Ongoing commissioning of heat recovery process in a central heating and cooling plant

Véronique Tremblay

A Thesis

in

the Department of

Building, Civil and Environmental Engineering

Presented in Partial Fulfillment of the Requirements

for the Degree of Master of Applied Science

(Building Engineering)

At Concordia University

Montreal, Quebec, Canada

April 2013

CONCORDIA UNIVERSITY
School of Graduate Studies

This is to certify that the thesis prepared

By: Véronique Tremblay

Entitled: Ongoing commissioning of heat recovery process in a central heating and cooling plant

and submitted in partial fulfillment of the requirements for the degree of

Master of Applied Science (Building Engineering)

complies with the regulations of the University and meets the accepted standards with respect to originality and quality.

Signed by the final examining committee:

Dr. M. Zaheeruddin   Chair

Dr. G. Vatistas   Examiner

Dr. P. Fazio   Examiner

Dr. R. Zmeureanu   Supervisor

Approved by   _____

Chair of Department or Graduate Program Director

_____

Dean of Faculty

Date   April 3, 2013

ABSTRACT

Ongoing commissioning of heat recovery process in a central heating and cooling plant

Véronique Tremblay

Ongoing commissioning aims at assessing and maintaining the performance of HVAC components in operation. Benchmarks describing the reference state are required in order to compare the incoming data collected by the building automation system against expected values. One approach is to develop inverse models from measured normal performance.

The current thesis is based on data collected in a central heating and cooling plant operated in Montreal. As a measure of energy efficiency, heat rejected by the plant chillers is recovered for re-heating needs in the summer. This thesis presents the analysis of the plant thermal performance over three years of operation with a focus on the heat recovery process and the key equipment, a plate heat exchanger.

Then, the proposed benchmarking approach is described. This is likely the first published ongoing commissioning methodology targeting liquid-to-liquid heat-recovery. It is based on a collection of metrics targeting the heat exchanger (Type A), and the process (Type B). Observations on the pertinence of including both perspectives are presented. The impact of the benchmarks training strategy is discussed, and the general formulation into a graphical user interface is described.

Acknowledgements

Table of Contents

List of figures

List of tables

List of Equations

Nomenclature and abbreviations

AHU	Air handling unit
ANN	Artificial neural network
ASHRAE	American Society for Heating, Refrigeration and Air-Conditioning Engineers.
BAS	Building automation system
c	Condenser (as subscript)
c_p	Specific heat at constant pressure [kJ/(kg°C)]
C_{XX}	Heat capacity rate for the fluid XX [kJ/°C]
CH	Chiller
CHW	Chilled water stream
CND	Condenser water stream
CSB	Concordia Science building
COP	Coefficient of performance
COP_{RE}	Compound coefficient of performance for heat recovery
CT	Cooling tower
ev	Evaporator (as subscript)
ECBCS	Energy conservation in buildings and community systems
FDD	Fault detection and diagnosis
HVAC	Heating, ventilation and air conditioning
HW	Heating water stream
IEA	International Energy Agency
in	Inlet (as subscript)
$\dot{m}$	Mass flow-rate [kg/s]
NaN	Not a number (missing data)
out	Outlet (as subscript)
P	Electrical power [kW]
PI	Performance Index
PX	Pump number X
RER	Recovery efficiency ratio (recovery / auxiliary power)
RH	Relative humidity of air
RL	Ratio of loads (recovery / demand)
RR	Recovery ratio (recovery / condenser load)
RMSE	Root-mean squared error
Q	Load or Heat transfer rate [kW]
Q_{HW}^{HX3}	Heat transfer rate measured on the cold side of heat exchanger 3 [kW]

Q_{HW}^{CSB}	Heating load for the CSB [kW]
Q_{CHW}^{CSB}	Cooling load for the CSB [kW]
RER	Recovery efficiency ratio
RR	Recovery Ratio
r	Return (as seen from the device; equivalent to inlet)
rec	Recovery
S_x	Standard deviation for the distribution in the sample of the variable x
s	supply (as subscript)
T	Temperature
T_{avg}	Average stream temperature ($|T_{in}+T_{out}|/2$) [°C]
T_{OA}	Dry-bulb temperature of the outside air [°C]
T_{CNDs}	Temperature of condenser water leaving a chiller
T_{diff}	Temperature differential ($|T_{in}-T_{out}|$) [°C]
$T*_{diff}$	Difference between inlet temperature for the fluids entering HX3 [°C]
T_{HWr}^{HX3}	Temperature of the heating water returning to HX3 [°C]
T_{HWs}^{HX3}	Temperature of the heating water leaving HX3 [°C]
T_{CNDs}^{HX3}	Temperature of condenser water reaching HX3 [°C]
T_{CNDout}^{HX3}	Temperature of condenser water leaving HX3 [°C]
T_{CNDr}^{CT}	Temperature of condenser water returning to the cooling tower
T_{HWs}^{CSB}	Temperature of heating water supplied to the CSB
T_{HWr}^{CSB}	Temperature of heating water returning from the CSB
U	Overall heat transfer coefficient [W/°C·m²]
V	Volume flow rate [l/s]
UA	Conductance-area product [W/°C]
ε	Effectiveness of heat exchanger [dimensionless]
ε_{cl}	Effectiveness in initial (clean) state [dimensionless]
ρ	density [kg/m³]
ρ_v	volumetric density [kg/l]
$\$_{electricity}$	Rate for electrical energy [¢/kWh]
$\$_{gas}$	Rate for natural gas [¢/m³]
$\$_{heat}$	Rate for thermal energy [¢/kWh]

1. Introduction

The sector of commercial and institutional buildings accounts for roughly 15% of total energy consumption in Canada [1], a share comparable to the one of the residential sector (17%). Surveys mention that about 30% of the energy used in commercial buildings is actually wasted [2]. Maintaining comfort and optimal operation costs is a challenge. Proper design and installation, careful maintenance as well as retrofit and fine tuning of heating, ventilation and air conditioning (HVAC) equipment can lead to a significant reduction of energy usage. These observations underline the interest into the field of building systems commissioning; the focus is put here on the HVAC.

The term commissioning describes a process in which the HVAC systems are planned and delivered with a special attention on the correspondence between the owners' project requirements and the actual performance. It is thus a risk reduction approach for the investor. The process logically extends to the occupation phase, to support operation and maintenance when equipment degradation and changes in building function are likely to occur. The terms continuous or ongoing commissioning are then used.

The current study focuses on non-invasive analysis of HVAC equipment performance through the measurements made by the building automation system (BAS). The goal is to develop analysis methods and benchmarks for the energy performance of installed components in order to support ongoing commissioning.

Heat recovery is a key element in energy efficiency strategies being included in new constructions and existing building retrofits, but very few commissioning directives are

available, especially at plant scale. The current project is thus a contribution to the performance assessment methods of such processes. It could thus have impact on computational tools development for automated fault detection and diagnosis (FDD).

2. Literature review

2.1.Building Commissioning

The stronger regulations on comfort and environment quality, the necessity to use resources efficiently and the development of new technologies make building systems more complex. The interest in commissioning increased with this complexity. The American Society for Heating, Refrigeration and Air-Conditioning Engineers (ASHRAE) released in 1989 the initial version of *The Commissioning Process*, a guideline for new buildings which has been updated twice since, in 1996 and 2005 [3]. It describes extensively the procedure which includes (but is not restricted to) review of design documentation, functional testing performed during equipment installation as well as the production of an operation manual. This initial commissioning ideally starts from pre-design phase and is completed at building delivery. Although not yet mandatory, commissioning is required for high performance building accreditations such as LEED® Canada for new constructions [4]. Indications about the continuity of the process within the occupation phase are also given.

The interest for existing building commissioning emerged a little later, through guidelines such as the 1999 publication by Haasl & Sharp [5]. Liu, Claridge and Turner [6] mention an average of 20% of utility savings with simple paybacks often under two years for this process. It was service marked under the name of Continuous Commissioning[SM] by Texas Engineering Experimental Station's Energy System Lab [6]. This contributes to some confusion in the terminology because two types of commissioning activities are

included under this term. Both are ongoing or continuous in the sense that they occur during the occupancy phase. They are indeed complementary.

1. **General investigation and corrective measures implementation.** A systematic analysis event in an optimization perspective is performed to plan and implement retrofits. Occupants' comments, utility bills and data measured by the BAS or manually are analyzed. Solutions are suggested, installed and validated. Guidelines are available, such as [7]. The process can apply to an existing building that was never commissioned, in which case it is called retro-commissioning. For buildings that were initially commissioned, the term re-commissioning is preferred.

2. **Ongoing commissioning** and analysis of building behavior. This type presumes that initial, retro or re-commissioning has been performed, and the goal is to maintain its benefits. Ongoing commissioning includes performance tracking [3, 8] by detecting the degradation of equipment or changes in the functions of the building. The time basis for ongoing commissioning can be quarterly or shorter, according to the needs, scope or budget [6]. It is thus likely to outline issues early.

The International Energy Agency (IEA) published in 2010 the Annex 47 [9] of the Energy Conservation in Buildings and Community Systems program (ECBCS). It mentions the early stage of existing building commissioning in Canada. When submitting a project for accreditations such as LEED Canada for existing buildings [10] or BOMA BESt [11], both of the aspects mentioned above must be addressed. The current study is

however primarily aimed at the second category, ongoing commissioning, through the development of analysis methods and benchmarks.

2.1.1. Benchmarks

In whole-building energy analysis protocols (for instance Energy Star [12]), the annual energy use is compared to values from similar buildings; these are called building benchmarks [13].

To keep track of energy savings [5] or to make sure performance is maintained, the benchmarks or reference values are more complex. This higher level of analysis is also called energy tracking [14]. Energy tracking can be focused on the building or on certain systems. To properly compare the energy use for different conditions, the key factors must be corrected for the independent variables such as weather, loads or occupancy. In this case, the benchmarks are mathematical *models* using the data acquired by the BAS as inputs. The comparison between the model prediction and actual performance before and after a retrofit, for instance, allows for the validation of savings [15]. By extension, advanced benchmark models also enable fault detection. The Annex 25 [16] and Annex 34 [17] of the ECBCS referred to such usage of benchmark models. It is assumed that due to faults or degradation, the measured value will be significantly different from the modeled one, because the latter corresponds to expected performance under reference state [18].

Extensive analysis and advanced models are required for fault diagnosis [14], because of the complex interactions among HVAC components. A given symptom can have multiple causes; the effect of individual or combined faults must be known [19].

Passive or active testing of the systems against the benchmarks is possible, the latter involving forcing the BAS into specific states to verify the reaction of the various equipments in given conditions. This intrusive approach is usually performed within a short testing time, for instance during unoccupied hours [19].

2.1.2. Energy modeling

For a building, HVAC process or equipment, models describing the interaction between the influential parameters and the systems allow, among other things, energy tracking. As described in chapter 19 of the ASHRAE fundamentals 2009 [20], a modelling approach can be either forward or reverse. The forward (classical or white-box) models are based on physical and engineering principles. They are particularly appropriate for design. In order to apply them to an existing system, a model calibration must however be performed. This time-consuming operation requires high technical knowledge.

Data-driven (inverse or reverse) models are by nature more appropriate for the analysis of installed, existing systems [20]. For one specific installation, they are defined based on measured data from actual behavior; by nature allowing self referencing [13]. They are typically simpler and often more precise than forward models. The identification of operation patterns, as described by Baumann [21] can be a preliminary step to reverse modeling development. Black-box approaches such as purely empirical statistics-based parametric models and artificial neural networks (ANN) models can perform very well [22]. Gray-box reverse models and expert knowledge are also used.

One more distinction must be done concerning the time dimension: the transient or steady-state nature of the model. A steady-state behavior assumes no time variation in the

inputs and outputs of a system. For varying inputs or properties, models involving differential equations are generally necessary [23]. The ASHRAE [20] mentions that in building systems analysis, hourly or sub-hourly measurements will generally display transient behaviour. Daily to monthly data are more likely to be compatible with steady-state models. It is thus possible to define the analysis time-scale so that a quasi-steady state model approximates a transient phenomenon.

Performance indexes (PI), also called performance metrics, are measurable quantities that provide insight on the performance of an equipment or system. Qualities of a PI include a clear definition and the ability to indicate state or progress toward a performance goal [9]. In an ongoing commissioning perspective, the output of an inverse benchmark model can be a performance index. The measured values characterizing the operation conditions (temperature, flow, power usage, etc.) are candidate model inputs. The actual PI value can be compared against the value predicted by the PI benchmark model, to compare the current state to the expected, standard behaviour. Discrepancies between observed and predicted PI may indicate the presence of a fault. The training sample and method have impact on the benchmark model and its accuracy. Monfet [24] proposed methodology for the development of large primary HVAC components benchmarks and demonstrated it on chillers, using the coefficient of performance (COP) as PI.

2.1.3. Automation of ongoing commissioning process

The ongoing commissioning of HVAC systems consists in collecting continuously measured data that is important for the evaluation of energy performance of equipment, including the degradation of performance, detection of faults and assessment of the need

for maintenance. Data is analyzed, either online or offline, indices of performance are displayed, and messages or reports are sent to the operating team. The selected indices of performance are compared with benchmarks (reference values) that are either target values or are models representative for the normal operation of the system.

The Annex 25 [16] of the ECBCS presented in 1995 a collection of procedures, concepts as well as a fault database for HVAC equipment. The United-States Air-Conditioning and refrigeration technology institute released a similar report in 2003 [8]. The generic goal of these documents is to support the development of advanced functionalities for the BAS, in order to allow automated fault detection and diagnosis (FDD) in HVAC systems. The Annex 34 of the ECBCS [17] described the early state of the FDD field in 2001.

The experts consulted for the projects mentioned above [8, 16, 17] gave priority to air-side components such as air handling units (AHU). Interest for the water systems is more recent; as outlined by Deng *et al.* [25] there are significant opportunities on the central chilled and hot water plants and the corresponding water networks (local or district). This 2002 publication gave recommendations for re-commissioning or retro-commissioning of plants and suggested the use of simulation tools to assist operations and support decision making (ongoing commissioning).

The Annex 47 of the ECBCS [9], released in 2010, covers commissioning needs for existing and low energy buildings. The report described automated and semi automated commissioning tools. All tools remained at prototype level, with limited FDD capabilities, and only one targeted heating and cooling plants.

2.2.Ongoing commissioning of heat recovery processes in HVAC

Heat recovery in HVAC systems is one of the pillars of energy efficiency in buildings. Various strategies are available, ranging from relatively passive (heat-exchanger based) to active (heat-pump based) approaches. The term "active" here applies to the heat transfer process and not the auxiliary consumption of energy, for instance by circulation pumps. The most common example targets the ventilation; specialized units recover sensible and latent heat from the exhaust air.

These air-side equipments were very briefly discussed in [8]. The ANSI/ASHRAE standard 84-2008 defines laboratory methods to measure and test the performance of air-to-air heat recovery systems [26] in a rating perspective. The Annex 47 [9] referred to a few software tools supporting the ongoing commissioning of AHU equipped with heat recovery functionalities.

Liquid-to-liquid heat transfer can be used to take advantage of the heat rejected by chiller condenser. In such applications, standards and computer aided commissioning tools appear to be inexistent. There are no scientific publications about the ongoing commissioning of liquid-to-liquid heat-recovery processes in HVAC systems or other fields. As a matter of fact, the very definition of relevant performance indices needs to be achieved.

The discussion here is limited to the liquid-to-liquid, passive case. Such a system involves valves, circulation pumps and at least one heat exchanger. Temperature, liquid flow rates and pressure sensors are often also present. Assuming proper sensor calibration

and the simplest possible pumps and valves (ON/OFF), the key component is the heat exchanger itself, for which the possible faults are few; the most common is fouling.

Fouling generates a gradual decrease of the heat transfer performance caused by the accumulation of deposits or dirt on the exchange surfaces. There are some cases, mostly with shell and tube exchangers, where the fouling level reaches a plateau; the inclusion of a safety margin in the heat exchange surface area at design is sufficient to mitigate the effect. Things are different with plate heat exchangers due to the smallest cross section for the fluid circulation [26]. They might even reach a critical state involving blocked flow. Fouling in the heat-exchanger is likely the main problem susceptible of affecting the heat recovery process, but its level cannot be measured directly. The consequence is that even under optimal conditions, the performance of the heat recovery process may decrease. A complete maintenance strategy for a heat exchanger involves defining the proper cleaning schedule and method, based on mechanical, economic or energetic criteria [16] in its specific operation context.

The following sections introduce two groups of performance indices intended to support the preventive maintenance of heat recovery system in an ongoing commissioning approach. The main component is the heat exchanger, and as an initial analysis perspective, this equipment is the center of attention (section 2.2.1). Fault detection for heat exchangers is based on various properties. They are listed in a literature review and, if applicable, the approach according to which they have been used for ongoing analysis or monitoring is presented.

Although the heat exchanger is the key component, it seems pertinent to also define criteria for the heat recovery process as a whole. The idea is to take into account the integration and interdependence of the processes involved. The second section (2.2.2) thus lists process-scale PI likely to complement the analysis.

2.2.1. Performance indices for heat exchangers

Kuhlmann presented in 2000 "MonitEx" [27], a computational tool designed to support preventive maintenance of heat-exchangers used in district heating. The tool analysed temperature measurements to identify current fouling level (described through the fouling resistance R_f (°C·m²/W)) and predict the moment where a pre-set fouling limit would be reached. The tool was developed and applied for shell and tube heat-exchangers.

The 2003 study performed by Cui and Wang [18] on chillers and based on synthetic data involved the analysis of their evaporator and condenser, which are heat exchangers. In their experiment, the PI was the measured log-mean temperature difference (Δt_m). It was compared against a parametric benchmark model having as inputs the cooling load, the chilled water supply temperature and the returning condenser water temperature. Discrepancies between measured and predicted values were observed in the presence of faults, allowing for their detection.

In 2009 Zhou [28] compared outlet fluids temperature, thermal effectiveness and conductance-area product (UA, (kW/°C)) as candidates for monitoring the performance of heat exchangers included in a HVAC system. The UA value appeared as the most pertinent PI. It was mimicked through a second order parametric model. Here too,

simulated faults corresponded to measured values of UA diverging from the model prediction.

In 2011 Monfet [24] calibrated a model of a heating and cooling plant with TNRSYS simulation program. She observed that the UA for a heat exchanger was about 50% lower than the design value. However the change had no impact on the performance of the heat recovery system under analysis. A significant change in UA may thus not be detectable. The 2011 publication of Tatara *et al* [29] mentioned that field data for heat exchangers are often characterized with very large uncertainty (up to 900%) in the calculation of UA.

Mohanty [30] introduced in 2011 the use of the C-factor calculated as the ratio of flow to pressure drop on one side of the exchanger and illustrated its evolution during the 20 days-long chemical cleaning of a shell and tube device. The C-factor shows a certain correlation to the overall heat transfer coefficient (U, (kW/ °C·m²)).

In 2012 Pogiatzis *et al* [31] modeled the time-variation of the resistance for the fouling layer R_f and used the classical ε-NTU method to compute the corresponding heat transfer. Their goal was to optimize the heat exchanger cleaning cycle. The 2013 paper by Markovski *et al* [32] used a similar approach for a network of heat exchangers. The authors applied steady state analysis by a combination of averaging and data selection.

The 2012 paper by Genić *et al* [33] is one of very few scientific studies involving plate heat exchangers operated in district heating. The authors performed two campaigns of measurements, the first shortly after installation and the second one year later. They used the classical ε-NTU method to evaluate the actual fouling resistance R_f and manufacturer design software to obtain the water shear stress. For a first group of heat exchangers

(radiators), they observed an average fouling resistance of 0.048 °C·m²/kW per heat-exchanger side, which is slightly above the design recommendations. There was no significant variation of R_f in time, which appeared to indicate no fouling development. For the second group (domestic water heaters), the measured R_f increased significantly. After one year, it showed a strong correlation to the shear stress.

It must be mentioned that in all the studies presented above except [24, 30, 32 and 33], synthetic data was used for analysis. Moreover, the heat exchanger models were all steady-state models with no time-lagged values. Measurements were performed under steady-state conditions.

Other authors studied the dynamic behavior of heat-exchangers. In 2000 Weyer *et al* [34] generated synthetic data with a lumped discrete-time model and then used a white-box recursive scheme to compute the overall heat transfer coefficient U stepwise. They analyzed its variation in order to detect the simulated faults. Hu *et al* in 2005 [35] stated that in HVAC applications, first principle models were insufficient to predict the behavior of heat exchangers due to strong non-linearity in the phenomena. Their ANN showed good accuracy for modeling the heat transfer rate in the heat exchanger for an AHU. The algorithms were presented as good candidates for control optimization, not performance monitoring tools. Astorga-Zaragosa *et al* in 2008 [36] used an adaptive algorithmic observer, tolerant to the expected slow decrease of U caused by fouling while being sensitive to abrupt changes due to settled material breaking off. The ongoing monitoring was thus not based on comparison between the measured and expected value of the performance index, but on the time scale and intensity of the variation it would

undergo. All these studies used synthetic data whereas [36] also included laboratory testing. Authors [34, 36] insisted on the necessity of filtering and smoothing input data in regards of the high impact of noise. In all these studies of dynamic models, the sampling time was between 1.5 seconds and 1 min.

2.2.1.1. Existing tools for heat exchangers ongoing commissioning

The Siemens Maintenance System company released in 2010 a maintenance application called "HeatXchMon" [37, 38] that performs the ongoing commissioning of fluid-to-fluid tube bundle heat exchangers used in industrial applications (not for HVAC systems). It uses as inputs the inlet and outlet temperatures of both streams and corresponding mass flow rates. The measurements lead to the estimation of actual heat transfer flow rate, which is compared with two reference values that are estimated by numerical simulations: the heat transfer flow rate: 1) under clean conditions, and 2) under maximum tolerable fouling state. Warnings and alarms are issued when the heat transfer performance is below the acceptable limits.

Figure 2-1 Plate heat exchanger

14

It is worth mentioning that the Siemens application for plate heat exchangers requires the simulation model of each manufacturer to estimate the two reference heat transfer rates and is not supported in the available version.

2.2.2. Performance indices for heat-recovery process

The 2012 ASHRAE Handbook on Systems and equipments [26] devotes an entire chapter to air-to-air heat and energy recovery exchangers. It includes methods for rating based on seven criteria: the sensible, the latent and total effectivenesses, the supply and exhaust air pressure drops, the fraction of exhaust air transferred to the supply air and the ratio of supply inlet to outlet air flow. These seven criteria are laboratory tested for two sets of conditions simulating winter and summer. They allow for classification and comparison among technologies and are expected to vary significantly in field conditions compared to laboratory measurements.

Considering performance assessment for the overall process, the handbook introduces the notion of Recovery Efficiency Ratio (RER). The case of a liquid-to-liquid application is simpler because leakage effects are not considered, the analysis requires no significant correction for fluid dilatation and no condensation is present. The heat transfer rate occurring across such a heat exchanger is purely sensible and is calculated from:

$$Q = \dot{m}c_p(T_2 - T_1), \qquad \text{Equation 2-1}$$

where $\dot{m}$ is the mass flow rate (kg/s), c_p the mean heat capacity (kJ/kg°C) and T_2 and T_1 respectively the outlet and inlet temperatures for the fluid. In the absence of heat losses to the environment, the magnitude of Q for each stream should be the same. The RER for a passive, liquid-to-liquid heat-exchanger based process becomes the ratio of

heat rate through the exchanger ($Q_{recovered}$), divided by the total electrical power P of the pumps circulating the cold and warm fluids on each side:

$$RER = \frac{Q_{recovered}}{P_{electrical}}$$

This quantity is similar to the one called "COP" in 2009 by Hortelan [39]. For measurements performed in a cooling and heating plant, he also quantified the recovery rate (RR), defined as the ratio of the heat recovery rate divided by the total rejected heat at the condensers.

A few definitions for the coefficient of performance (COP) of compound cooling and heat-recovery processes can be found in literature. Durkin [40] used in 2003 a ratio of heat flow rates to electric power to characterize a dedicated heat recovery chiller. Kaushik [41] used a similar approach in 2011 to evaluate the performance of a simulation-based recovery system:

$$COP_{rec} = \frac{|Q_{cool}| + |Q_{recovered}|}{P_{electrical}}$$

where Q_{cool} (kW) is the evaporator load, $Q_{recovered}$ (kW) is the heat recovered and $P_{electrical}$ is the electrical input of the equipment involved in the processes. This includes the chiller's compressor, circulation pumps and cooling tower fan. The system was not actually built, but COP was obtained from simulation (synthetic) data.

Gong [42] suggested in 2010 a recovery COP formulation involving exergy analysis of a system from recovering heat from an air conditioning device to pre-heat domestic hot water.

2.3. Summarizing remarks after literature review

Only a few publications are available on the topic of heat recovery in HVAC that could be applied to the ongoing commissioning. The process is likely to be mostly affected by the degradation of equipment, here a heat exchanger. Under the hypothesis that thermal performance degrades due to fouling, ongoing commissioning could be based on a comparison of measured performance of the heat exchanger with a benchmark corresponding to a theoretical performance limit. It also appears pertinent to quantify the impact of the degradation on the processes put into interaction by the heat-recovery loop. Complementary indices thus seem interesting, and they could also allow insights on the operation and its evolution.

Most publications are based on synthetic data; the application to measured data as presented in this thesis is a new contribution to the field. In addition, most experiments involve shell and tube exchangers; the study of a plate heat exchanger is also distinctive.

2.4. Objectives of thesis

The general objective is the development of an analysis and benchmarking methodology for the ongoing commissioning of liquid-to-liquid heat recovery in HVAC systems. Benchmarks are developed for a corpus of measured data generated by the BAS of a central heating and cooling plant in which heat is recovered from condenser water. The study is performed offline, but the data is analyzed in a chronological approach similar to the incoming of operation data through the season.

The benchmarks are defined from standard operation data, or at least data assumed to be free of faults. Here are the two sets of benchmarks against which incoming data is tested:

A. TYPE A: "limit of performance" approach for the main equipment (heat exchanger). The incoming data is compared to a limit expressed in terms of effectiveness and based on the following criteria

- o Power : minimum and limit based on ASHRAE 90.1 [43];

- o Cost: minimum.

B. TYPE B: with process-scale performance indices. For some of them, benchmark models are developed, following the methodology of Monfet [24]. The measurements can then be compared with benchmark predictions.

In a real-time operation of the method, the detection of a discrepancy with respect to the benchmarks is supposed to trigger an alarm, recommending maintenance or further analysis. Simple fault detection through performance assessment is envisaged, without diagnosis.

The data collected from the central cooling and heating plant provides an opportunity to analyze the fouling for a plate heat exchanger operated in HVAC; the fouling growth regime and R_f are described and discussed.

3. Description of the plant

3.1. Concordia Science building and central plant

The R. J. Renaud building, also called the Concordia Science building (CSB), was inaugurated in 2003 on the Loyola campus of Concordia University, Montreal. The building contains classrooms, laboratories and offices for a total floor area of 32 000 m^2. In 2011 a new wing was delivered; the Genomic pavilion has four floors plus a basement (total 5350 m²) and its heating and cooling water loops are connected to those of the CSB. Monfet [44] studied the CSB through a calibrated simulation; the building was observed to be more sensitive to internal loads variation than to weather. The temperature changes were stronger in the heating and cooling water loops than in the ventilation air.

Figure 3-1 Concordia R.J. Renaud Building (right) and Plant (left)

A central plant (the RF) provides the CSB with two hydraulic loops for heating water and chilled water, both intended to space conditioning. Steam is also produced for various needs. The heating water loop is active all year long. In the cold and shoulder seasons, two small chillers located within the building provide for low cooling loads. The plant large chillers are active only when the building chillers are not sufficient, generally

between April and the end of October. The plant chilled water loop then provides for two buildings, AD and CSB, but the main share is devoted to the latter.

The Figure 3-2 illustrates the plant in cooling mode. For simplification, the steam boilers and SOFAME are not illustrated.
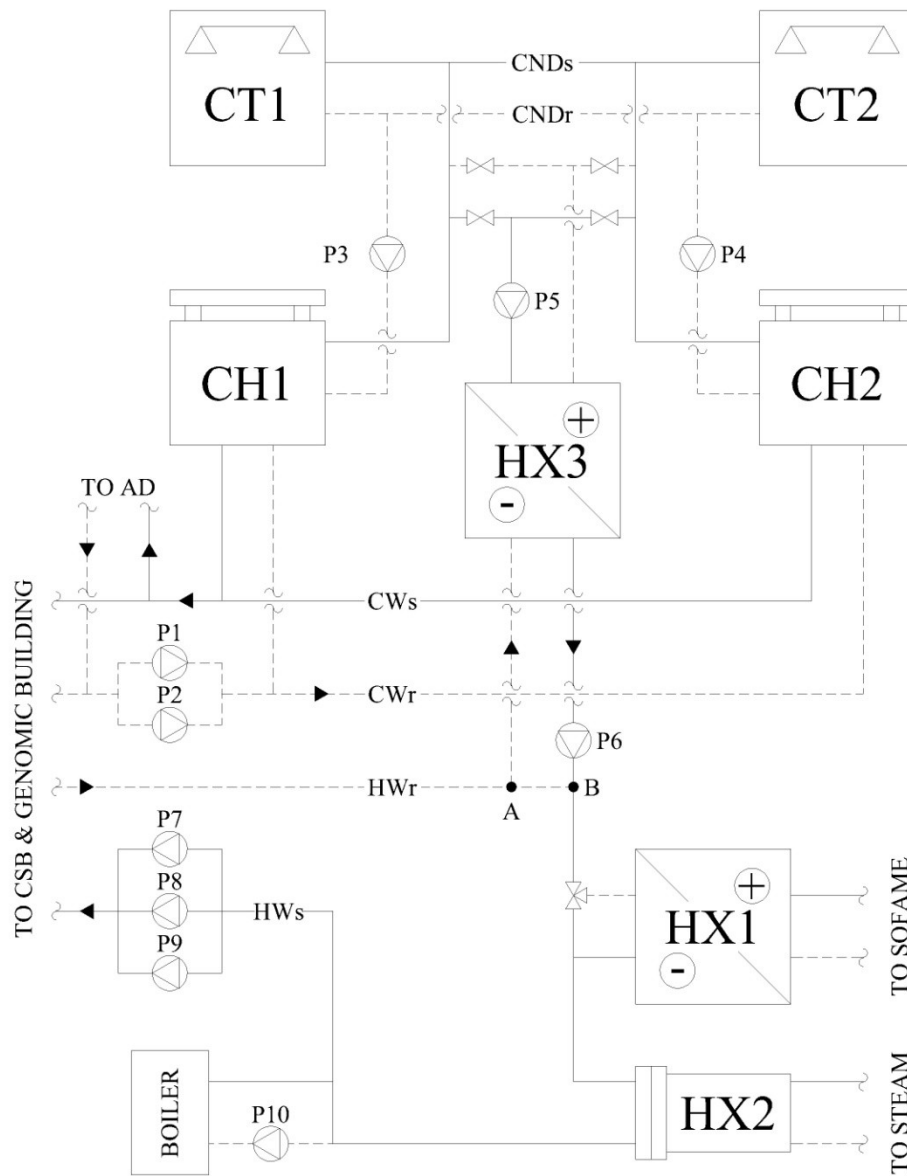
Figure 3-2 Plant schematic in cooling mode

Heat recovery is a key element in the design integration of the heating and cooling systems. During the cold season, energy recuperated from the flue gas of the steam

20

boilers provides for most of the heating needs in the CSB. This operation is accomplished with the means of a boiler economizer (the SOFAME) and a plate heat exchanger identified as HX1 on Figure 3-2. During the warm season, when chillers are in operation, heat is recovered from the condenser loop of the first-to-start chiller using a plate heat exchanger identified as HX3. There is no simultaneous operation of the plant chillers and boiler economizer; HX1 and HX3 are never operated together. All year long, when heat recovery is not sufficient, steam can be used to complete water heating through a shell and tube exchanger identified as HX2. In 2011, an electrical water boiler was added downstream the HX2; its operation is restricted by the total electrical usage and contract electric power for the campus.

Monitoring data generated by sensors of the plant and CSB are collected through the BAS for analysis. The measurements can be used to assess the performance level and its evolution as well as to develop and test benchmark models. The collected data allows the analysis of two main processes:

1) Heating water production through heat recovery:

    a) For reheat during the summer and shoulder seasons (main heat source = HX3)

    b) For winter-time heating (main heat source = HX1)

2) Chilled water production (summer and shoulder seasons)

Previous studies on this corpus of data have mainly focussed on the chilled water production [24, 39, 45, 46, 47]. The current analysis extends the approach to the equipment involved in the heat recovery process operated in the warm season.

3.1.1. Chilled water production

When the plant 3165 kW (900T) centrifugal chillers are operating, chilled water is circulated by either one or two of the constant-speed pumps P1 and P2. The chilled water temperatures and flow in the CSB loop are measured and recorded.

Each chiller is connected to a cooling tower (CT). The cooling towers are operated when required by the chillers load. They are equipped with variable speed fans. The CT outlet temperature and the fan relative variable frequency drive (%VFD) are measured and recorded. The constant-speed pumps P3 and P4 are devoted to the condenser loops. It was observed that the association pump/chiller/cooling-tower is maintained from 2009 to now; for instance chiller 2 (CH2) is operated with chilled water pump P2, cooling-tower CT2 and condenser water pump P4.

A single chiller is required during most of the season, the second one being added for high loads, about 10 to 25% of the time. The transition from one to two chillers occurs around 2500 kW of total cooling load at the plant. When operated in tandem, the chillers were observed to share the total cooling load evenly. Over the warm season, the roles of the chillers are inverted a few times to prevent them from ageing too differently (first-to-start versus back-up). Temperatures are measured and recorded at the inlet and outlet of chillers evaporators and condensers. The electrical power input to each chiller is also measured and recorded.

The notion of cooling group is sometimes used in the text. It refers to chilled water production involving a chiller, a cooling tower (if necessary), a condenser water pump

and a chilled water pump all in action. The first-to-start cooling group feeds the heat recovery process involving HX3.

At low cooling loads (winter and parts of the shoulder season) the plant chilled water loop is not active; the 352 kW (100T) chillers located in the CSB provide chilled water. They are not operated with cooling towers; the extracted heat is rather transferred to the heating-water loop, yet another example of heat recovery.

The start-up of a plant chiller thus involves effects on both water networks. 1) The chilled water loop between the plant and the building becomes active. 2) The heating water loop starts receiving heat from the condenser of the plant chillers rather than from the building's. The heat rejection is not necessarily performed at the same temperature for the building and plant chillers. Upon heat recovery start-up, the heating water loop behavior does not change significantly hydraulically but it might do thermally.

3.1.2. Heat recovery process during the warm season

Figure 3-3 presents a simplified schematic of the equipment involved in heat recovery, with the location of sensors and the identification of the measurement point. Only one cooling group is illustrated, for simplification. This is coherent with the fact that only one group at a time provides for the heat-recovery process.
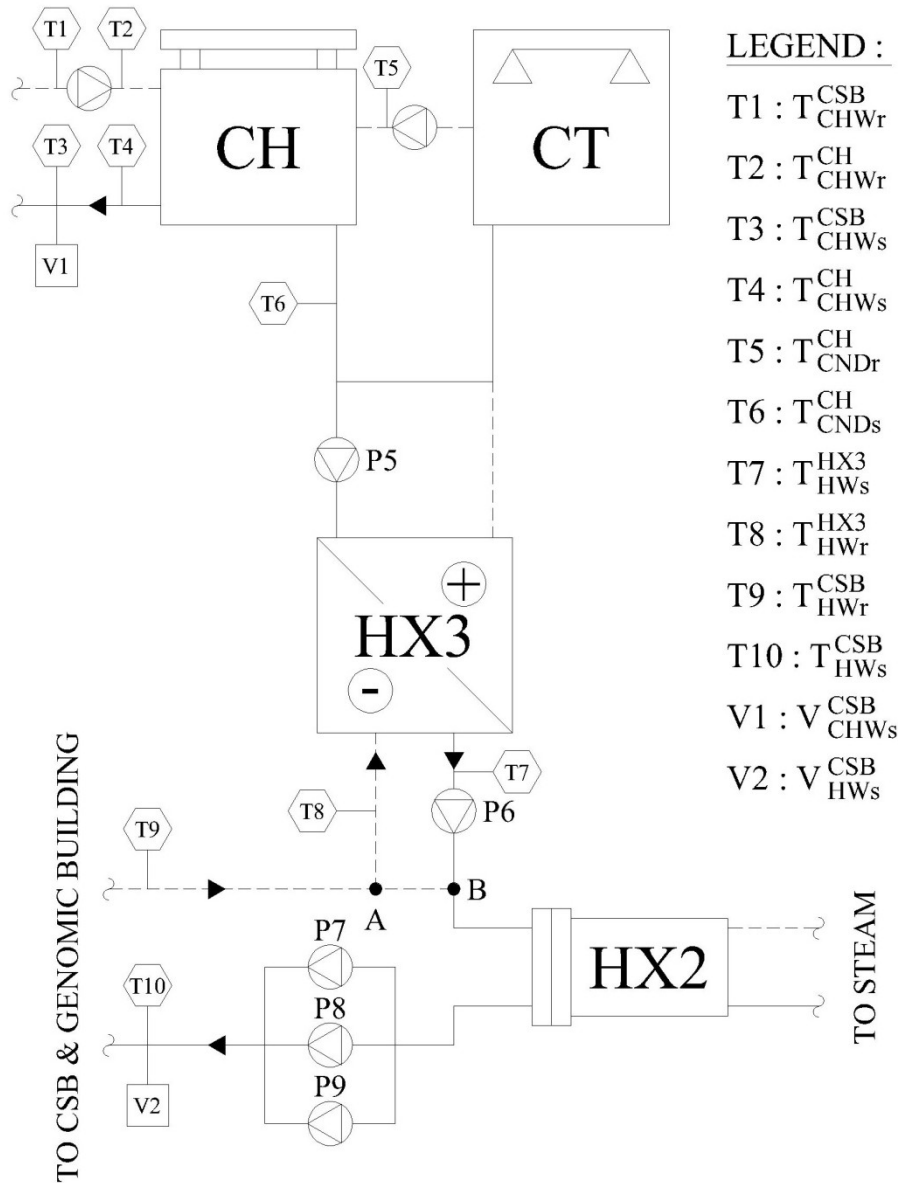
Figure 3-3 Measurement points location

Heat recovery through HX3 takes place when at least one of the plant chillers is in operation. The exchanger receives condenser water (CND) from the first-to-start chiller. The recovery process uses two constant speed pumps: P5 circulates the warm fluid on the CND side, and P6 circulates the cold fluid on the heating water (HW) side. This recovery process is always (and only) done when chilled water is produced in the plant. The heat

extracted from the condenser loop through heat-recovery reduces the load on the corresponding cooling-tower, and thus the electricity used by the fan [39, 47].

The inlet and outlet temperatures on both sides of the exchanger change value over time and are thus the key variables involved in the study of the warm season heat recovery process. Three temperatures are actually measured: 1) the return T_{HWr}^{HX3} and 2) the supply T_{HWs}^{HX3} temperatures on the HW side of the exchanger as well as 3) the temperature of the water leaving each condenser T_{CNDs} on the CND side (measured upstream of P5).

The heating water circulation between the plant and the CSB is maintained by three variable frequency drive pumps (VFD) P7 to P9 for which the VFD, a value between 0 and 100, is measured and recorded. The pumps action is controlled automatically, adjusting in real-time. There is also a flow meter for this loop. The HW does not circulate through the building itself; plate heat exchangers allow the heat to be transferred to a glycol-water loop. Adjustable valves controlled by the BAS modulate the HW flow for these heat exchangers. No measured data were recorded for the glycol-water heat exchangers.

A specificity of the HW (cold side) of the HX3 exchanger is to be mentioned. The HW loop is connected to the heat exchanger loop with a common pipe [48]. The water flow rate driven by Pump 6 (107 L/s) is greater than the CSB heating water loop during the cooling season (around 50 L/s). This generates a re-circulated water flow rate from point B to point A of Figure 3-3. The temperature of the water entering HX3 (T_{HWr}^{HX3}) is thus warmer than the temperature of the heating water return (T_{HWr}^{CSB}) from the CSB due to mixing with heated water at temperature T_{HWs}^{HX3}. Additional heat can be added to the HW

loop downstream of HX3 through HX2 and electrical boiler (after 2011) to complete the heating load.

3.2. Plant equipment as-operated

Monfet [47] presented an evaluation of the performance of the plant in 2009. Her results demonstrated differences between the design and as-installed properties of the equipment. The as-operated parameters estimated in 2009 will be used here; design values are presented in Appendix A. The other characteristics are cited from the plant operation manual and equipment specifications produced by the consortium in charge of the construction [49].

Table 3-1 Operation equipment properties in 2009

Item	Description	Capacity	Power input
Chiller (each of 2)	Trane CenTraVac CVHF 0910	Q_{max} = 3165 kW	525 kW
Chilled water pumps	Bell & Gosset series 1510 3BC	86.75 ± 0.90L/s	75 kW
Cooling Towers (each of 2)	Baltimore Aircoil model 3676A	Q_{max} = 4750 kW	Fan P_{max} = 30kW
Condenser water pumps (each of 2)	Bell & Gossett VSCS 10X12X11 75 hp 1800rpm	110 L/s ±1.2	56 kW
HX1	Alfa Laval plate heat exchanger, single pass, counter-current		None
HX2	Shell and tube		None
HX3	Alfa Laval M20-MFG plate exchanger single pass, counter-current 133 gasketed plates, 0.5 mm AISI 136 Exchange surface = 111.31 m² Designed for 1035 kPa, 107°C		None
Heating-water pumps (each of 3, P7 P8 P9)	Bell & Gosset series 1510 4BC 3500 RPM	V_{max} = 53 L/s	56 kW
Pump 5 HX3, condenser water side	Bell & Gossett VSCS 6X8X9¾ 40hp 1800 rpm	60±0.6 L/s	30kW
Pump 6 HX3, heating water side	Bell & Gossett VSCS 6X8X9¾ 40hp 1800 rpm	107.25±0.75 L/s	30kW
Pump (2) for glycol loop, in CSB 612	Bell & Gossett series 1510 4E 1800 rpm, 10 hp	36.6 l/s	14.9 kW
Pumps (2) for glycol loop, in CSB 470	Bell & Gossett series 1510 2E 1800 rpm, 20hp	14.5 l/s	7.5 kW (10hp)
Electric water heater (added in 2011)	Cleaver brooks WB-243 1020kW 3 phases /600V /60Hz	Q_{max} = 1020kW at 600V	Max 1020kW
Pump to Electric heater	Armstrong 4030-3x2.5x6-1.5	11 L/s	1.2 kW

All constant speed pumps and fans are considered to be operated at rated rpm. The power usage by circulation pumps and fans is also the rated value; no electrical readings were performed in the context of this study.

3.3.Data collection

Data collection is performed through the BAS. Time series for more than 100 points recorded every 15 minutes are available. Most measurements correspond to the numerical value (temperature, pressure, etc.) at the end of each interval or to the current state (ON/OFF). Some measurements, however, the logger only updates according to a pre-defined sensitivity. The heating water pumps variable drive is an example; the recorded value (%VFD) is not updated if a change less than 10% away from the previously recorded value occurred during the interval.

The Concordia physical plant provides an access to a weekly report for a selection of points. It takes the form of a spreadsheet with the state data as well as numerical values for seven consecutive days. The spreadsheet is automatically transferred to our research group by email. The selection of the points was made in the perspective of a previous ongoing commissioning project by Monfet [24]. Most of the data used for the analysis of the 2008-2010 period thus corresponds to archives. The current analysis, including filtering and averaging, is based on the original spreadsheets.

In the context of the current project, the list of measurements and state data to be included in the report was updated. Several onsite visits as well as verbal and written communications with the operation employees provided information complements such as sensors specifications and details on the operation sequence. Finally, a verification of

27

the flow for the streams driven by constant speed pumps was performed with the cooperation of Canmet Energy in October 2012.

4. Methodology

The measurements are presented and briefly analyzed first; the plant general thermal performances as well as the properties of the heat exchanger are calculated. These results are presented in chapter 5.

The general ongoing commission approach for the heat recovery system is the following. At the end of each evaluation period, for instance each day of operation, the ongoing-commissioning functional block computes the daily value for the relevant performance indices. They are grouped in two categories: main equipment state (heat exchanger effectiveness) and process PIs. This information is compared to the benchmarks, which are the reference values for these quantities, and warnings are generated if investigation seems required.

This chapter contains three main sections. The first (4.1) presents the benchmarking approach for the heat exchanger, and the second presents the process performance indices (4.2). Finally a discussion on the benchmarks training is presented (4.3). The demonstration of the approach on the measurements is performed in chapter 6.

Dynamic studies of heat exchanger performance [34, 35 36] require a sampling rate of one minute or less, whereas the data acquisition at central plant is performed four times per hour, which seems insufficient to track the transient phenomena. The current study will thus be limited to steady-state.

4.1. Limits of performance for main equipment (Type A)

The heat recovery process described here is characterized by a relatively small electrical usage from circulation pumps; hence it is considered as passive. The system is susceptible of diminishing efficiency as the equipment degrades due to heat exchanger fouling. Valve, pumps and meter failure are not considered, the available measurements not allowing the assessment of their state.

The common practice [50] in heat exchanger design is to oversize the capacity based on a constant value of fouling resistance R_f. The allowance is based on empirical knowledge and can be seen as to correspond to the effect of fouling over the designated service cycle for the facility. Heat exchanger fouling is complex; the decrease in heat transfer properties, often combined with an increase in pressure drop, is site and process-specific. It is not possible, nor desirable, to model and predict the fouling here, but rather to determine the level that can be tolerated.

A minimum or limit performance can thus be established beyond which heat exchanger cleaning should be undertaken; this corresponds to Type A benchmarking. Performance limits are defined according to energy and financial arguments. The tolerance here is not based on safety of the mechanical equipment; it is not possible to know at what level of fouling the flow is so impaired that the pumps cannot work the fluid through either side of the exchanger. The hypothesis must be made that the power and cost limits are such that they are reached before the mechanical limit.

The limits are formulated here in terms of the heat exchanger effectiveness, ε. This choice is somehow equivalent to working in terms of fouling resistance (R_f) or UA.

Effectiveness (ε), as will be further discussed (4.1.4), is an intermediate value in UA and R_f assessment and has thus lower uncertainty bands.

When detailed design data is available, it can be used to determine the numerical values for the limit performance benchmarks. This is not the case here and operation data will be preferred. The 2008 season is the first available and serves here as the reference operation state. Measurements were performed under conditions assumed to be normal.

4.1.1. Effectiveness of a heat exchanger

The heat exchanger effectiveness (ε) is an intrinsic property for the equipment that is typically constant under constant operation conditions, unless fouling occurs. For a heat exchanger ε is defined as the ratio of the actual to the maximal thermodynamic heat transfer rate; it thus varies between 0 and 1. No publications involving ε as a performance index in the context of ongoing commissioning of heat recovery processes or heat exchanger were identified, but the evaluation of ε is normally used as support in scheduling cleaning operations [30]. Moreover, this quantity is compatible with the available measurements and allows for the calculation of all other heat exchanger properties (see 4.1.4 below). Limited to steady-state approach, ε of a heat exchanger is [51]:

$$\varepsilon = \frac{Q}{Q_{max}} = \frac{Q}{C_{min}\left(T_{hot_{in}} - T_{cold_{in}}\right)}, \qquad \text{Equation 4-1}$$

where Q is the heat flow rate (Equation 2-1) and C is the heat capacity rate (in kJ/°C), obtained from the product of the mass flow rate $\dot{m}$ and heat capacity c_p. For the case of HX3 the water flow on the condenser side (V_{CND}) is lower than the water flow

rate on the heating water side (V_{HW}); hence $C_{min} = C_{CND}$. The effectiveness is then calculated as follows:

$$\varepsilon = \frac{V_{HW}\rho_{HW}c_{p_{HW}}\left(T_{HWs}^{HX3}-T_{HWr}^{HX3}\right)}{V_{CND}\rho_{CND}c_{CND}\left(T_{CNDinlet}^{HX3}-T_{HWr}^{HX3}\right)} = \frac{C_{HW}\left(T_{HWs}^{HX3}-T_{HWr}^{HX3}\right)}{C_{CND}\left(T_{CNDinlet}^{HX3}-T_{HWr}^{HX3}\right)}. \qquad \textbf{Equation 4-2}$$

The value used for $T_{CNDinlet}^{HX3}$ corresponds to the temperature supplied by the condenser connected to the heat-exchanger; T_{CNDs}. The numerator of Equation 4-2 is based on cold side temperatures and properties because these measurements are available here.

The degradation in heat transfer due to fouling should translate into a decreasing effectiveness. Type A benchmarking limits are expressed here in terms of ε and comparison is performed using data averaged at daily scale. This is in concordance with the ASHRAE [20] recommendation restricting the use of steady-state models to daily or larger scale in order to remove time-lag effects.

4.1.2. Limit performance based on Power

When the heat recovered through the heat exchanger HX3 cannot satisfy the demand Q_{HW}^{CSB} for heating water in the building, additional heat is provided through the steam exchanger HX2 or the electrical boiler BR1 (after 2011). Assuming that Q_A is the additional heat:

$$Q_A = Q_{HW}^{CSB} - Q_{HW}^{HX3} \qquad \textbf{Equation 4-3}$$

According to ASHRAE 90.1 standard [43], reheat is not permitted in a zone except if at least 75% of the energy comes from onsite recovery (including condenser heat). There is no specific provision concerning heating and cooling plants; the interpretation of the standard here is thus the following. The sum of the additional heat and the electric input

of the two pumps used to operate the heat recovery loop should not exceed 25% of the building's reheat demand.

$$Q_A + (P_{P5} + P_{P6}) \leq (1 - X)Q_{HW}^{CSB},$$

where X = 0.75 and P only includes the heat recovery pumps.

For a given period of operation (e.g. day or week), if the mean measured effectiveness is greater than ε_{lim} it is assumed that the condition imposed by the standard is satisfied, and therefore the cleaning is not required. Under this approach, the heat-exchanger cleaning should be scheduled when ε becomes equal to ε_{lim}, the minimum effectiveness value allowing compliance with the standard which is for HX3:

$$\varepsilon_{lim} \geq \frac{1}{C_{min}^{HX3}} \frac{0.75Q_{HW}^{CSB} + P_{P5} + P_{P6}}{\left(T_{CNDs} - T_{HWr}^{HX3}\right)}$$

The solutions to Equation 4-5 are obtained by substituting the operation conditions, the constant quantities and eventually relations between some variables. Estimation could be obtained from design information, but the value of T_{HWr}^{HX3} poses a challenge since recirculation makes it dependent upon the flow. The Equation 4-5 can be compared to the effectiveness corresponding to net-zero power recovered, or power balance. In that rather basic case, the limit is reached when the electric input exceeds the recovered heat transfer rate:

$$\varepsilon_{Pmin} \geq \frac{1}{C_{min}^{HX3}} \frac{P_{P5} + P_{P6}}{\left(T_{CNDs} - T_{HWr}^{HX3}\right)}$$

If the heat transfer through HX3 is reduced by fouling, one consequence it the increase of the load on the cooling tower; the non-recovered heat must be rejected to the environment. To refine Equation 4-5, the power usage term could thus include the

additional electrical power usage at the cooling tower fan caused by the current value of ε. This would require the calculation of a reference, initial fan power usage in the absence of fouling, for the initial value of effectiveness ε_{cl}.

4.1.3. Limit performance based on cost

The heat recovery becomes a source of expense (instead of a savings opportunity) when its operation costs more than the usage of an alternative heat source. In this perspective, the minimal acceptable effectiveness can be expressed based on the cost balance. The information used in the calculation of the heat and electricity cost is summarized in Table 4-1.

Table 4-1 Information for operation cost calculation

Alternative heat source	Shell and tube steam/water heat exchanger, assumed ε=1
	Natural gas steam boiler, rated efficiency η=81.6%
	Heating value at sea level G=37.3 MJ/ m³= 10.35 kWh/m³ [chap 28 of ref 20]
Rate	$\$_{electricity}$= 4.41 ¢/kWh (Hydro-Quebec M-Rate) [52]
	$\$_{gas}$= 44.83 ¢/m³ (commercial customer, using 2010 average rate from [53])

The cost of producing complementary heat is calculated from the properties of the furnace, steam exchanger and fuel. Data from Table 4-1 are combined to obtain the cost per kWh of heat:

$$\$_{heat}\left[\frac{\$}{kWh}\right] = \varepsilon_{steamHX} \times \frac{1}{\eta_{boiler}} \times \frac{1}{G_{gas}\left[\frac{kWh}{m^3}\right]} \times \$_{gas}\left[\frac{\$}{m^3}\right]$$

$$\$_{heat}\left[\frac{\cent}{kWh}\right] = 1 \times \frac{1}{0.816} \times \frac{1}{10.35\left[\frac{kWh}{m^3}\right]} \times 0.4483\left[\frac{\cent}{m^3}\right] \qquad \text{Equation 4-7}$$

$$\$_{heat} = 5.31\frac{\cent}{kWh}$$

Cost balance corresponds to a condition where the cost of operating heat recovery is equal to the cost of simply heating the water by using natural gas. This is based on the assumption that heating might be required, and is available, at any time when the needs are not fulfilled by the recovery. The power demand of the recovery pumps and heating demand of complementary heat should cost less than the cost of heating provided only by natural gas. :

$$(Q_{CSB} - Q_{HX3})\$_{heat} + P_{pumps}\$_{electricity} \leq Q_{CSB}\$_{heat} \qquad \text{Equation 4-8}$$

After simplification:

$$P_{pumps}\$_{electricity} \leq Q_{rec}\$_{heat}$$

Expressed in terms of ε:

$$\varepsilon \geq \varepsilon_{minCost} = \left(\frac{\$_{electricity}}{\$_{heat}}\right)\frac{P_{pumps}}{Q_{HX3max}} \qquad \text{(from Equation 4-9)}$$

where $\$_{electricity}$ (¢/kWh) is the price of the electric energy and $\$_{heat}$ (¢/kWh) is for the thermal energy. The final formulation in terms of effectiveness and energy costs is:

$$\varepsilon_{minCost} \geq \frac{(P_{P5}+P_{P6})5.31}{Q_{max}^{HX3}4.41} = 1.2\frac{P_{P5}+P_{P6}}{Q_{max}^{HX3}}, \qquad \text{Equation 4-9}$$

It might not be desirable to reach such a trivial limit. The power and process industry introduced [54] the notion of optimal servicing cycle in its practice. It is especially important in installations where heat exchanger operation is continuous and when various

cleaning options (chemical versus mechanical) are available, as mentioned by Pogiatzis [31]. The goal is to identify the optimal cycle duration minimizing the total operation cost while maximizing the throughput, here the reheat energy. The cost of the cleaning operation and the detrimental effect of effectiveness losses are part of the required input data. This method however does not appear compatible with a HVAC case for numerous reasons such as the variation in the inlet temperatures and the discontinuous operation. Moreover, the optimization is based on increasing costs of the complementary heat, but as will be discussed below (5.5.1), the system actually sees no increase in Q_A.

4.1.4. **Other steady state formulations for Type A limits**

The limits introduced above were formulated in terms of ε. The conductance-area product UA and the fouling resistance R_f are derived from ε and alternative, complementary formulations of the limits are possible.

4.1.4.1. Conductance-area product (UA)

The function linking ε and the conductance-area product UA depends on geometry and flow arrangement. It involves an intermediate quantity, the number of transfer units (NTU). For counter-flow arrangements [51]:

$$NTU = \frac{1}{C_r - 1} ln\left(\frac{\varepsilon - 1}{C_r \varepsilon - 1}\right),$$
<div align="right">Equation 4-10</div>

where the capacity ratio $C_r = C_{min}/C_{max}$. The dimensionless number NTU allows for the calculation of UA as follows:

$$UA = C_{min} NTU.$$
<div align="right">Equation 4-11</div>

The overall value of UA depends on fouling, but also on the properties of the heat exchanger material as well as on the convection coefficients in each fluid, the latter being sensitive to the temperature.

4.1.4.2.   UA from the log mean temperature difference

The temperature difference between both inlet fluids can be seen as the driving force of the heat transfer through the heat exchanger. It is also possible to combine the four fluid temperatures into one quantity, the log mean temperature difference Δt_m, defined according to the flow pattern. The heat-recovery plate heat-exchanger HX3 is counter-flow and single-pass, thus:

$$\Delta t_m = \frac{\Delta T_1 - \Delta T_2}{\ln (\Delta T_1 / \Delta T_2)}$$

Equation 4-12

$$\Delta T_1 = T_{hot,in} - T_{cold,out} \qquad \Delta T_2 = T_{hot,out} - T_{cold,in}$$

Equation 4-13

This quantity provides an alternative way of computing UA.

$$UA = \frac{Q}{\Delta t_m}$$

Equation 4-14

In the case of HX3, only three out of the four temperatures are measured. An energy balance between streams is applied, with the hypothesis of no thermal inertia and no heat losses, to generate the missing temperature value ($T_{hot,out}$).

$$C_{HW}(T_{HWs}^{HX3} - T_{HWr}^{HX3}) = C_{CND}(T_{CNDs}^{HX3} - T_{CNDout}^{HX3}),$$

Equation 4-15

from where:

$$T_{hot,out} = T_{CNDout}^{HX3} = T_{CNDs}^{HX3} - \left(\frac{C_{HW}}{C_{CND}}\right)(T_{HWs}^{HX3} - T_{HWr}^{HX3})$$

Equation 4-16

4.1.4.3.　　Fouling resistance R_f

The conductance-area product UA is expected to change as fouling builds up. Knowing the heat exchange surface (A = 111 m²) and assuming that the initial heat transfer coefficient U in clean state is U_{cl}, the fouling resistance can be obtained from [50]:

$$R_f = \frac{1}{U} - \frac{1}{U_{cl}}$$

The value of U is obtained from measurements. In this study, we used as reference conditions, that is the clean state, the year of 2008. Hence, the closest equivalent value to $1/U_{cl}$ is the y-intercept in a time plot of $1/U$ for the reference season (2008). The R_f is then proportional to the time-varying term, if variation in the fouling resistance is present (not asymptotical).

By nature, the value of R_f at a given time is only a property of the fouling material thermal properties and layer thickness, unlike U and U_{cl} varying with the temperature and flow. Considering that flows are constant and that the temperature span in which each stream varies is relatively small (±10°C), it is assumed that the effect of temperature is negligible.

4.2. Process performance indices

This section presents a number of performance indices (PI) from their first-principle definition. They are used as metrics to provide an insight to the heat recovery process. They have the advantage of spreading the analysis beyond the limits of the heat exchanger, encompassing the processes linked together by heat recovery: cooling, heating

and pumping. In the current discussion, the term "Type B" is used for the benchmarks derived from this group of metrics.

4.2.1. Performance indices for the heat recovery process

Four performance indices are calculated in the current project.

Table 4-2 Heat recovery process performance indices

	Equation
Recovery Efficiency Ratio	$$RER = \frac{Q_{HX3}}{(P_{P5} + P_{P6})}$$
Compound Recovery COP	$$COP_{RE} = \frac{|Q_{HX3}| + |Q_{ev}|}{(P_{P5} + P_{P6}) + (P_{CW} + P_{CND}) + (P_{P7} + P_{P8} + P_{P9}) + P_{fan} + P_{CH}}$$
Relative Load	$$RL = \frac{Q_{HX3}}{Q_{HW}^{CSB}}$$
Recovery Ratio	$$RR = \frac{Q_{HX3}}{Q_c}$$

The RER is adapted from the rating of air-to-air heat-recovery systems; it was introduced in section 2.2.2, like the compound recovery COP_{RE}. For the calculation of the latter, only the electric input to pumps and fans of the group involved in the heat recovery process (first-to-start) are considered here. The back-up group, if active, is ignored. For instance, if chiller 2 is the first-to-start for this period, then $P_{CW} = P_{P2}$, $P_{CND} = P_{P4}$, $P_{fan} = P_{CT2}$ and $P_{CH}=P_{CH2}$. This index appears interesting since the decrease in Q_{HX3} due to fouling and its expected effect (higher cooling tower fan power usage) affect the PI by lowering COP_{RE}.

The Relative Load (RL) and Recovery Ratio (RR) are simply the heat rate through HX3 divided by the re-heat needs for the first, and the available heat from the condenser for the second.

The power input (P) of fans and pumps is obtained from specification sheets in the case of constant speed motors. For variable drives, it is possible to use monitored relative frequency drive (%VFD) to obtain a power value in the absence of power measurement from pump affinity laws [51].:

$$P = \left[\frac{(\%VFD/100)RPM}{RPM_{design}}\right]^3 P_{maxFan} \qquad \text{Equation 4-18}$$

where, RPM is the rated rotational velocity in revolutions per minute, RPM_{design} is the design revolution velocity and P_{maxfan} the fan full capacity (kW).

4.3. Inverse benchmark development

The question of the training set for benchmark development must be addressed. As inverse benchmarks and models, they are defined, or trained, based on operation data. A complete season is theoretically the ideal set, since it is representative of all the possible operation conditions. For practical reasons, such a large set may not be available; a one-month set is thus tested too. The benchmarks obtained from seasonal and monthly sets are compared to one another.

For the Type B benchmarks, inverse models are developed. The PI value is obtained from its definition (Table 4-2). It is then mimicked by a linear parametric model. Given the inputs x, y, and z, such a model takes the form presented in Equation 4-19. The fifth term takes into account colinearity between x and y if present; the sixth is for second-order dependence.

$$PI = a + bx + cy + dz + exy + fx^2 + \cdots \qquad \text{Equation 4-19}$$

The goal is to solve for the parameters (a, b, c, …) through ordinary least square (OLS) calculation. The selection of the regressors (x, y, z…), is supported by understanding of the process and statistical tools (covariance, p-statistic, t-statistic). It can thus be seen as a gray-box inverse model. For the same selection of regressors and terms, different training sets will generate slightly different parameter values, thus different benchmarks.

The internal performance of a model can be analyzed through the coefficient of determination; a perfect fit leads to $R^2 = 1$, whereas the absence of correlation is equivalent to $R^2 = 0$ [23]. For a linear fit, R^2 is:

$$R^2 = \frac{\sum_{i=1}^{n}(\hat{y}_i - \bar{y})^2}{\sum_{i=1}^{n}(y_i - \bar{y})^2},$$ Equation 4-20

where y_i is the individual observation, $\bar{y}$ is the mean value of the n observations and $\hat{y}_i$ is the individual value predicted by the model. For a n points sample, the normalized version of the coefficient of determination R^2 is used if the number of parameters (k) is higher than two.

$$\overline{R^2} = 1 - (1 - R^2)\frac{n-1}{n-k}$$ Equation 4-21

For a given PI model, the benchmarks obtained from the various training sets can thus be compared based on $\overline{R^2}$. Another interesting criterion for model evaluation is the root mean squared error [23], the RMSE, measuring the precision of the model:

$$RMSE = \sqrt{\left(\frac{\sum_{i=1}^{n}(y_i - \hat{y}_i)^2}{n-k}\right)}$$ Equation 4-22

The benchmark model leading to the highest RMSE is the least precise. The RMSE can also be used to assess the external accuracy of a model. In that case, the remaining sample is compared against the predictions from the benchmarks.

5. Analysis of measurements

This chapter first presents the sensors and their precision (5.1). The generic description section (5.2) includes mean seasonal values. Observations on the time behaviour are presented. Significant co-dependences are also described. The key aspects of heat recovery are then introduced: effectiveness, UA and R_f are discussed in 5.3, heat transfer through the heat exchanger in 5.4 and the sources of additional heating in 5.5.

The addition of the Genome building and new equipment to the CSB hydronic loops in 2011 involved major modifications to the plant loads, especially those related to the heating water. For this reason, the data is fractioned into two subsets, 2008-2010 and 2011-2012; the first is analyzed in this chapter while the latter is presented in Appendix B.

5.1. Precision and uncertainty

According to standards such as the IPMVP [15], ASHRAE standard 14 [55] or ASHRAE guideline 2-2005 [56], a field data (x) must be presented with the corresponding uncertainty (U_x), a two-digit value bearing the same dimensions as x and denoted by the symbol plus-or-minus ($\pm$). Uncertainty has two components: the bias error (B_x), which is not affected by the number of readings, and the random component (Ru_x):

$$U_x = \sqrt{B_x^2 + (Ru_x)^2}$$ **Equation 5-1**

Coleman [57] recommends, in the absence of any information on meter precision, to use one half of the smallest digit of digital displays as bias. It is then assumed to correspond to the 95% confidence interval recommended in HVAC [56]. This applies here for

instance to the power usage of the chillers; a recording of 579 kW for chiller 1 is interpreted as $P_{CH1} = 579.00 \pm 0.50$ kW.

Sensor specifications are available for temperature and flow sensors installed in the plant as well as for the portable flow-meter used in 2008 and 2012 [47]. They are summarized in Table 5-1. When uncertainty reported by the manufacturer is presented as a global quantity, like for the first two sensors, Coleman [57] recommends applying it entirely as bias component.

Table 5-1 Precision of temperature and flow meters

Sensor	Rated precision	Calculation
Endress + Hauser Electromagnetic Flow meter Promag 50W 50w2h-ul0a1ra0b1aa/DM-1	0.5% + 1mm/s	$B_V = 0.005V + V_{min}$ **Equation 5-2** V is the measured flow (L/s) and V_{min} is the flow corresponding to 1 mm/s velocity
Siemens building technologies Temperature sensor 544-577 rtd 1000 ohm platinum -40-240F	0.3 + 0.005T °C	$B_T = 0.005T + 0.3$ **Equation 5-3** T is the measured temperature (°C)
Controlotron Strommeter ultrasonic portable flow-meter model 1010WDP1	Bias: • 0.5% of calibratable accuracy • zero drift <15 mm/sec Random : 0.15% repeatability	$B_V = 0.005V + V_{min}$ **Equation 5-4** $Ru_V = 0.0015V$ **Equation 5-5**

Sensors from Table 5-1 have a precision varying with the magnitude of the measured quantity. The following example illustrates the use of the Controlotron on the cold stream reaching heat exchanger HX3. The diameter of the pipe is 20.3 cm (8 in) and the reading is 107.2 L/s. The minimum fluid velocity in mm/s is calculated from:

$$V_{min} = Fluid\ velocity \ \times pipe\ section = \frac{1mm}{s}\left(\frac{\pi(20cm)^2}{4}\right) = 0.032 \text{ L/s} \quad \text{\textbf{Equation 5-6}}$$

$$B_V = 0.005 \times 107.2 + 0.032 = 0.57 \quad \text{(from Equation 5-2)}$$

During the measurement campaign of 2012, the display flickered of ~0.5 L/s during all readings. This effect is considered here as a random component, and adds up:

$$U_V = \sqrt{0.57^2 + (0.50)^2} = 0.75 \text{ L/s (according to Equation 5-1)}$$

Finally, $V_{HW}^{HX3} = 107.20 \pm 0.75\ L/s$. The same reasoning was applied to other values resulting into Table 5-5:

Table 5-2: 2008 Measurements and precision on constant flow pumps

Item	Pump Tag	Diameter at measurement point	Flow (L/s)	Uncertainty (L/s)
CH water pump	P1, P2	25.4 cm (10 in)	86.75	0.90
CND pump	P3, P4	30.5 cm (12 in)	110.00	1.25
HX3 (CND) pump	P5	20.3 cm (8in)	60.00	0.59
HX3 (HW) pump	P6	20.3 cm (8in)	107.20	0.75

Unless stated otherwise, the symbol $\pm$ in the current document refers to the uncertainty on the value. The random component of Ru_x is considered zero for the 15-minute recordings. The total uncertainty is calculated based on the above or on error propagation. In that case, the uncertainty on a quantity (y) derived from measurements (X_1 X_2… X_i) combines the error contribution from each input. The generic formulation suggested by [15, 23, 56, 57 and 58] is, for the bias component:

$$B_y = \sqrt{\sum_{i=1}^{n}\left(\frac{\partial y}{\partial X_i} B_{Xi}\right)^2} \qquad \text{Equation 5-7}$$

This is an approximation assuming uncorrelated inputs with independent bias; correlations among inputs are usually neglected in engineering analysis [58].

5.2. Generic description

The current study focuses on the heat recovery performed on the condensers loop during chilled water production by the plant. For the recorded period, the combination was

observed to be systematic: if a cooling group (chiller, cooling tower and pumps) is started, the recovery system is activated.

Figure 5-1 presents the moment and duration for each chilled water production event on a common monthly view; each solid bar corresponds to an event. April and May are typical of discontinuous chilled water production in shoulder seasons. The longest event corresponds to Chiller 2 (gray) operated from mid-June to the mid-August 2008, with Chiller 2 (black) added in peaks.
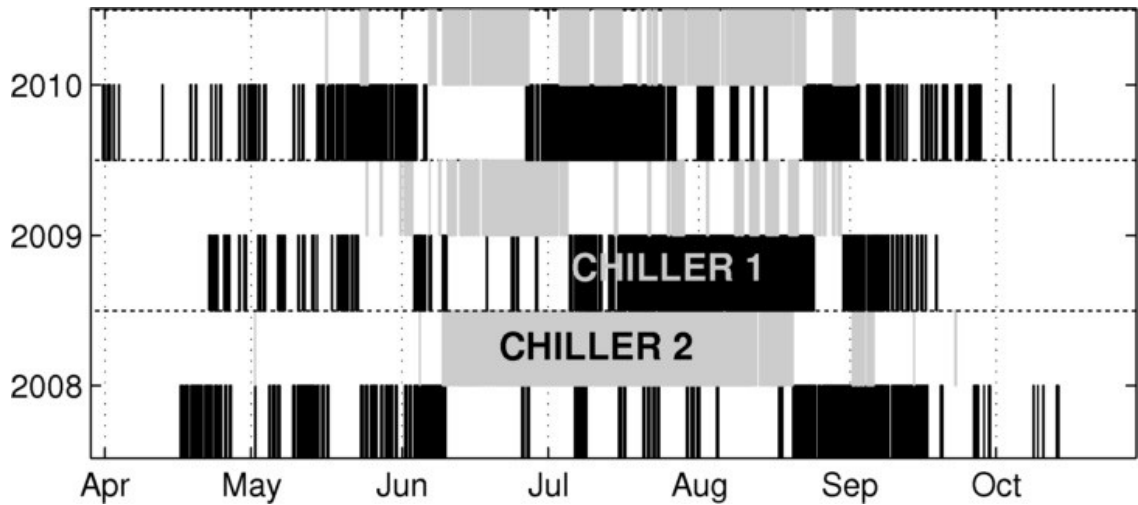
Figure 5-1 Operation pattern for the cooling groups, 2008-2010

Table 5-3 summarizes the duration of operation of the heat recovery system and chillers over the chilled water production seasons of 2008, 2009 and 2010. The duration associated with HX3 corresponds to the total number of operation hours for the heat recovery process. This number is inferior to the sum of the hours of operation for CH1 and CH2 because they operate in tandem (simultaneously) in a certain proportion of the season.

Table 5-3 Description of the operation

	2008			**2009**			**2010**		
	CH1	CH2	HX3	CH1	CH2	HX3	CH1	CH2	HX3
Total (h)	1457	1685	2914	1600	883	2136	1849	1448	2656
Total plant (h)	2954 h			2207 h			2702 h		
tandem (%)	9.2%			14%			23.7%		
Number of events	64	29	63	60	38	77	64	36	78
Short events (<24h)	53	22	47	53	31	66	51	22	59

5.2.1. Constant speed pumps

Flows of constant speed pumps were first measured in September 2008, then in October 2012 with the same equipment and methodology. When applicable, the sensors were put in the same location on the pipe. The N/A values for 2008 flows are the consequence of maintenance operations ongoing in the plant at the time of measurements, making one group non operable.

Table 5-4 Water flow rate for constant speed pumps

Item	Design L/s	2008 measurement L/s	2012 measurements L/s
Chilled water pumps			
P1	72.6	N/A	72.50 ± 0.86
P2		86.75 ± 0.90	71.50 ± 0.86
Cooling tower pumps, value used for condenser flow			
P3	131.5	N/A	110.3 ± 1.3
P4		110±1.2	117.0 ± 1.3
Heat exchanger 3			
P5 (CND)	107.3	60.00 ± 0.59	37.80 ± 0.53
P6 (HW)	107.3	107.25 ± 0.75	105.00 ± 0.74

The heat exchanger HX3 was designed for equal flows on each side, but is operated differently. As seen in Table 5-4, a significant reduction (~30%) in flow occurred on the condenser side of HX3 between 2008 and 2012, which corresponds to the flow driven by pump P5. The hypothesis can be made that this flow reduction is caused by fouling. This stream is exposed to outdoor air which carries various contaminants such as pollen or

dust. The heating water side of HX3, circulated by P6, is a closed loop and was not as significantly affected. The cooling tower flows (P3, P4) changed moderately while the chilled water flow (P1, P2) was reduced by ~17%. This diminution is probably linked to the major modification in the hydraulics following the addition of the Genome building to the CSB loops in 2011.

The flow values for 2008 listed in Table 5-4 are used in the analysis for the 2008-2010 period, and they are considered constant. Section 5.3.3 discusses the impact of this decision on the analysis of HX3.

5.2.2. Measurements of relevant variables during chilled water production

Table 5-5 presents the average values and standard deviation (S) for relevant variables. The sample used for Table 5-5 considers only the periods during which heat recovery and chilled water production was active based on the ON-OFF states of the components. The samples include start-up points.

The chiller power input was not available in 2008. The heating water flow rate on Monday to Thursday morning was not recorded from 2008 to the fall of 2011.

Table 5-5 Mean and standard deviation during chilled water production

Variable	unit	2008		2009		2010	
		Mean	S	Mean	S	Mean	S
Toa	°C	21.6	4.8	22.5	4.5	23.2	4.8
RH	%	42	23	40	22	42	23
V_{CHW}^{CSB}	L/s	86	18	91	23	100	26
T_{CHWs}^{CSB}	°C	7.03	0.69	7.12	0.30	7.07	0.41
T_{CHWr}^{CSB}	°C	11.0	1.8	11.5	1.5	11.4	1.5
V_{HW}^{CSB}	L/s	42.4	8.3	46	7	52	8
T_{HWs}^{CSB}	°C	32.2	1.8	31.8	1.6	30.7	1.4
T_{HWr}^{CSB}	°C	29.6	1.3	29.1	1.2	28.2	1.1
T_{cs}^{CH1}	°C	32.4	2.0	33.2	1.9	32.3	1.5
T_{cr}^{CH1}	°C	28.3	0.52	28.3	0.5	28.36	0.44
T_{evs}^{CH1}	°C	6.78	0.52	6.75	0.41	6.8	0.5
T_{evr}^{CH1}	°C	10.4	1.9	11.2	1.6	11.1	1.5
P_{CH1}	kW	NaN	NaN	303	94	288	80
$VFDT_{CT1}$	%	41	16	43	14	47	17
T_{cs}^{CH2}	°C	33.3	1.7	33.1	1.6	32.4	1.3
T_{cr}^{CH2}	°C	28.50	0.45	28.52	0.45	28.50	0.35
T_{evs}^{CH2}	°C	6.73	0.32	6.73	0.28	6.74	0.42
T_{evr}^{CH2}	°C	10.9	1.3	11.0	1.4	11.3	1.4
P_{CH2}	kW	NaN	NaN	292	85	297	77
$VFDT_{CT2}$	%	42	12	47	15	55	20
T_{HWin}^{HX3}	°C	31.1	1.7	30.6	1.7	29.5	1.3
T_{HWout}^{HX3}	°C	32.0	1.8	31.5	1.9	30.4	1.4

The measurements generally display a normal, symmetrical, distribution. The exceptions are the presented below:

1. The relative humidity in the outside air is of asymmetrical distribution (non-gaussian), a large proportion of measurements are in the range 15% to 23%.
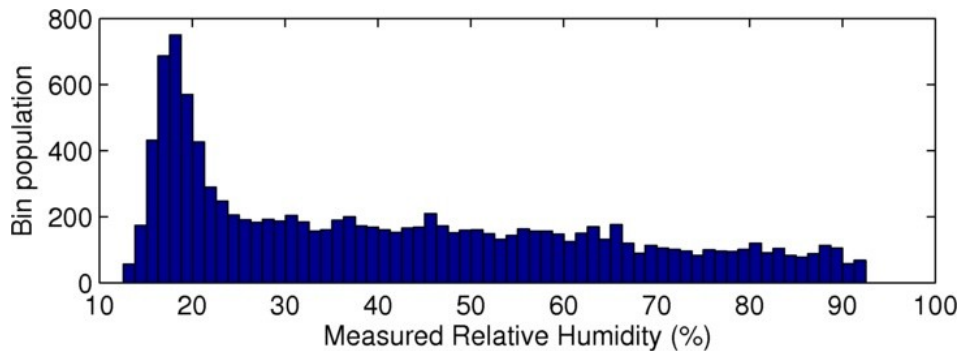

Figure 5-2 Histogram of relative outdoor air humidity for 2008

2. The chilled water flow distribution has two lobes (Figure 5-3), due to the fact that the flow is maintained by either one or two constant-speed pumps.
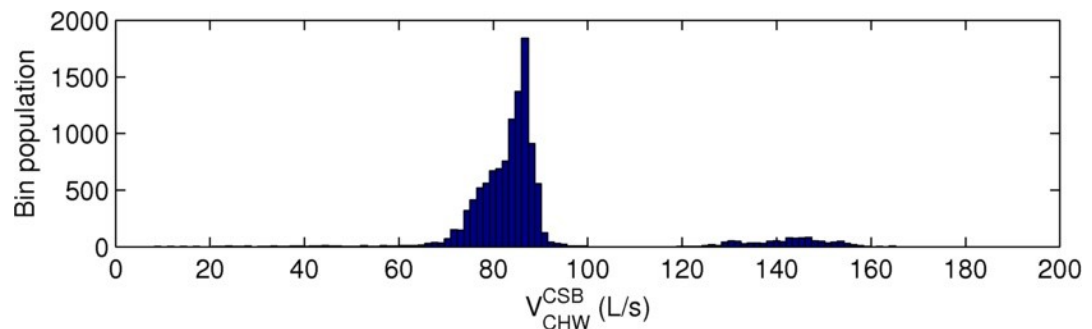
Figure 5-3 Histogram of CSB chilled water flow rate for 2008

The peak value for each lobe is not equal to the measured value for the corresponding pump established in 2009 [47]. Various reasons explain this. First, flow is measured at the CSB level whereas the loop also provides for another building. Second, two pumps operated in parallel do not generate a total flow equal to twice the effect of only one of them [26]. Finally, it was observed that the flow-meter records a small non-zero value when the pumps are OFF. This can be considered here as part of the instrument's bias (-0.23 L/s).

3. The measurement for the heating water variable speed pumps (VFD) are discontinuous, assuming values over defined ranges. This is due to the sensitivity limit programmed in the logger (not updating measurement if change is < 10%).

4. The cooling tower fans do not operate in the range of VFD =1% to VFD =29%, but all values from 30% to 100% are possible. The distribution is thus atypical.

5.2.3. Heat transfer rates and loads

For each stream, the mean temperature (T_{avg}) is calculated from:

$$T_{avg} = \frac{|T_{in} - T_{out}|}{2}$$

Equation 5-8

49

Season	Seasonal T$_{avg}$ of the water streams (°C)						
	CH1ev	CH2ev	CSB CHW	CH1c	CH2c	CSB HW	HX3 HW
2008	8.58	8.79	9.03	30.39	30.92	30.92	31.57
2009	8.98	8.87	9.31	30.74	30.82	30.47	31.04
2010	8.92	9.00	9.25	30.33	30.44	29.46	29.97

Table 5-6 summarizes the season-averaged mean water stream temperatures for the evaporators, the chilled water loop, the condensers and heating water loop and the cold side of the heat exchanger. The properties ρ and heat capacity c$_p$ are calculated at each point for the stream mean temperature.

The Table 5-7 presents the stream temperature differentials (T$_{diff}$), all in absolute value. The temperature differential is the difference between the inlet and outlet fluid temperature for a given stream.

Table 5-7 Mean temperature differentials

Season	Seasonnal T$_{diff}$ for the water streams (°C)						
	T_{diff}^{CH1ev}	T_{diff}^{CH2ev}	$T_{CHW\,diff}^{CSB}$	T_{diff}^{CH1c}	T_{diff}^{CH2c}	$T_{HW\,diff}^{CSB}$	T_{diff}^{HX3}
2008	3.60	4.13	4.00	4.09	4.84	2.62	0.87
2009	4.45	4.29	4.38	4.87	4.61	2.68	0.93
2010	4.31	4.52	4.37	3.93	3.89	2.42	0.94

As T$_{diff}$ is a derived quantity, Equation 5-7 is applied to the calculation of its uncertainty. The bias uncertainty at the mean stream temperature (Table 5-6) for 2008 is obtained from Equation 5-3.

$$B_{Tin} = B_{Tout} = 31.57 * 0.005 + 0.3 = 0.46°C$$

And applying Equation 5-7:

$$B_{T_{diff}^{HX3}} = \sqrt{\left(\frac{\partial T_{diff}^{HX3}}{\partial T_{in}}\right)^2 (B_{Tin})^2 + \left(\frac{\partial T_{diff}^{HX3}}{\partial T_{out}}\right)^2 (B_{Tout})^2}$$

$$B_{T_{diff}^{HX3}} = \sqrt{(1)^2 (0.46)^2 + (-1)^2 (0.46)^2} = 0.65°C$$

It is worth mentioning that the bias uncertainty on temperature measurements is conservative; although the sensor displays up to the second decimal, the rated precision is fifty times wider. The temperature differential measured at HX3 is nevertheless larger than its bias uncertainty (0.87 ± 0.65 °C) and therefore statistically significant. The use of a temperature bias more coherent with the display (second decimal) would result into a B roughly ten times smaller. The rated bias is however used below.

The heat transfer rate is another derived quantity. The error takes the following form:

$$B_Q = \sqrt{\left(\frac{\partial Q}{\partial V}\right)^2 (B_V)^2 + \left(\frac{\partial Q}{\partial T_1}\right)^2 (B_{T1})^2 + \left(\frac{\partial Q}{\partial T_2}\right)^2 (B_{T2})^2 + \left(\frac{\partial Q}{\partial \rho}\right)^2 (B_\rho)^2 + \left(\frac{\partial Q}{\partial c_p}\right)^2 (B_{c_p})^2} \quad \textcolor{blue}{\textbf{Equation 5-9}}$$

$$B_Q = \sqrt{(\rho c_p \Delta T)^2 (B_V)^2 + (V\rho c_p)^2 (B_{T1})^2 + (-V\rho c_p)^2 (B_{T2})^2 + (V c_p \Delta T)^2 (B_\rho)^2 + (V\rho \Delta T)^2 (B_{c_p})^2}$$

Here is an example of uncertainty calculation of heat transfer rate at condenser for the mean daily values on 2008-07-15.

$V = 110.0 \pm 1.2$ L/s $= 0.110 \pm 0.001\ 2$ m³/s

$T_1 = 29.00 \pm 0.44°C$ and $T_2 = 32.00 \pm 0.46°C$ (bias evaluated from Equation 5-3).

The water properties ρ and c_p are evaluated at the mean stream temperature $T_{mean} = 30.50 \pm 0.65°C$. Using the upper and lower bounds of the mean temperature to estimate their variation:

ρ=995.59 ± 0.28 kg/m³ and c_p = 4.178 000 ±0.000 097 kJ/kg.

After numerical substitution in Equation 5-9:

$$B_Q = \sqrt{1.6E08(0.0012)^2 + 2.1E05(0.44)^2 + 2.1E05(0.46)^2 + 1.9(0.28)^2 + 1.1E05(9.7E - 05)^2}$$

$$B_Q = \sqrt{224 + 4.2E04 + 4.2E04 + 0.15 + 0.001} = 292 \; kW \qquad \text{Equation 5-10}$$

The two last terms of Equation 5-10 should be ignored, which is equivalent to assuming water properties are absolute values. The first term, caused by bias on flow, is also very small compared to the contribution of the temperature bias. Finally, the rate is (from Equation 5-1)

$$Q = V\rho c_p(T_2 - T_1) = 1372.65 \; kW$$

With the appropriate formulation: Q_c = 1370 ± 290 kW.

The evaporator and condenser loads as well as the heat exchanger heat transfer rate were calculated using Equation 2-1. The flow measurement performed on the chilled water loop was used for Q_{ev} calculation (see justification in 5.2.5 and Figure 5-14); when two chillers are in operation, the total measured flow is divided evenly between the evaporators.

The mean seasonal loads and heat rates are summarized in Table 5-8 along with the corresponding calculated uncertainty. Here too, the reduction of the temperature bias to the second digit would result into dividing the total error by roughly ten.

Table 5-8 Mean heat transfer rates during chilled water production

item	Seasonal mean heat flow rate (kW)								
	2008			2009			2010		
Q_{ev}^{CH1}	1200	±	160	1530	±	170	1460	±	160
Q_{ev}^{CH2}	1400	±	160	1470	±	170	1540	±	170
Q_{CHW}^{CSB}	1500	±	180	1720	±	190	1890	±	210
Q_{c}^{CH1}	1870	±	310	2220	±	290	1800	±	290
Q_{c}^{CH2}	2200	±	310	2110	±	290	1780	±	290
Q_{HW}^{CSB}	440	±	110	490	±	120	500	±	140
Q_{HW}^{HX3}	390	±	290	410	±	290	420	±	280

The Figure 5-4 presents the averaged value of the cooling and heating loads for the plant as a function of the outside air temperature; error bars are not presented, for clarity. The plant cooling load corresponds to the instantaneous sum of the evaporator load of the chillers. The outdoor air temperature T_{OA} definitely has impact on cooling loads whereas the re-heat load appears to be relatively constant

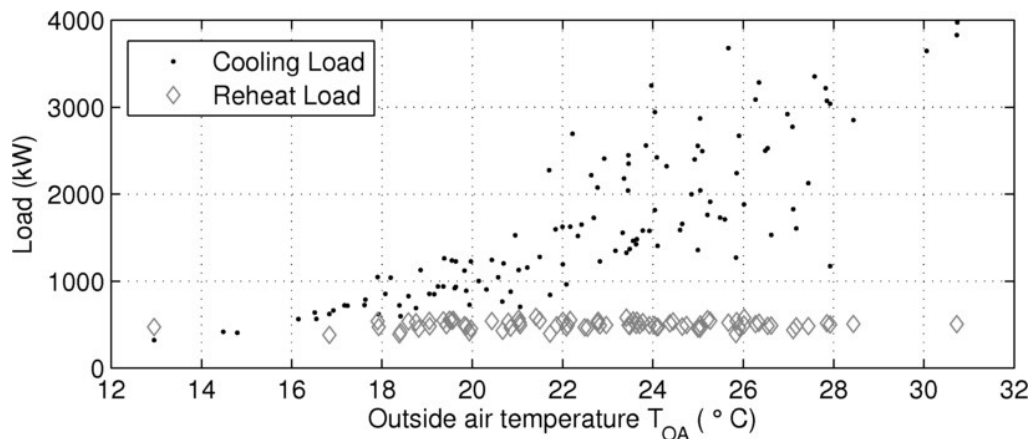Figure 5-4 Mean daily loads vs outside air temperature, 2010 season

The heat flow rate observed through HX3 is generally inferior to the corresponding heating load of the CSB; for instance, the mean $Q_{HW}^{CSB} = 440\ kW$ while the mean $Q_{HW}^{HX3} = 390\ kW$ in 2008. It is likely that pumping, through friction effects, adds a certain quantity of heat accounting for a significant proportion of the observed difference.

The difference between the recovered heat and the HW load is further investigated in section 5.5.

5.2.4. Time behavior of temperature and heat flow rate

On Figure 5-5, one event of chilled water production and heat recovery is illustrated through the temperature of fluids for May 17th 2008, a day from the shoulder season. The bias uncertainty bands of roughly 0.46°C for all measured temperature were not included to simplify visualization. Temperatures are not constant; the condenser water supplied temperature is affected by cooling load variations.
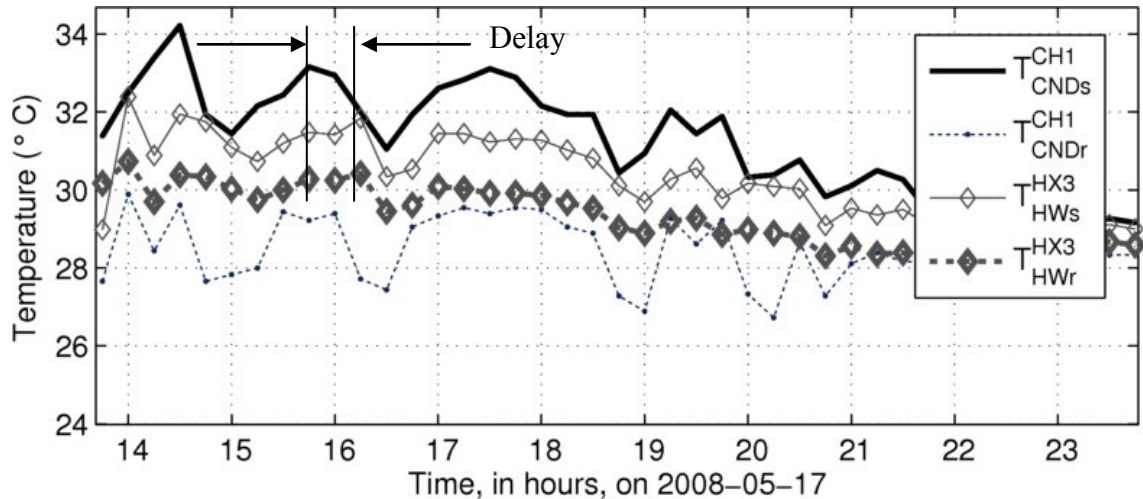
Figure 5-5 Time-variation of water temperatures during chilled water production

A delay of one to two 15 minute time-steps is often noticed before the temperature fluctuation on the condenser fluid is propagated on the HW side (Figure 5-5). The reason might be a combination of the following factors. The length of piping between the condenser outlet and the HX3 inlet may delay the occurrence in HX3 of a change occurred at CNDs. Second, there may be some thermal inertia.

Since there is no measurement point at the inlet of HX3 on the condenser side, the temperature value used for calculations is the one measured at the condenser outlet

(T_{CNDs}^{CH1}), upstream of pump 5 (Figure 3-3). When operated in tandem, the chillers share the load evenly. In Figure 5-6, CH2 is the first-to-start; when adding CH1 at high cooling load, there is a rapid drop of fluids temperature of roughly 4°C within less than one hour (Figure 5-6). As a counterpart, the interruption of CH1 involves the temperatures to rise rapidly. The effect is transferred to the HW side of the heat exchanger
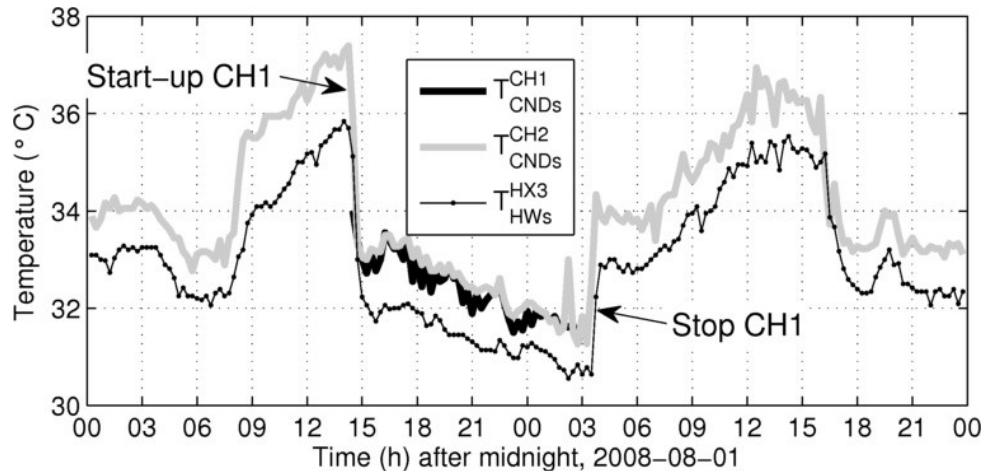

Figure 5-6 Effect of chiller operation mode on temperatures for August 1rst 2008

The time variation in temperatures does not systematically mean that steady-state approximation is impossible; the classical ε-NTU approach for instance depends on temperature differentials, which appear to be relatively stable.

The temperature differential (T_{diff}), which corresponds to the difference between the inlet and outlet temperature for a given fluid, is investigated below. All 2008 heat-recovery events were aligned on a common time-axis from their beginning (Figure 5-7). The mean value undergoes a relatively steep increase involving a sign change within the first two time steps, followed by stabilization (Figure 5-7 A). The dispersion of points decreases significantly within the first hour, as illustrated by the decreasing standard deviation

(Figure 5-7 B). The variations in T_{diff}^{HX3} should affect the ε, especially in the first hour of operation.
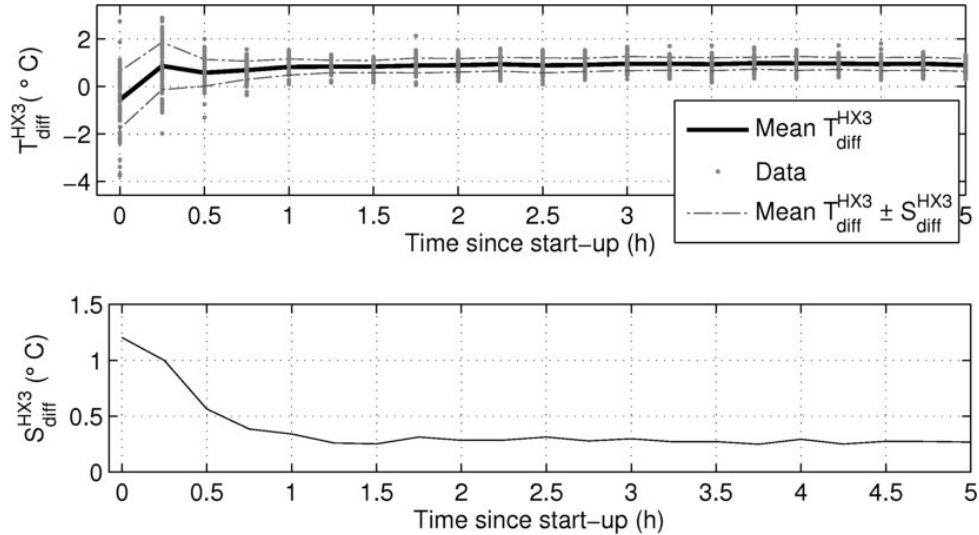
Figure 5-7 Time variation of (A) Mean T_{diff} and (B) S_{diff} for HX3 in 2008

The temperature differential was evaluated for the evaporator and the condenser. At the time-resolution available, it is not possible to identify a delay between the evaporator and condenser temperature variation for a given chiller. Figure 5-8 illustrates this for chiller 1 (T_{diff}^{CH1e}, T_{diff}^{CH1c}).
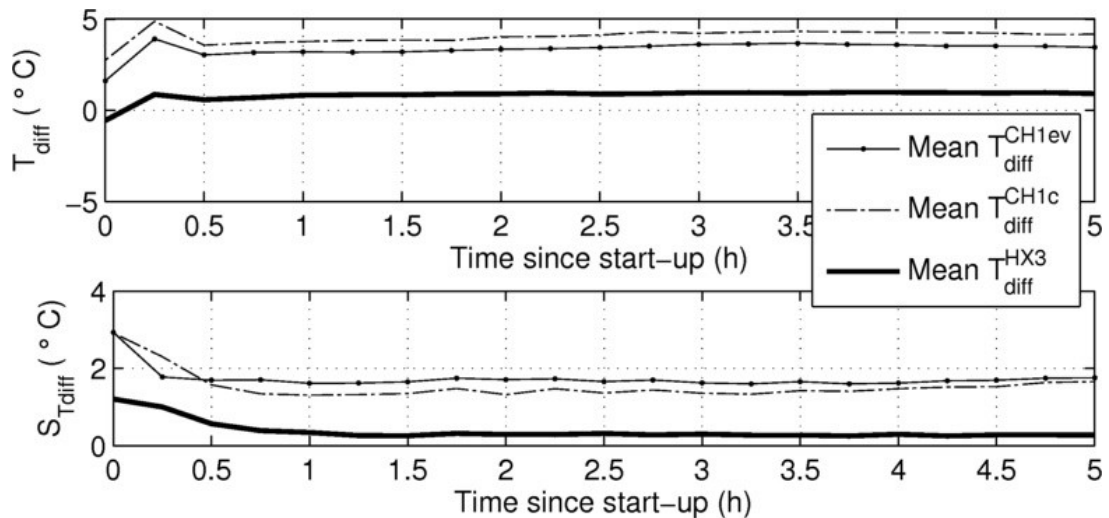

Figure 5-8 Time-variation of (A) mean T_{diff} and (B) S_{diff} for CH1 in 2008

56

A similar analysis was made for the last ten hours before turning OFF the chillers and interrupting heat recovery (not illustrated). No significant change in the dispersion (constant S) appears to be linked with stopping the process, from chiller as well as from heat-exchanger perspective.

A start-up effect followed by stabilization is however observed when considering temperature differentials. The use of quasi steady-state models might be possible after the stabilization; in other words the first few time-steps of all events should be considered transient. Visual inspection of Figure 5-8 allows for the distinction of the boundary between transient and quasi-steady state around one hour for chillers for HX3.

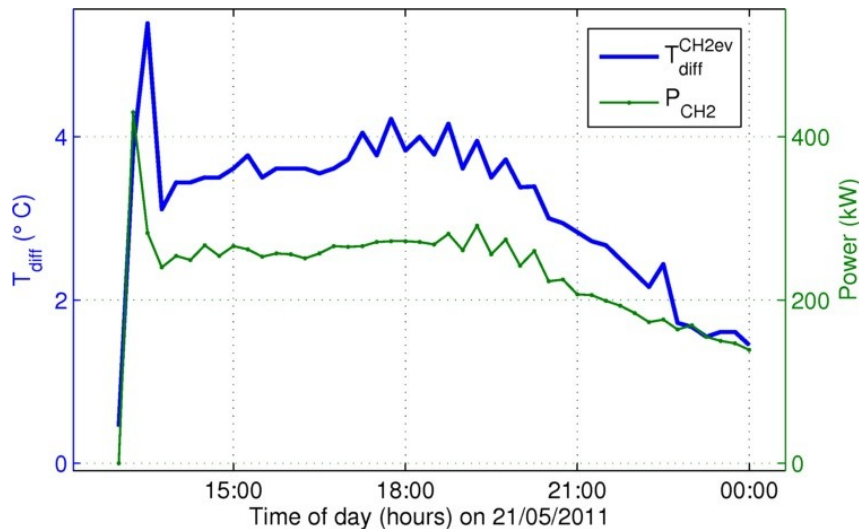**Figure 5-9 Time variation of T_{diff} and P_{CH2} during a chilled water production event**

An additional argument to separate data based on a distinct pattern at start-up arises from the corresponding electrical power input measured at the compressor (Figure 5-9). The shape of the temperature differentials and electric input are similar for a given chiller. A peak is present during the two or three first readings.

For the complete 2008 season, the points considered transient according to this criterion represents 2.6% of the total recorded time for chilled water production and heat recovery. The data filtered from the start-up points will be referred to as quasi steady-state (QuasiSS) from now on and no dynamic analysis will be performed.

5.2.5. Relevant co-linearities

The temperature of the water leaving the condenser is proportional to the cooling load measured at the evaporator, as illustrated in Figure 5-10 for the case of chiller 1.
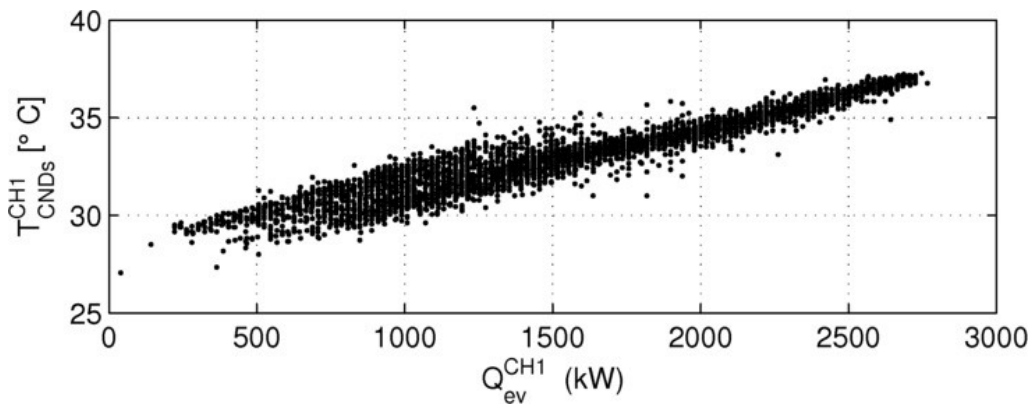
Figure 5-10 T_{CNDs} as a function of Q_{ev} for CH1, 2009 15-min QuasiSS data

The heat recovery process through HX3 is fed by only one condenser loop at a time. An important change in regime occurs when the plant goes from one to two operating chillers, a condition in which they share evenly the high cooling load. Since HX3 receives colder water from a condenser operated in tandem mode, the possible temperature gain is lower. As a consequence, the supplied reheat water temperature for the building decreases when both chillers are in operation (Figure 5-11). This transition occurs around 2600 kW of total cooling load as measured at evaporators.
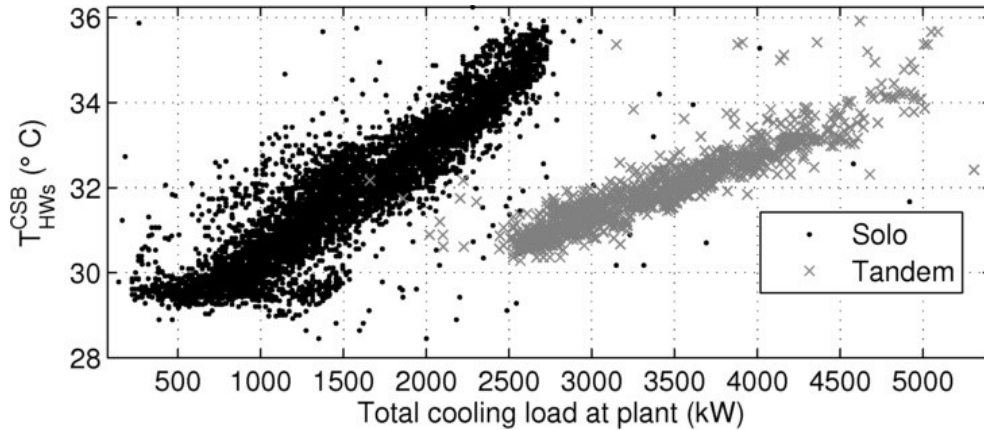
Figure 5-11 Building HW supply temperature as a function of cooling load

This observation suggests that heat recovery analysis in terms of total plant cooling load is less pertinent than simply focusing on the chiller providing for the heat recovery at a given time.

The co-linearity of all temperatures related to the heating water (HW) and their dependency upon the available condenser water temperature is to be mentioned. The variation of four temperatures as a function of T_{CNDs} is presented in Figure 5-12.
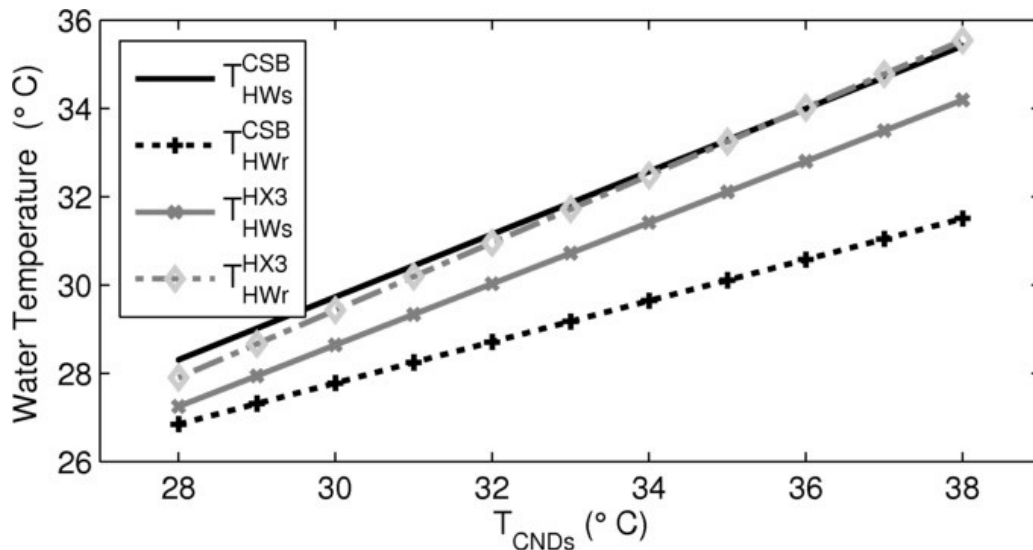
Figure 5-12 Heating water temperatures as a function of T_{CNDs}, 2009 15-min data

Figure 5-13 presents the filtered 2009 15-min flow measurements for the CSB heating water with respect to inlet temperature. This dependence is observed for all cooling seasons.
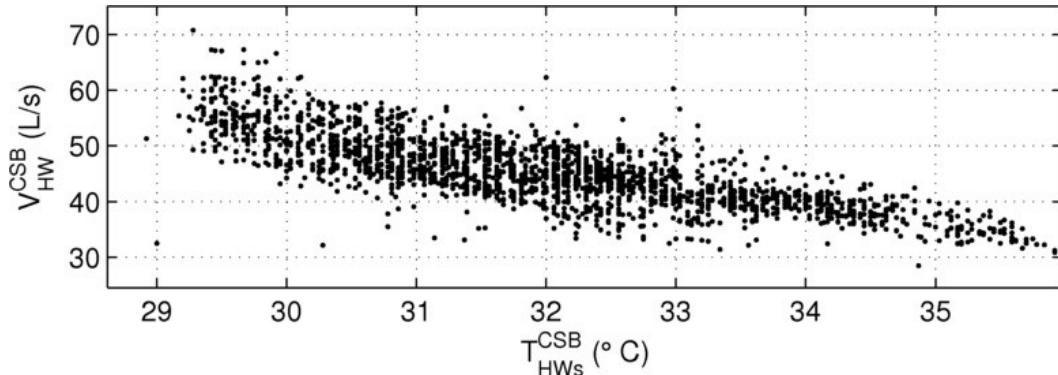
Figure 5-13 Heating water flow rate vs supplied temperature at CSB, 2009 15-min data

There is a flow measurement redundancy for chilled water. The available continuous flow measurement is performed on the CSB loop; it does not include the stream leaving for the AD (illustrated in Figure 3-2). The CSB building is however by far the main contributor to total plant load.
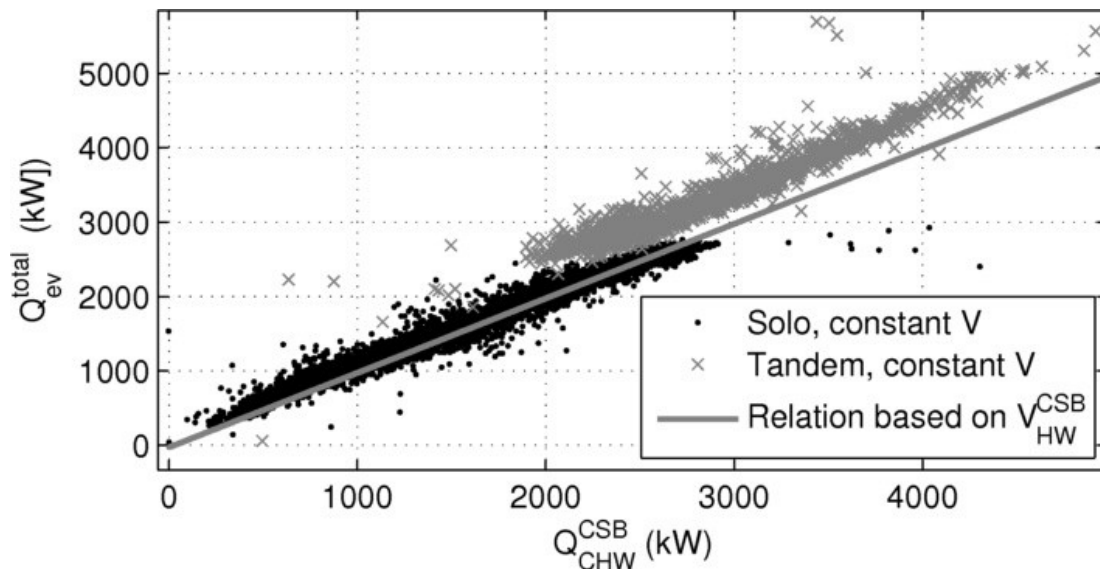
Figure 5-14 Total load at evaporator versus CSB cooling load, 2009 QuasiSS data

When only one chiller is in operation, the correlation between the plant evaporator load and building load (Figure 5-14) is directly proportional (slope = 1) with an intercept of -

29.4 kW for the 2009 Quasi SS dataset. This represents 2% of the average plant load in that mode and the value can be interpreted as the mean AD cooling load.

The difference is much larger (~500 kW or 30%) for the cases where chillers are operated in tandem due to the overestimation of the flow resulting from calculations based on the constant rated value. The measured flow recorded in the building is thus more precise (and exact) than the rated constant flow for load calculation and is thus preferred here.

The chiller power input (P) is measured for all seasons except 2008. This value is required to compute process-scale performance indices. In order to include the 2008 data in the analysis, a replacement P value is used. A linear parametric inverse model (Equation 4-19) of the chiller power usage in 2009 was developed to obtain P from data available in 2008.

The relative amperage (%RLA) measurement for the chillers is available for the whole three-years sample. Before 2009 P was generated by an equation system based on constructor data, %RLA and Q_{ev} was used [39, 47]. Here a stepwise OLS was applied to the following candidate regressors: RLA (%), Q_{ev}(kW), Q_c(kW), as well as second order and interaction terms (total of nine regressor candidates), using the complete 2009 QuasiSS, 15-min data as training sample. In the stepwise method, a term is added or removed if it improves the fit [23]. Despite the co-linearity in the regressors, the interaction terms did not improve the model significantly. No strong residual pattern was observed. It resulted into a four-parameter fit, Equation 5-11, valid for both chillers:

$$P_{CHmodel} = -19.4 + 4.24 RLA + 0.0166 Q_{ev} + 0.0187 Q_c \qquad \text{Equation 5-11}$$

For the Equation 5-11, $\overline{R^2}$=0.97, which means the fit is significant. Here, RMSE = 15.22 kW, from which the replacement value and precision on the model prediction are obtained based on [24]:

$$Y = Y_{model} \pm zRMSE$$ **Equation 5-12**

The factor z is defined by the confidence interval [23]. For two-sided normal distribution considering 95% tolerance, z = 1.96 in large samples (n>30). The t-statistic is used for smaller samples.

Finally, the chiller power model is:

$$P_{CH} = P_{CHmodel} \pm 30 \; kW$$ **Equation 5-13**

5.3. Experimental value of effectiveness (ε)

This section uses daily averaged measurements, which are more compatible with steady state. In the averaging process, only the quasi steady-state points were retained (see 5.2.4). The shoulder seasons involve processes that can be active a few hours each day. It could happen that the day-time average includes 24h of recording while the chiller only operated during six hours. To rigorously combine averaged versions of the measured quantities, the same sample - here the six hours of chilled water production- must be used. For this reason, process-specific daily averages were calculated.

According to the ASHRAE guideline 2.2005 [56], a set of repeated measurements can be considered a multi-sample experiment. In that perspective, the individual readings used to

compute, for instance, the mean daily value allow the determination of a random uncertainty component based on statistics:

$$Ru_x = z \frac{S_x}{\sqrt{n}}$$

In Equation 5-14, S_x is the standard deviation in the sample, n the number of readings. A random uncertainty component of zero was assigned to the 15-min time step data. The data-reduction process generating the mean daily values however results in the determination of a random component for each one-day sample. The uncertainty calculation is illustrated here for a day in the peak season. The daily mean for the water temperature at the inlet of HX3 is based on 96 individual measurements and corresponds to 31.26°C with a standard deviation of S_T=1.15°C. The temperature sensor determines the bias component:

$$B_T = 0.005 \times 31.26 + 0.3 = 0.46\ °\text{C} \qquad \text{(based on Equation 5-3)}$$

The random component is calculated from S_T;

$$Ru_T = 1.96 \frac{1.47}{\sqrt{96}} = 0.23. \qquad \text{(from Equation 5-14)}$$

The total uncertainty on the daily mean value is obtained from:

$$U_T = \sqrt{0.46^2 + 0.23^2} = 0.51 \qquad \text{(from Equation 5-1)},$$

This results in the mean daily measurement of $T_{HWr}^{HX3} = 31.62 \pm 0.51°\text{C}$.

The calculation of the uncertainty on the experimental ε involves error propagation analysis. The general form for the ε of HX3 is:

$$\varepsilon = \frac{V_c(\rho c_p)_c(T_{co}-T_{ci})}{V_h(\rho c_p)_h(T_{ci}-T_{hi})} \quad \text{(from Equation 4-1)}$$

Values for the July 15th 2008 are used. The bias, presented between parenthesis (), is calculated from information available in Table 5-1.

- V_c = 107.25 (0.75) L/s, V_h=60 (0.59) L/s
- T_{ci} = 31.26 (0.46) °C, T_{co}=32.21 (0.46)°C and T_{hi}=33.82 (0.47)°C
- $k = (\rho\ c_p)_c/(\rho\ c_p)h = 1.003$ (no bias)

The numerical value of ε for these conditions is 0.822. The calculation of uncertainty on ε is based on Equation 5-7:

$$B_\varepsilon = \sqrt{\left(\frac{\partial\varepsilon}{\partial V_c}\right)^2(B_{Vc})^2 + \left(\frac{\partial\varepsilon}{\partial V_h}\right)^2(B_{VH})^2 + \left(\frac{\partial\varepsilon}{\partial T_{ci}}\right)^2(B_{Tci})^2 + \left(\frac{\partial\varepsilon}{\partial T_{co}}\right)^2(B_{Tco})^2 + \left(\frac{\partial\varepsilon}{\partial T_{hi}}\right)^2(B_{thi})^2}$$

After numerical substitution:

$$B_\varepsilon = \sqrt{(\sim0)^2(0.75)^2 + (\sim0)^2(0.59)^2 + (-0.47)^2(0.46)^2 + (0.87)^2(0.46)^2 + (-0.40)^2(0.47)^2}$$

$$B_\varepsilon = \sqrt{\sim0 + \sim0 + 0.05 + 0.16 + 0.04} = 0.49$$

A similar analysis is then performed for the random components of temperature values. (Ru_{Tci} = 0.23°C, Ru_{Tco}=0.26°C and Ru_{Thi}=0.31°C). The total random uncertainty on ε is Ru_ε=0.28. Finally, both contributions are summed according to Equation 5-1, resulting in the daily value: ε = 0.82±0.56, or a relative error of 68%. The bias-dominated error is a consequence of the high rated temperature sensor bias.

Despite filtering, some calculated ε values in 2008 are non-physical (>1); they are more common for samples including less than 24 hours, as illustrated in Figure 5-15 A. These incomplete sets are less numerous than true daily means, as described by the histogram of

Figure 5-15 B. Although their wider error-bars cover the physical range, it seems justified to ignore these values.
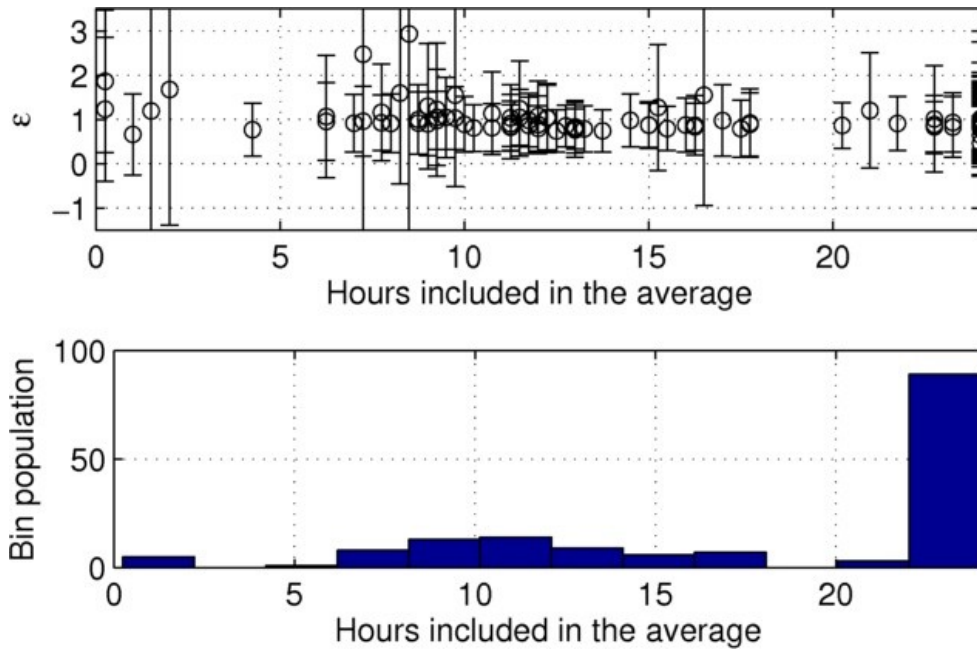
Daily mean values actually calculated from less than 12 hours of operation are rejected as well as non-physical ε. The resulting average seasonal values are summarized in Table 5-9:

Table 5-9 Mean annual effectiveness

YEAR	ε
2008	0.85 ±0.63
2009	0.76 ±0.51
2010	0.60 ±0.38

The mean daily filtered effectiveness as a function of time is plotted in Figure 5-18 for the three available years. The process is not active between November and April.
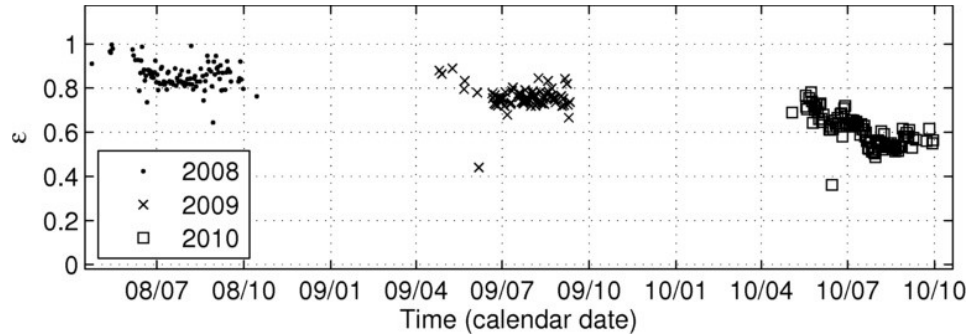
Figure 5-16 Evolution of mean daily ε over three years

Despite the wide error bars (not illustrated), a global decrease seems to be present. Seasonal patterns were also investigated. In Figure 5-17, the time-axis is the date in calendar days, within the chilled water production season.
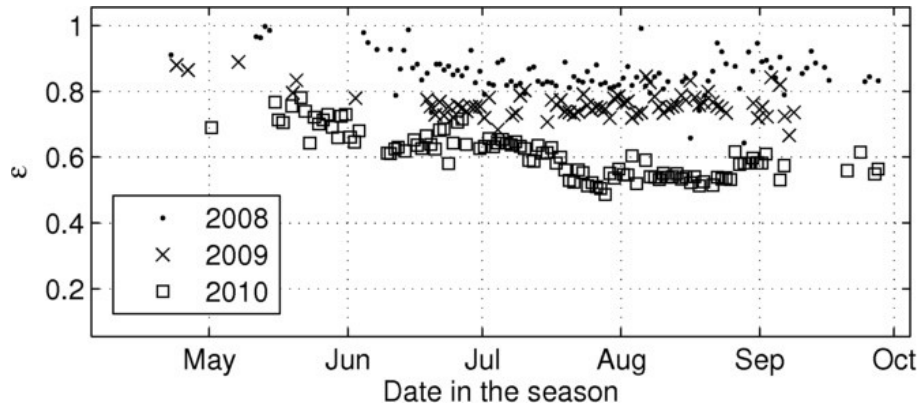
Figure 5-17 Evolution of mean daily ε over the season

For each season, the shoulder periods (May, September) show a slightly higher mean ε than the remaining data. It is likely due to the fact that the cooling load is then lower, which results in lower temperature for the condenser water. This makes the denominator smaller in the definition of ε (Equation 4-2). The same applies to weekend versus week-day values, generating oscillations in the daily average visible in the 2008 curve of Figure 5-17. For the peak season (mid-June to September), ε is relatively constant in 2008 and 2009. The 2010 season includes a decrease in July. It was not possible to link it to maintenance or changes in operation (no log is available).

66

The dependence upon the operation conditions throughout each season makes it hard to assess a *true* value for the effectiveness. For instance, the ε decrease observed in the first half of June 2008 (Figure 5-17) could have been incorrectly linked to fouling; but ε goes back to high mean values in September 2008. It appears that for the case study, a complete season of operation is required to determine the general pattern and the range of ε values.

The measurements show a significant decrease of ε over the three-year period, coherent with fouling build-up. It is interesting to mention that although several months passed between each season, the measured values show no significant gap at the transition. This indicates that the property does not change when the exchanger is not in operation
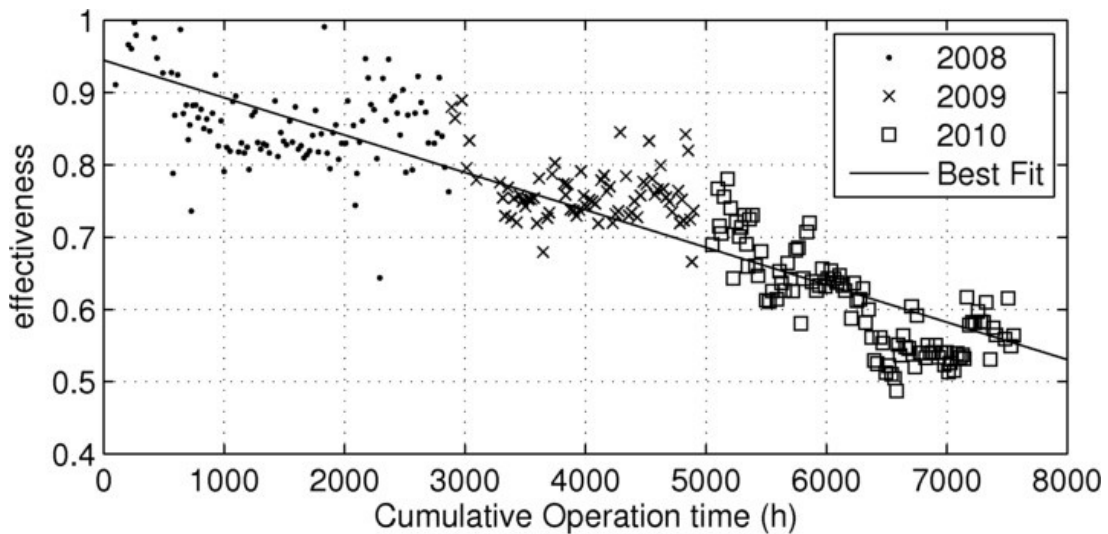
Figure 5-18 Mean daily ε as a function of the operation time, 2008-2010

The time dependence of ε in terms of calendar-day (Figure 5-18), $R^2=0.08$, is very poor. Hence, there is no significant time dependence of ε in terms of calendar days. Alternatively, since the heat recovery process is discontinuous, the ε can be expressed in terms of the cumulative sum of operation hours as a time-reference (Figure 5-18), in other words a time-frame specific to the heat exchanger operation.

It was possible to obtain a model of the variation of effectiveness ε as a function of the cumulative sum of operation hours. For the three-year period, $R^2=0.76$, which indicates that the variation of ε in terms of operation time is statistically significant. The fit is:

$$\varepsilon = 0.94 - 5.1 \times 10^{-5}h \qquad \text{Equation 5-15}$$

where h is the total number of operation hours for HX3.

It is worth mentioning that fit parameters (intercept and slope) require numerous points to reach stabilization. An ordinary least square regression was performed for the data set using an incremental approach. According to that method the sample size was incremented by adding chronologically all available points and performing OLS upon each addition. The parameters (slope and intercept) took roughly 3000h to stabilize (Figure 5-19), which corresponds to more than one season of operation.
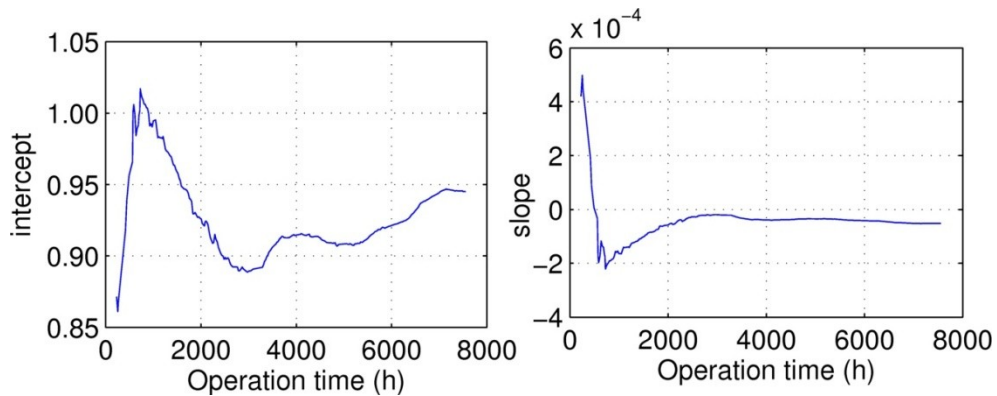
Figure 5-19 Stabilization of parameters for effectiveness-time fit

To complement the analysis of the fit of ε as a function of operation time, the R^2 and normalized RMSE (Equation 4-22) (CVRMSE), are used [23].

$$CVRMSE = \frac{RMSE}{\bar{y}} \qquad \text{Equation 5-16}$$

68
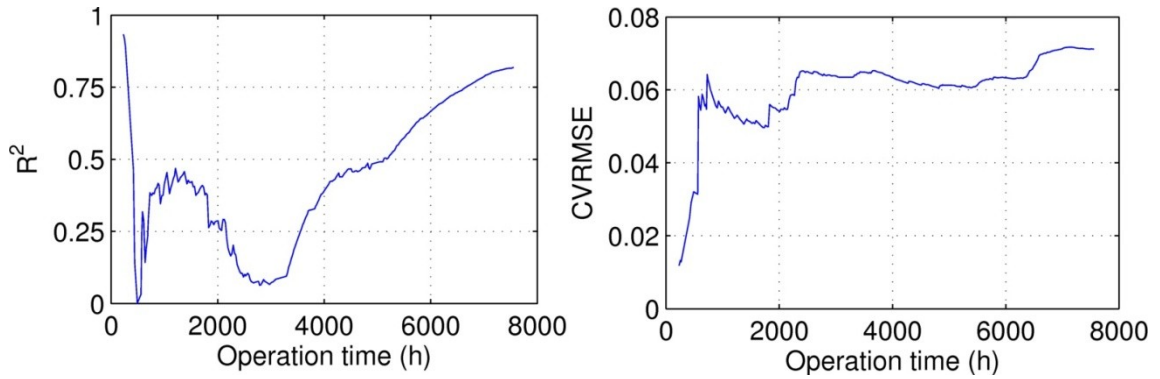
Figure 5-20 Statistical analysis of the effectiveness-time fit

The strong variation in R² in the 3000 first operation hours (Figure 5-20) confirm the impossibility to conclude after only one season (2008) that ε does decrease. Although the R² reaches the critical value of 0.75 around 6600 hours of recorded operation, the increase in error (CVRMSE) continued. The model error increases with the sample size.

5.3.1. Experimental value of UA

The value of UA as a function of ε was calculated for values representative of HX3 (Figure 5-21). Close temperature differentials (ΔT) correspond to high values for ε, which means high UA.
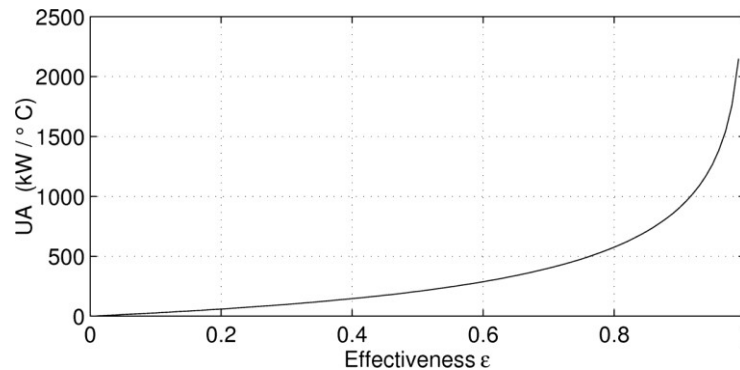
Figure 5-21 Dependence of UA on ε for HX3

The calculation based on log-mean temperature and ε-NTU lead to very similar results; discrepancies arise for limit cases where the ΔT are very close to one another, challenging the stability of Equation 4-12.

The ε-NTU method combines Equation 4-1, Equation 4-10 and Equation 4-11. Even for the daily averaged QuasiSS data, filtered from low reliability (<12hours of recovery for the day) and non-physical values of ε, the UA values are strongly dispersed, especially in 2008, as illustrated in Figure 5-22.
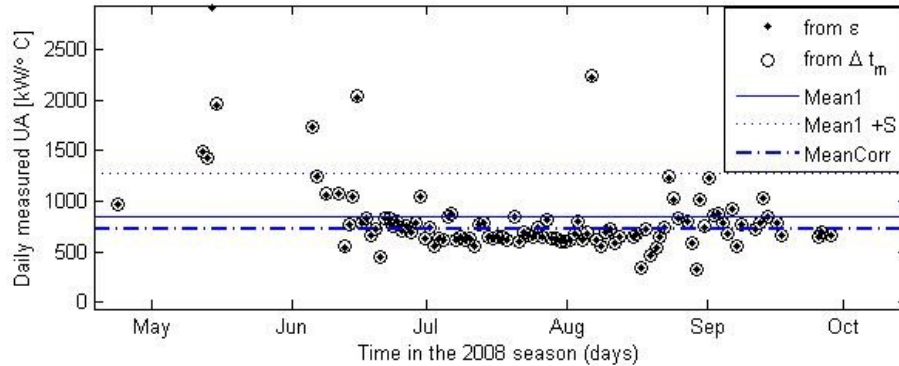
Figure 5-22 Mean daily UA through the 2008 season

After rejection of the points more than one standard deviation away from the mean, the corrected mean UA for the 2008 season becomes $UA_{2008MeanCorr}$= 720 kW/°C. The design UA for the heat exchanger is 882 kW/°C, based the design fluid temperatures and flows (Appendix A), and with glycol in the HW fluid. The seasons of 2009 and 2010 show a less dispersed UA, and no correction to the mean was performed.

Uncertainty calculations based on the partial derivative method for error propagation were made. The total error is very high; in Table 5-10, the total uncertainty on UA based on temperature measurement precise to the second decimal is also presented.

Table 5-10 Mean seasonal values for UA

Year	UA (kW/°C)	Using corrected bias error
2008	720 ± 1900	720 ±848
2008	490 ± 850	490 ± 383
2010	287 ± 340	287 ±130

The experimental uncertainty is outside acceptable bounds, even when using a more reasonable temperature bias. One reason is the random component, inherent to the

measured quantity, which remains significant. The simplified approach for error propagation presented in Equation 5-7 is apparently insufficient here. Additional terms taking variables co-linearity into account might be required. This advanced uncertainty approach, only briefly presented in [23] and [57], is beyond the scope here. Even in a paper discussing the uncertainty for heat exchangers in the nuclear plant industry [29], the authors did not use it. They mentioned 900% error was observed in some *in situ* experiments involving small temperature difference. The traditional error calculation was also considered invalid by Markovski [32].

The dispersion in the calculated values for UA (Figure 5-22) is however smaller than the calculated error. It will thus be assumed here that UA is valid, to allow R_f analysis. A seasonal variation is present: the measured UA in the peak season is lower than in the shoulder months. This is linked to the condenser water temperature, as previously observed concerning ε.
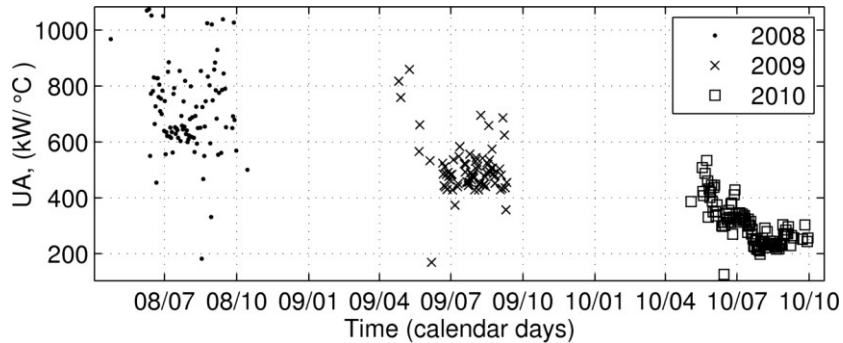
Figure 5-23 Evolution of the mean daily UA 2008-2010

5.3.2. Experimental value of R_f

A fit of 1/U as a function of the total number of operation hours was performed in order to identify the dependence and the intercept. The result is a statistically sound quadratic

fit ($\overline{R^2}$ =0.85, RMSE = 0.056) for which the intercept is $1/U_{cl}$=0.14°C·m²/kW. As mentioned in 4.1.4.3, this value is linked to the conductance-area product in reference state. The corresponding UA_{cl} =792 kW/°C, is coherent with the mean 2008 value. The resistance of the fouling deposit R_f, is calculated as follows:

$$R_f = \frac{1}{U} - \frac{1}{U_{cl}} \qquad \text{(from Equation 4-17)}$$

For the three-year sample, the experimental growth regime of R_f is:

$$R_f = \frac{1}{U} - 0.14 = 6.2 \times 10^{-9}h^2 \qquad \text{Equation 5-17}$$

where h is the total number of operation hours. The growth pattern of R_f as a function of operation time is presented for the filtered mean daily data in Figure 5-24.
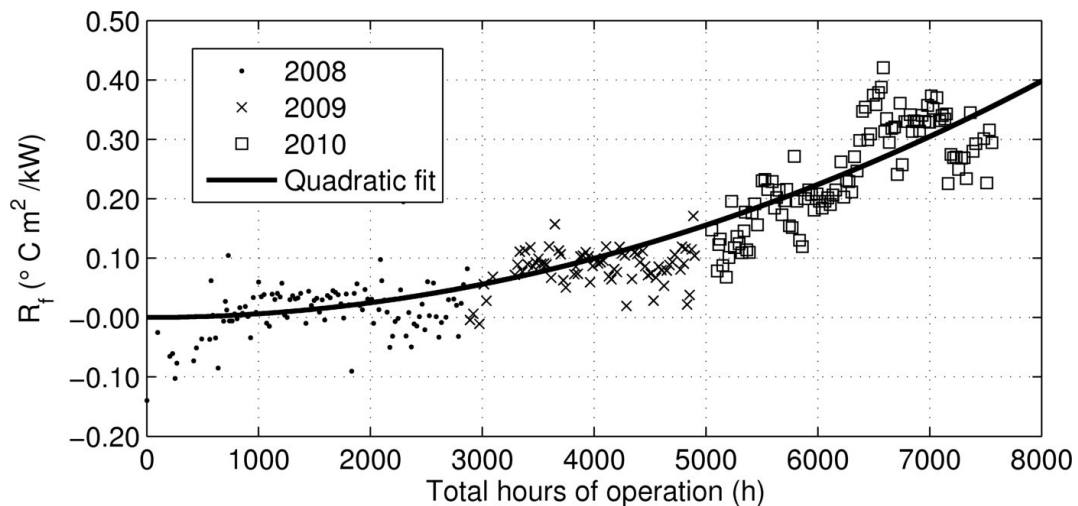
Figure 5-24 Fouling resistance as a function of the operation time

The measurements of 2008 alone do not confirm fouling build up. The main reason is the seasonal variation; the variation of the U_{cl} term caused by temperature fluctuations is not smaller than the effect of fouling. The hypothesis of negligible temperature effect (done in section 4.1.4.3) was thus incorrect. Normalizing for T (as Kuhlmann [27]) would

reduce oscillations in Figure 5-24, but this is not possible without detailed manufacturer data.

It is likely that the fouling was developed mostly on the condenser side because of atmospheric particles brought from the cooling towers. This is coherent with the significant flow loss observed for the corresponding stream over the 2008-2012 period (Table 5-4). Although the heat exchanger was designed for equal flow rates, the condenser-side flow rate is smaller than the heating water flow rate. Low flow favors fouling by reducing shear stress between plates [54].

Genić [33] listed various fouling resistance values used for the design of plate heat exchanger such as R_f between 0.035 and 0.045 °C·m²/kW per side for treated cooling tower water. The HX3 reached total values five times larger by the end of the 2010 season.

5.3.3. Considering flow variation between 2009 and 2012

On September 25th, 2008, a flow of 60.00±0.59L/s was observed on the condenser-side of the heat exchanger whereas on October 11th 2012, the value had decreased to 37.80±0.60 L/s. The growth of the fouling layer is assumed to be the cause of this flow reduction. The variation is assumed to have taken place linearly, like the variation on ε.

In section 5.3, it was observed that fouling takes place during the operation of the heat exchanger. Unfortunately, the total number of operation hours between the two measurements is unknown because of the several lost weeks of recording in 2011. The flow decrease is thus applied linearly in terms of calendar days. Using this corrected flow

73

value has impact on the calculated ε. This, in return, affects the time-variation of the total

thermal resistance 1/U.
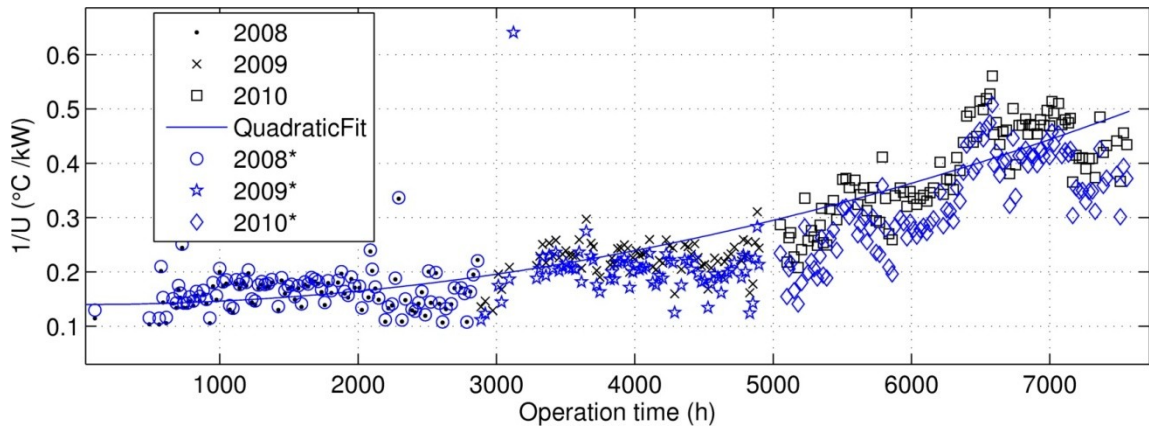
Figure 5-25 Thermal resistance vs operation time (constant and corrected CND flow)

The difference between the as-used and the corrected values is illustrated in Figure 5-26

for the ε and R_f.
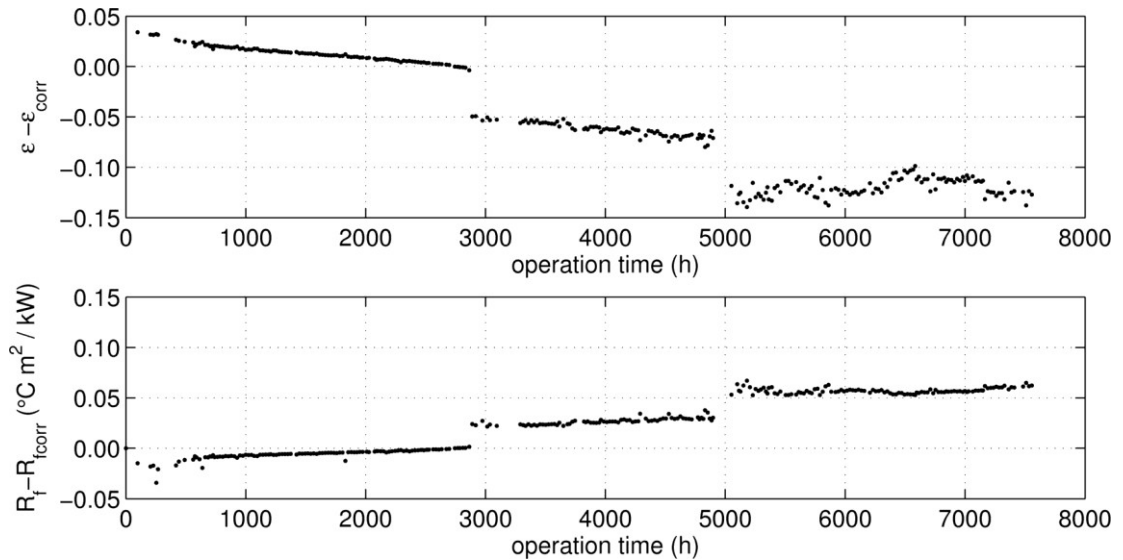
Figure 5-26 Effect of flow correction on the time-variation of ε and R_f

The use of a linear distribution of the flow decrease is the only possible approach here,

although the discontinuities in Figure 5-26 show it to be moderately appropriate. It

however allows for an estimation of the effect of flow variation. In general, it appears

that the hypothesis of constant flow leads to an over-estimation by 0.10 of the mean

74

seasonal ε in 2010, leading to an underestimation of 0.05 °Cm²/kW for R_f. This is roughly 15% of the assumed value for ε, and 25% for R_f. With this in mind, the constant value is however used for the remaining of the analysis.

5.4. Heat flow rate through the heat exchanger

The discussion on uncertainty from section 5.3.1 also applies here. The mean daily heat transfer rate through HX3 on the heating water side assuming constant flow rate from constant speed pumps is plotted as a function of the total hours of QuasiSS operation for the seasons 2008-2010 in Figure 5-27. A seasonal shape is present, with globally lower recovery rates in shoulder months. This is likely explained by a combination of the following: 1) lower reheat needs and 2) lower cooling loads resulting in lower temperature for condenser water T_{CNDs}. A split in two parallel subsets is visible in 2008 an 2009. It corresponds to week-end (lower) and weekdays (upper) operation of HX3.
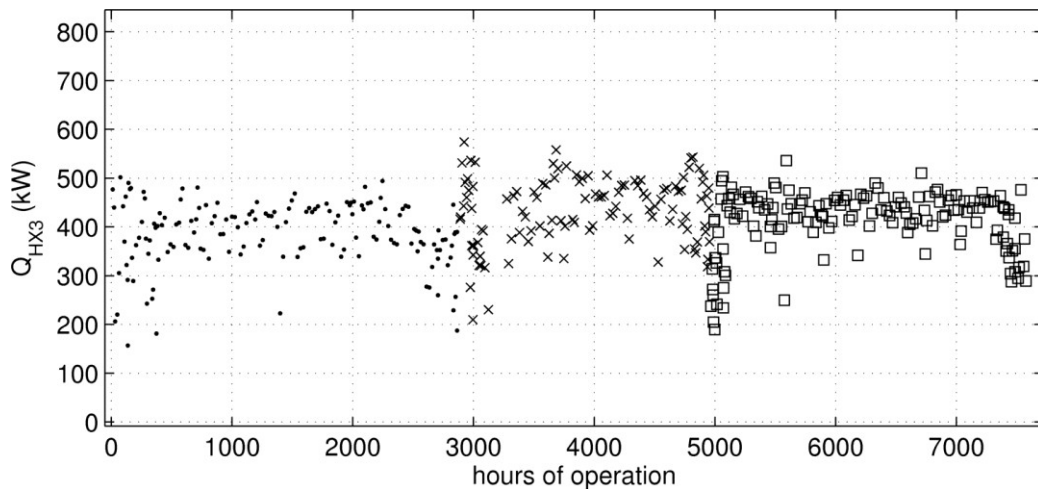
Figure 5-27 Heat transfer rate through HX3 as a function of operation time

As the total number of operation hours increases, the mean heat flow rate through the heat exchanger was expected to decrease due the fouling layer growth confirmed by the analysis of ε. The Figure 5-27 however indicates the opposite: there is a slow increase of

Q_{HX3} in time. The phenomenon is likely to be caused by a variation of the driving force: the temperature difference at inlet for both streams.

The Figure 5-28 shows that the maximum possible thermodynamic heat transfer rate through HX3 (Q_{max} defined in Equation 4-1) is not constant from a year to another. On the contrary, the daily mean increases. As a consequence of growing Q_{max}, the decay in heat exchanger heat-transfer properties (or R_f increase) did not result into lower heat recovery rate.
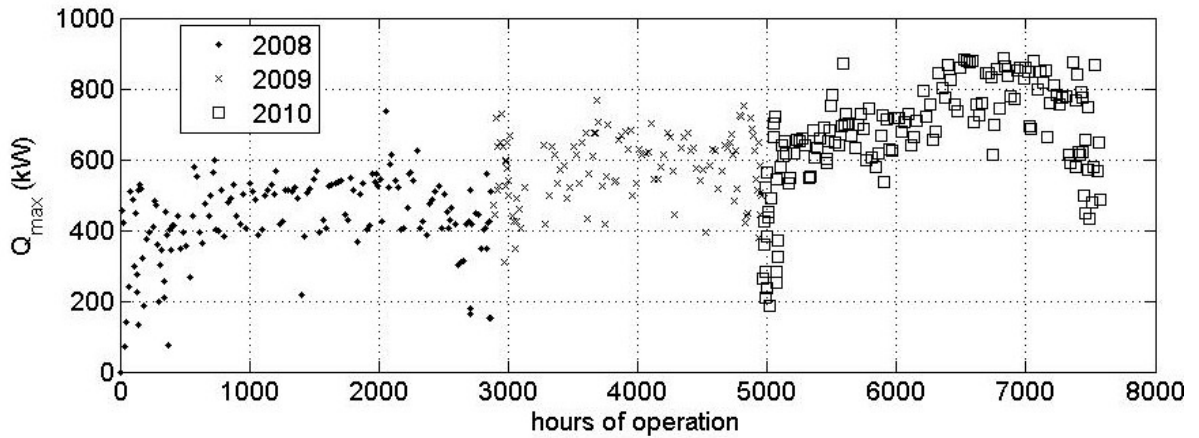
Figure 5-28 Maximal thermodynamic heat transfer rate at HX3 vs operation time

Both inlet temperatures of the fluids entering the exchanger tend to decrease over the 2008-2010 seasons, but the returning heating water does so four times faster than the condenser water as seen in the corresponding regression models (Table 5-11).

Table 5-11 Linear models for temperature, 2008-2010 daily data

$T_{HWr}^{HX3} = 31.2 - 2.78 \times 10^{-4}h$
$T_{CNDs} = 32.6 - 6.27 \times 10^{-5}h$

The decreasing tendency in the temperatures on the HW occurs above the set point of 28°C [49]. The whole loop operates at decreasing mean temperatures as the fouling builds-up, but the re-heat needs are still fulfilled and the minimal temperature is never reached, at which additional heat from HX2 would be required.

76

This critical limit could have been eventually observed in subsequent seasons, but these conditions did not occur. The modifications to the building and plant that took place in 2011 make the determination of this limit irrelevant here, but the use of regression models combining T_{HWr}^{HX3}, T_{CNDs} and ε could have allowed it.

5.5.Additional heat for the re-heat process

The notion of complementary or additional heat for the re-heat needs was introduced in section 4.1.2. It is obtained from Equation 4-3.

$$Q_A = Q_{HW}^{CSB} - Q_{HW}^{HX3} \qquad \text{(Equation 4-3)}$$

The result is plotted against the supplied temperature at HX3 in Figure 5-29 (only points averaged over more than 12h per day).
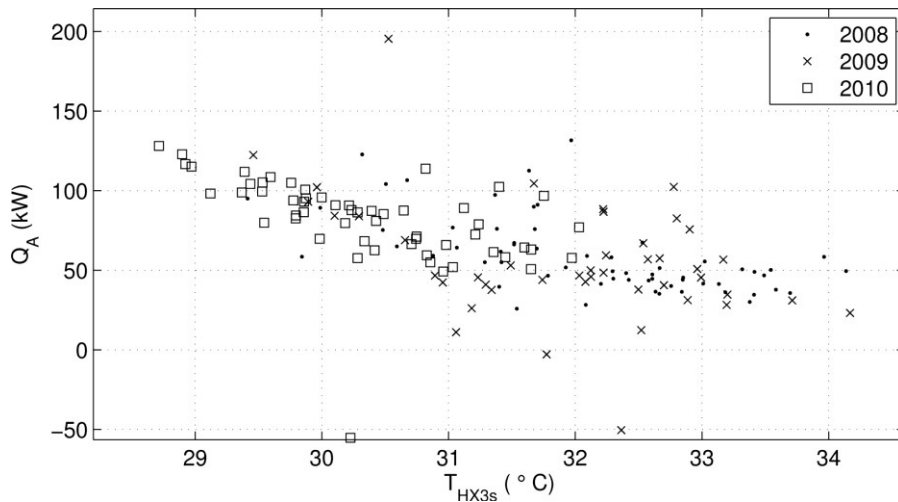
Figure 5-29 Additional heat as a function of outlet water temperature at HX3

A non-zero value for Q_A appears to be present in all the temperature range, decreasing to a relatively constant value of 40 kW as the water supplied by the heat exchanger HX3 reaches 31°C.

There is however no evidence as to the use of any additional heat in the re-heat process between 2008 and 2010. The plant operation sequence includes no automated action of the valves to HX2; after verification it appears they are acted upon manually in extreme cases only. The heat input described in Figure 5-29 is more likely an effect of the pumps: P6 between the outlet of HX3 and the main HW loop and the parallel variable speed pumps P7 P8 and P9 circulating the latter (Figure 3-2). The difference between the pump motor power (P_{motor}) and shaft power corresponds to losses susceptible of heating the driven fluid; an effect usually neglected [20]. The design information and manufacturer curves were used to obtain the efficiency η_P (ratio of shaft to motor power) at 2008 operation conditions for the concerned pumps.

Table 5-12 Pump parameters

Item	Design V / P (L/s / kpa)	Motor Power kW	η_P 2008
Pump 6 HX3, heating water side	107.25 / 179	30	0.82
P7 P8 P9 HW variable drive pumps Data for each	Max: 53.6 /657	Max = 56	0.76 at 100% speed 0.50 at 30% speed

The temperature rise from a centrifugal pump as a function of its mechanical efficiency is described in [59], from which the pump-related heat transfer rate can be calculated:

$$Q_{pumpHeat} = P_{motor} \frac{(1-\eta_P)}{\eta_P} \qquad \text{Equation 5-18}$$

According to this reasoning, P6 adds 6.5 kW to the stream. Each active HW pump will contribute between 1.5 and 18 kW depending on its operating point, based on Equation 4-18, Table 5-12 and Equation 5-18. The value of $T_{HWs}^{HX3} = 31°C$ corresponds roughly to 50 L/s in Figure 5-13; two HW pumps are required below this temperature.

The detailed analysis of heat input due to pumps as a function of recorded %VFD is beyond the scope here, but the general explanation is coherent with the greater Q_A observed at lower T_{HW}.

The general conclusion of this section is that although the building reheat demand at a given time is usually higher than the heat recovery rate through the heat-exchanger, the difference between the two quantities (Q_A) is not, strictly speaking, additional heat. It is generated by the operation of the circulation pumps, which are active by default. The total re-heat energy thus corresponds to recovered heat and by-effects at pumps.

The methodology introduced a limit ε defined according to an interpretation of the ASHRAE standard 90.1. The definition (Equation 4-5) was based on the existence of a Q_A provided by an alternative heat source. The analysis above invalidates the suggested limit.

5.5.1. System adaptation to degradation

Between 2008 and 2010, the effect of fouling was to gradually lower the temperature at the building inlet (5.4). The BAS could adapt to this degradation at HX3 by increasing the HW flow rate (see the temperature-flow correlation in Figure 5-30).
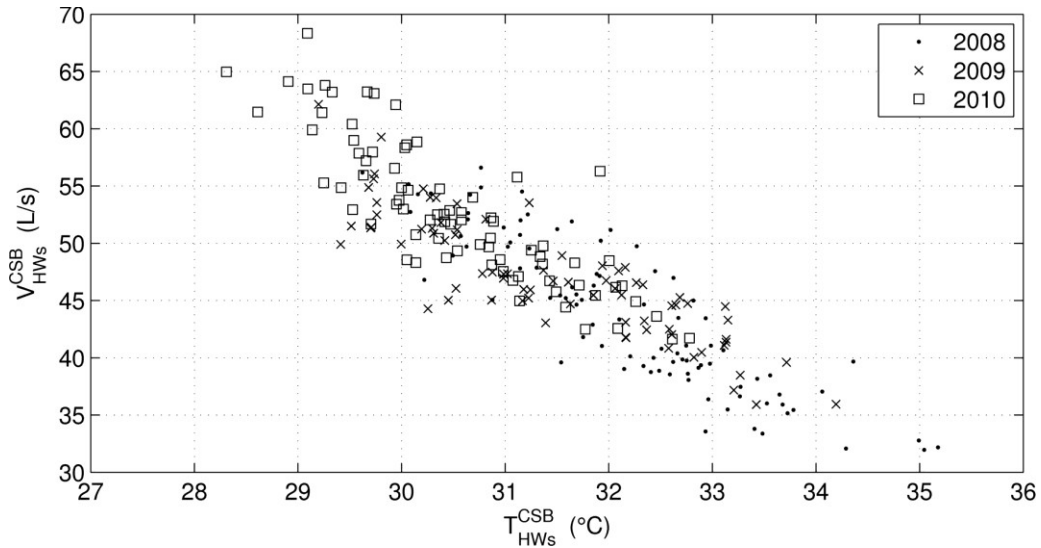
The mean values for the key quantities in the selected filtered set are summarized in Table 5-13. The heating water flow rate increase is the only detrimental effect associated to fouling actually observed in the system. The corresponding pump power usage was computed from measured drive data and Equation 4-18. The variation is very small.

Table 5-13 Mean QuasiSS seasonal values of key-quantities

YEAR	ε	Q_{HW}^{CSB} (kW)	Q_{HW}^{HX3} (kW)	T_{HWs}^{CSB} (°C)	V_{HW}^{CSB} (L/s)	P_{HW} (kW)
2008	0.86 ±0.63	453±54	402±153	32.23 ±0.49	42.1 ±1.6	28.0±2.0
2009	0.76 ±0.51	494 ±49	443 ±148	32.12±0.50	44.9±1.5	29.5±1.2
2010	0.61 ±0.38	512±49	437±112	30.67±0.50	53.0±1.6	29.6±1.2

Note that since the heat flow rate from the condenser loop to the HW did not decrease, the fouling of the heat exchanger did not have impact on the cooling towers. If, as was expected, the fouling had impaired the heat transfer, the load reduction at tower level would have become smaller. This would have involved a gradual increase in tower fan usage for a given condenser load.

5.6. Observation on the chillers

It was observed that the chillers behavior changed in the last week of May 2010. It takes the form of a reduction of the heat transfer at condenser Q_C (kW) for a given load at evaporator (Figure 5-31). Because no modification in the Q_{ev} and P dependency was observed, this indicates the condenser water loop is likely the cause.
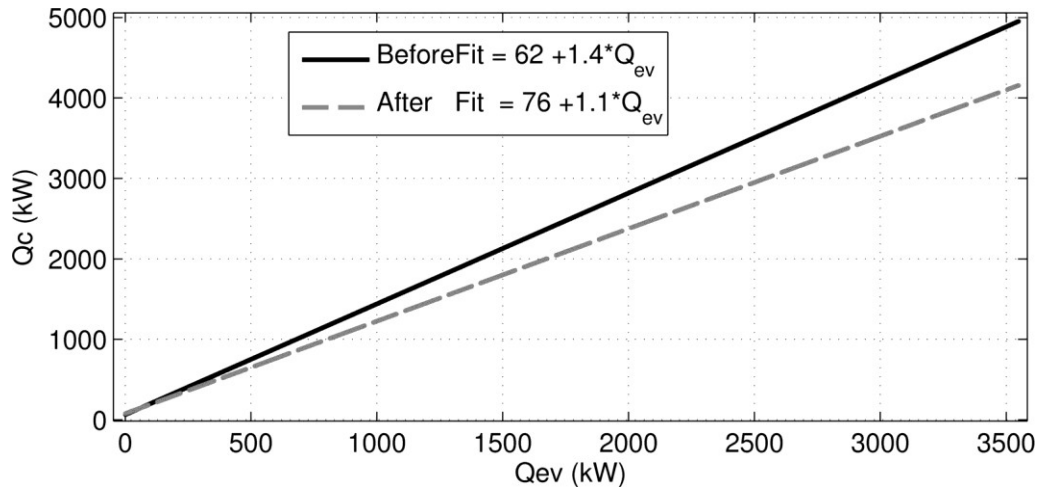
Figure 5-31 Curve rotation 2009-2010, Chiller 1

Increasing the flow would have as a consequence a lower mean temperature differential in the condenser water streams. The 2010 mean differentials (Table 5-7) are lower than those of 2008-2009.

Because these observations could not be validated, the flow values used in the analysis are the ones measured in 2008. It seemed pertinent to mention these facts in the case the data is used in other projects with a focus on the chillers.

6. Ongoing Commissioning

The previous section presented the thermal analysis of the heat recovery process and equipment. The current section presents the application of the proposed ongoing commissioning method to the heat recovery system. It presupposes an access to measured data allowing for the calculation of the mean daily value for relevant quantities. The most important are heat transfer at the exchanger, the inlet temperature of the fluid on both sides of the exchanger, the building heating demand, the condenser load and the auxiliary electrical power usage (pumps, fans, compressor) are required.

Type A benchmarks focus on the main equipment (heat exchanger) a selection of performance limits defined in terms of effectiveness (ε). Type B performance indices encompass the heat recovery process and its interactions with chilled water production and heating. This section first presents the calculated limits (Type A, in 6.1) and the PIs (for Type B, in 6.2).

Then, an illustration of the suggested ongoing commissioning approach is presented in 6.3. The benchmarks are inverse models, developed using operation data. They are trained based on specific samples, which mean calculating the numerical values of the PI and their models for the reference state. In regards of the seasonal variation of effectiveness (5.3), the complete 2008 season appears to be the ideal sample, as being the first set of data available to an energy auditor. One-month training sets are also tested and compared to the seasonal benchmarks. To encompass the seasonal variation of ε, a peak-

season month (July 2008) in which operation is roughly continuous is used, as well as a moth involving interruptions and variations in the loads (June 2008).

Finally, the remaining data is tested against the benchmarks. In the testing process, attention is given to the similarity of the training and testing sets.

6.1. Type A heat-recovery benchmarks

Basic limits of performance were described in section 4.1. The calculation of the benchmarks limits is illustrated here for the training set based on the ideal sample: the complete 2008 season filtered for QuasiSS behavior and valid ε. The operation characteristics for the sample are the following:

1. $P_{P5} + P_{P6} = 60$ kW for the constant speed pumps involved in the recovery. The value is considered exact here (no uncertainty).

2. The mean condenser supply temperature T_{CNDs} at HX3 is 33.06°C $\pm$ 0.51°C.

3. $V_{min}^{CSB} = 60.00$ l/s $\pm$ 0.59. Combined with the mean temperature, this allows the determination of the following heat capacity rate: $C_{min}^{HX3} = 249.3 \pm 5.7$ kW/°C

4. The mean temperature of the fluid returning to the exchanger after recirculation is $T_{HWr}^{HX3} = 31.15 \pm 0.51$ °C.

The value of ε corresponding to power balance is thus, from Equation 4-6:

$$\varepsilon_{minP} \geq \frac{1}{249.3(kW/°C)} \frac{60kW}{(33.06 - 31.15)°C} = 0.13 \pm 0.05$$

5. The 2008 mean maximal thermodynamic heat rate through HX3 correspond to $Q_{max}^{HX3} = 480 \pm 200$ kW.

83

The effectiveness value for cost-balance, applying Equation 4-9 is:

$$\varepsilon_{minCost} \geq 1.2 \frac{60kW}{480kW} = 0.15 \pm 0.06$$

6.2. Type B benchmarking: PI for heat recovery process

The values of the four performance indexes for the process (Table 4-2) are calculated for daily averaged, filtered, quasi steady state measurements during the available seasons. The PI calculation for the reference sample is presented first, using operation data and the plant as-operated constant properties (Table 3-1).

In the sample, the mean Q_{HX3} = 400 ± 290 kW. The Recovery Efficiency Ratio is, from Equation 2-2,

$$RER = \frac{Q_{HX3}}{(P5 + P6)} = \frac{400kW}{60kW} = 6.7 \pm 4.8$$

This ratio is moderately interesting here since the constant power usage of the pumps make it directly proportional to the heat transfer through HX3. The high uncertainty is a direct consequence of the error on Q_{HX3}.

For the sample, the mean Q_{ev} = 1200±160 kW, the mean total pumping power is 28±2kW, the mean cooling tower fan power is 2.4±0.4 kW and the mean chiller power 280±10kW. The Compound Recovery COP is then, from Equation 2-3:

$$COP_{RE} = \frac{|Q_{HX3}| + |Q_{ev}|}{(P_{P5} + P_{P6}) + (P_{CW} + P_{CND}) + (P_{P7} + P_{P8} + P_{P9}) + P_{fan} + P_{CH}}$$

$$COP_{RE} = \frac{|400|+|1200|}{(30+30)+(75+56)+(28.3)+2.4+280} = 3.16 \pm 0.63.$$

The mean chiller evaporator load is three times larger than the recovered heat. In addition, the power usage of the devices susceptible of eventually being affected by the degradation of the heat recovery process (the heating water pumps P7, P8 and P9 as well as the cooling tower fan P_{fan}) is also small compared to the chiller power usage P_{CH}. This indicates that the sensitivity of the COP_{RE} to degradation of the heat recovery process is likely to be low. The main contributor to the relative error of 20% is the precision on Q_{HX3}.

In the sample, the mean reheat load is $Q_{HW}^{CSB} = 450 \pm 110 \; kW$. The Relative Load is:

$$RL = \frac{Q_{HX3}}{Q_{HW}^{CSB}} = \frac{400}{450} = 0.88 \pm 0.67 \qquad \text{Equation 6-1}$$

Finally, using $Q_{cond} = 2100 \pm 310 \; kW$ the Recovery Ratio is:

$$RR = \frac{Q_{HX3}}{Q_{cond}} = \frac{400}{2100} = 0.19 \pm 0.14 \qquad \text{Equation 6-2}$$

The mean seasonal values for all PI are summarized in Table 6-1 along with the standard deviation S for each PI and season, to give an idea of sample quality. The discrepancies between the results of Table 6-1 and demonstration calculations above arise from the fact that the reported seasonal averages are calculated from all the available daily values, not filtered.

Table 6-1 Mean seasonal recovery process PI values

	2008		2009		2010	
	Mean	S	Mean	S	Mean	S
RER	6.70	0.72	7.38	0.98	7.28	0.56
COP$_{RE}$	3.16	0.55	3.47	0.53	3.51	0.50
RL	0.85	0.05	0.87	0.07	0.85	0.07
RR	0.21	0.07	0.20	0.01	0.25	0.05

The results in Table 6-1 indicate that the decreasing effectiveness and growing fouling level do not translate into lower performance indices at process scale.

While the RER and RL are roughly constant throughout a season, the COP_{RE} and RR assume distinct values according to the operation conditions. The benchmark for the first two will correspond to fixed values whereas benchmark *models* can be developed for the others.
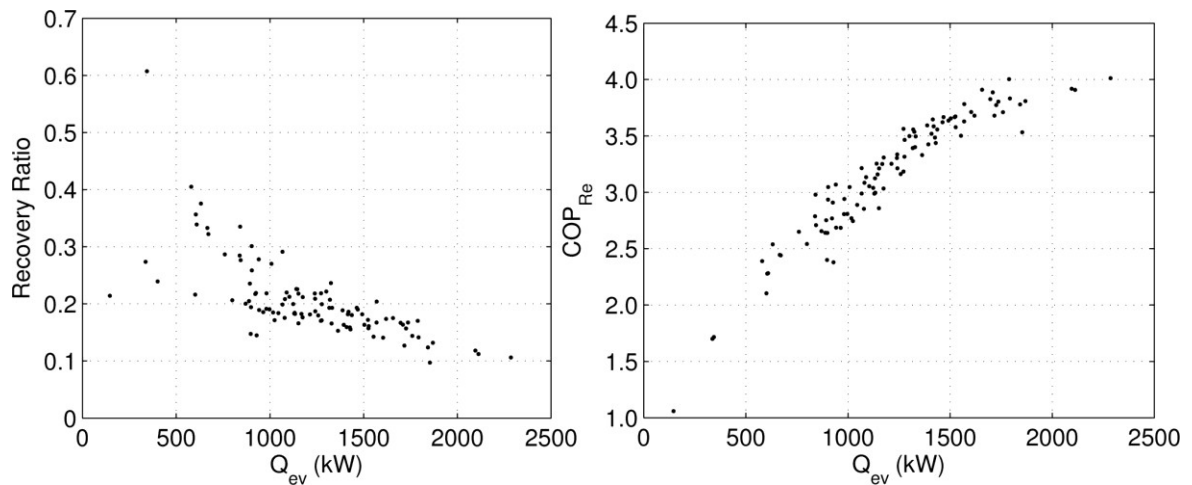
Figure 6-1 Performance indices as a function of Q_{ev} in 2008 A) RR and B) COP_{RE}

Since the heat-recovery process is passive and depends on the heat rejected by the chillers, the cooling load appears to be a relevant operation condition for analysis. The observations on the impact of solo versus tandem chiller mode (Figure 5-6, Figure 5-11) suggest that the notion of cooling load applies here to the chiller providing HX3 with condenser water rather than to the total building or plant cooling load. For the season of 2008, the dependence on Q_{ev} is illustrated in Figure 6-1.

For the purpose of this study, inverse parametric benchmark models are developed; they were introduced in Equation 4-19. The benchmark development is performed in section 6.3 for the selected training sets. A visual analysis of Figure 6-1 suggests to predict the RR for instance as a function of Q_{ev}. For the COP_{RE}, a quadratic dependence on Q_{ev} appears appropriate.

6.2.1. Time-variation of performance metrics

It is worth mentioning that unlike the heat exchanger ε, the performance indices selected here are not limited to steady-state analysis. The daily values were preferred here because the ongoing commissioning approach combines process and heat-exchanger benchmarks and is thus likely to require a daily calculation for the latter. Assessing the current state through a daily calculation appears sufficient and brings cohesion between the two benchmarking types. A brief investigation as to the sub-hourly variation of some of these PI was performed. As could be expected, they are strongly affected by transient effects at process start-up.

It is interesting to describe the evolution of the PI values as a function of the total number of operation hours for the heat recovery process, the same time frame that was used for the analysis of HX3.
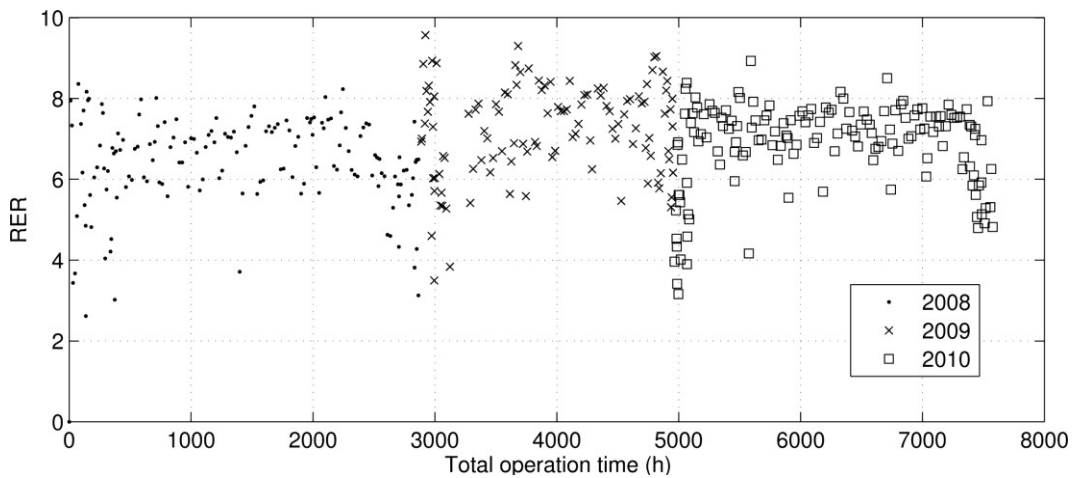
Figure 6-2 RER as a function of operation time

The time variation of the Recovery Efficiency Ratio is presented in Figure 6-2. It is affected by seasonal patterns, with higher dispersion at the beginning and end of seasons

and the split into two parallel clusters observed in 2008-2009 can be linked to occupancy patterns. A global increase in time seems to be present.

The COP_{RE} is also affected by a seasonal pattern (Figure 6-3) and global increase.
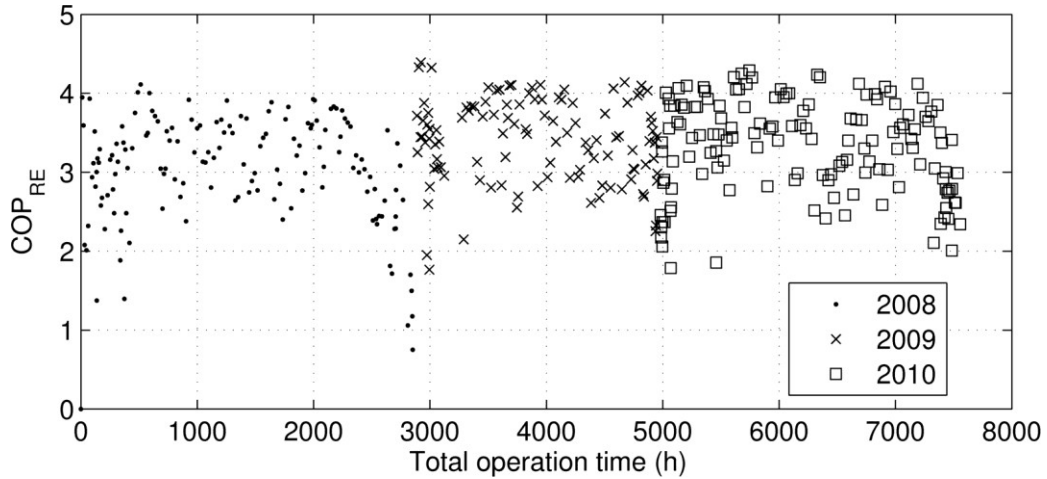
Figure 6-3 COP_{RE} as a function of operation time

The relative load, measuring the ratio of the recovery heat transfer rate on the building reheat load, is relatively constant, but significantly lower at the beginning and end of seasons, as seen in Figure 6-4. Unlike the two previous PIs, this one appears to decrease in time.
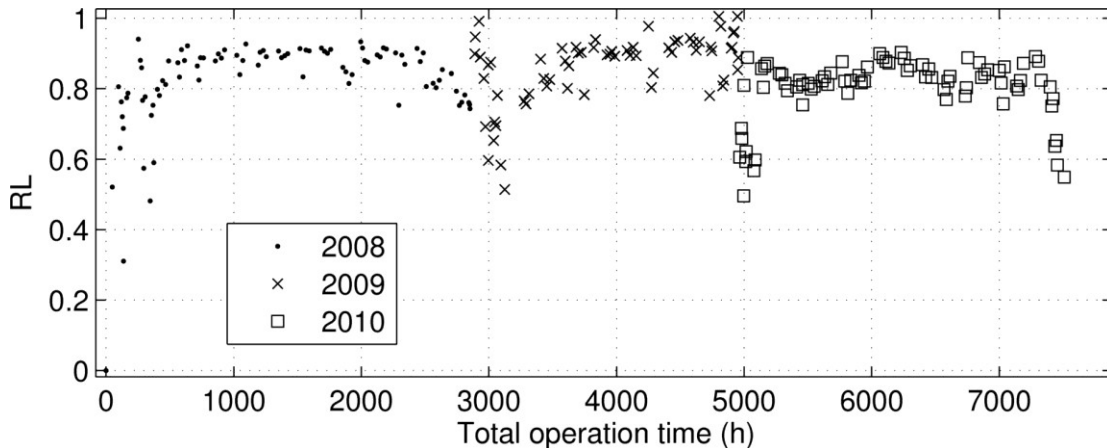
Figure 6-4 Relative load as a function of operation tome

And the relative load, comparing the recovery heat transfer rate to the available heat at the condenser is higher in shoulder seasons, and gradually increasing in time.
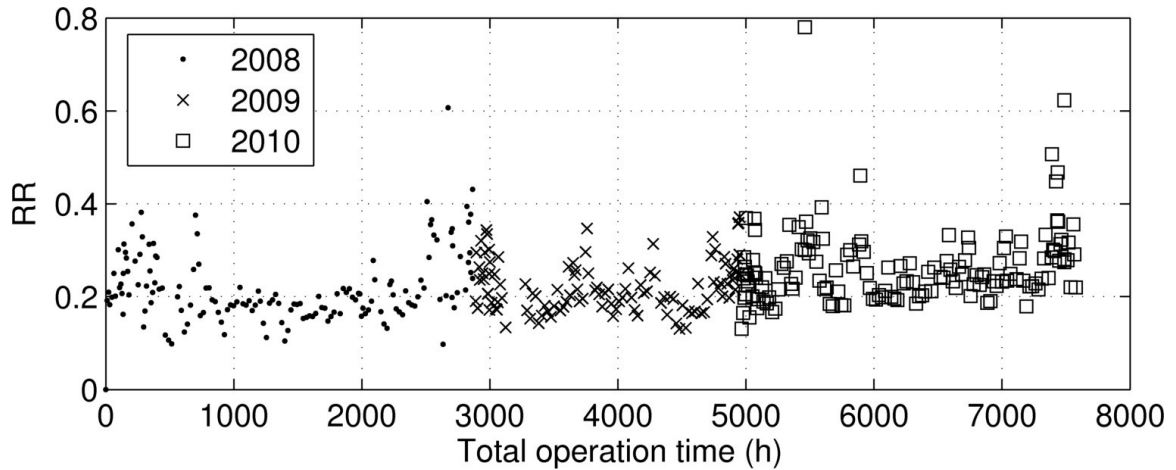
To complement the observations made above, the evolution of the selected driving variable, the load at the evaporator providing for the heat recovery process Q_{ev}, is also presented as a function of operation time for the process. Unlike the other significant quantity, the effectiveness, the global value of the condenser load is increasing.
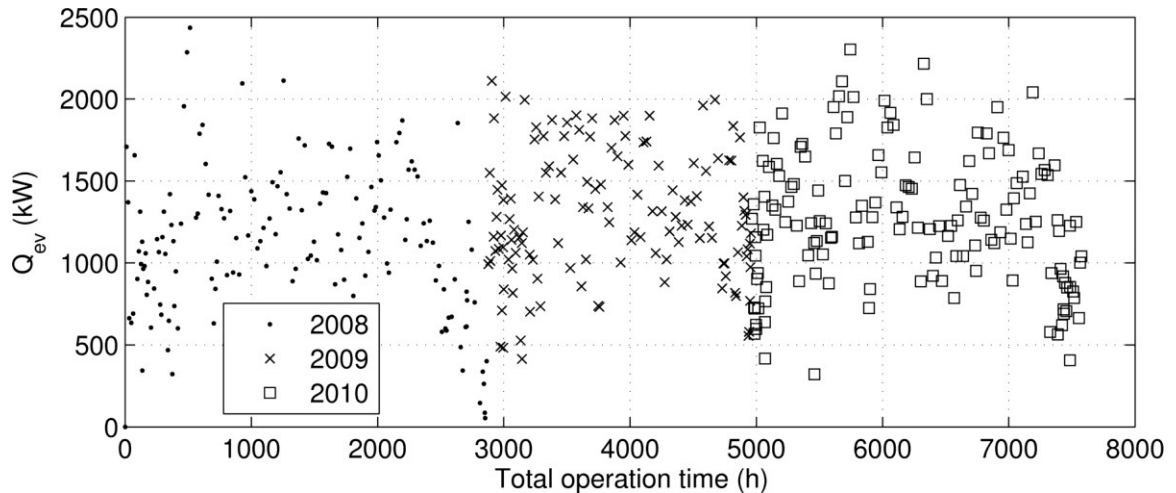
It seems pertinent to outline one fact: the performance indices used in Type B benchmarking are mostly sensitive on Q_{ev}. The increasing tendency of most indices is in contradiction with the growing fouling level. This is due to the system adaption (5.5.1), the ε could decrease while loads and thus the process performance indices increased throughout the years.

6.3.Illustration of proposed ongoing commissioning method

First, the benchmarks for the reference conditions are developed; which means that the numerical value of the constant benchmarks and the parameters of the benchmark models are calculated for the three training sets, for comparison purposes: A) June 2008 daily data, B) July daily data and C) all 2008 daily values. Benchmarks are divided here into Type A and Type B.

Type A benchmarks focus on the heat exchanger and correspond to limit values for ε. The calculated limit values for ε considering the three training sets are summarized in Table 6-2. The number of points indicates how many of the sampled days involved a physical value for ε (between 0 and 1). The valid days are those for which all inputs were actually recorded; the missing flow data on the building HW loop prevents the calculation of Q_{HW}^{CSB} and thus the sample. The number of valid points affects the tolerance; for samples below 30 points, the t-statistic [23] is used instead of z in Equation 5-14.

Table 6-2 Suggested limits for Type A benchmarking

Sample:			2008 season	June 2008	July 2008
Number of points (valid points)			106 (63)	23 (16)	31 (16)
ε_{cl} for the period			0.85 ±0.63	0.89 ±0.66	0.84 ±0.59
t-statistic			1.96	2.13	2.13
Limit	**Definition**				
Power Balance	$\varepsilon_{minP} \geq \dfrac{1}{C_{min}^{HX3}} \dfrac{P_{rec}}{(T_{CNDs} - T_{HWr}^{HX3})}$		0.13±0.04	0.13±0.04	0.12±0.04
Cost Balance	$\varepsilon_{minCost} \geq \dfrac{P_{rec}\$_E}{Q_{max}^{HX3}\$_H}$		0.15±0.06	0.15±0.06	0.15±0.06

The mean value of ε is smaller for the peak season sample (July 2008), but considering the large uncertainty, the impact of sample is moderate. The random uncertainty

component is small compared to the bias; the use of t instead of z has no significant impact. The numerical value of ε_{minP} and $\varepsilon_{minCost}$ is not significantly affected by the sample size either.

The Type B benchmarks target the process. Two are constant and two are functions of the operating conditions. For COP$_{RE}$ and RR, benchmark model predicting the expected PI value based on the load at evaporator is suggested along with a tolerance.

Table 6-3 Benchmark formulation for the Type B Performance indices

	Benchmark
RER	Constant RER ± t·S$_{RER}$
COP$_{RE}$	$COP_{RE} = aQ_{ev}^2 + bQ_{ev} + c$
RL	Constant RL ± t·S$_{RL}$
RR	$RR = d + eQ_{ev}$

The goal here is to illustrate the methodology, not to obtain high quality parametric models. Some elements such as the weekend/week-day patterns have been neglected. The benchmark models are presented in Table 6-4. The parameters (a to e) refer to Table 6-3.

Table 6-4 Benchmarks for the performance indices

PI	Numerical values	Training results		
		A 2008 Season	B June 2008	C July 2008
RER	RER	6.71	6.77	6.76
	S$_{RER}$	0.72	0.68	0.63
COP$_{RE}$	a	-5.79E-07	-6.15E -07	-9.56E -07
	b	2.72E -03	2.81-03	3.91E-03
	c	0.80	0.78	-0.11
	$\overline{R^2}$	0.94	0.87	0.83
	RMSE	0.14	0.19	0.10
RL	RL	0.86	0.87	0.89
	S$_{RL}$	0.05	0.04	0.03
RR	d	0.34	0.34	0.25
	e	-1.24E-04	-1.11E-04	-0.62E-04
	R²	0.50	0.53	0.58
	RMSE	0.05	0.04	0.01

In general, the greater cohesion in the July 2008 set favors small standard deviations and low RMSE. The fit quality for the COP_{RE} is acceptable in all training scenarios, but the whole season is slightly more reliable (high R^2) and precise (moderate RMSE). The fit for RR is poor, no matter the training set. The value of the constant PIs varies little and considering a benchmark formulated as CenterValue $\pm$ tS, the band considered as valid is very similar for RER in all training sets; the same applies to RR.

In order to explore the validity of the PI benchmarks developed from 2008 and presented in Table 6-4, testing sets are used. This external testing complements the internal testing provided by R^2 and RMSE within the training set [24]. Each PI developed for the three 2008 training sets is tested against the data from 2009, where three testing sets are defined. They are equivalent to the sets used for benchmark training: D) the complete 2009 season, E) June 2009 and F) July 2009. For each of the twelve 2008 benchmarks, three comparisons are thus performed. The comparison criterion here is the RMSE. Results are presented in Table 6-5.

Table 6-5 RMSE for 2008 benchmarks in 2009 testing sets

	Benchmark	Test set D Season 2009	Test set E June 2009	Test set F July 2009
Training set A Season 2008	RER_A	1.18	0.88	1.23
	COP_A	0.22	0.18	0.18
	RL_A	0.08	0.11	0.05
	RR_A	0.72	0.62	0.74
Training set B June 2008	RER_B	1.15	0.88	1.20
	COP_B	0.22	0.19	0.16
	RL_B	0.08	0.12	0.05
	RR_B	0.70	0.60	0.72
Training set C July 2008	RER_C	1.16	0.88	1.20
	COP_C	0.23	0.15	0.19
	RL_C	0.08	0.14	0.04
	RR_C	0.72	0.62	0.73

All benchmarks developed from 2008 perform equivalently in the overall 2009 season (Test set D), with slightly lower RMSE for the June 2008 benchmarks. Considering the June 2009 set (Test set E) the global performance for all benchmarks is similar. The June 2008 benchmarks are a little more coherent with the July 2009 testing set (Test set F). In general, harmonizing the testing and training sets does not favor cohesion.

Based on these observations as well as on the discussion on the limit values for ε, it appears there is no significant improvement in using the whole 2008 season as opposed to a shoulder season month (June) for benchmark training. The four benchmarks for June 2008 are illustrated in combination with the 2009 season data in Figure 6-7. The tolerance bands were defined based on Equation 5-12, where the z=1.96 value is replaced by the appropriate t-value = 2.13. The standard deviation was corrected similarly for the constant value benchmarks.
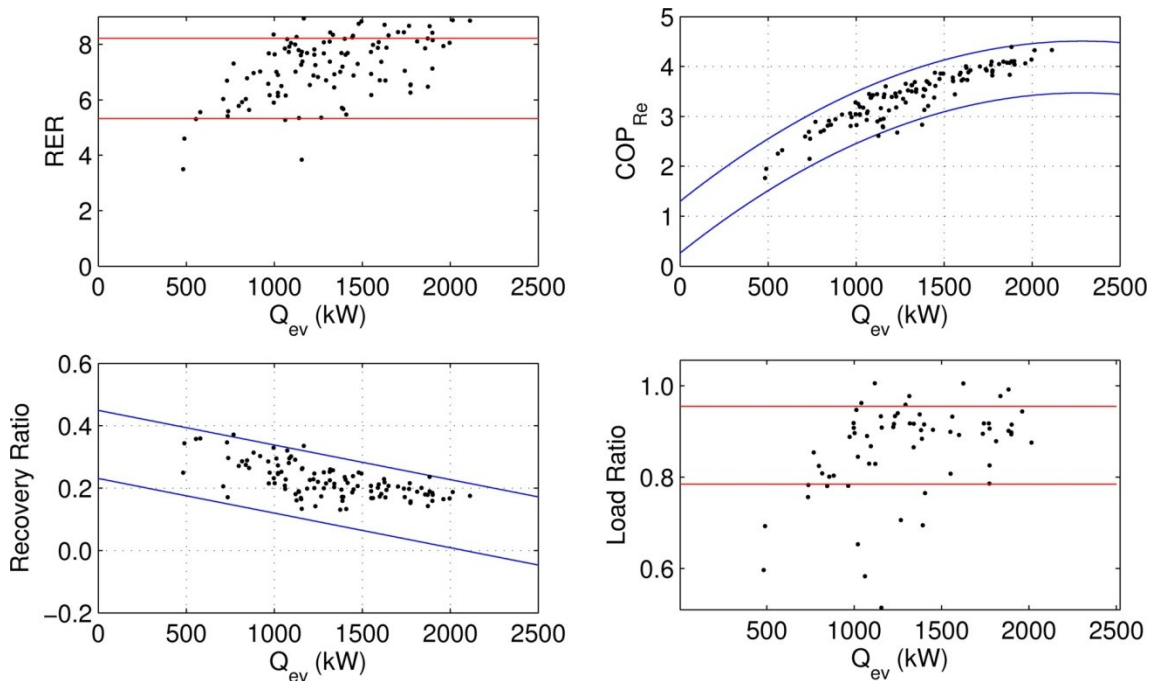
Figure 6-7 Comparison of the 2009 season data with June 2008 benchmarks

The PI benchmarks as well as the limit effectiveness values can be combined and used as follows. At the end of each day of operation, the ongoing-commissioning functional block computes the derived measured value of ε and the PI from definition. Upon the detection of off-bands values for a PI or when reaching a pre-set limit for the heat exchanger's effectiveness, a fault is suspected. A warning message is sent and the operation personal can view the current system state in an interface. It is illustrated in Figure 6-8 on page 95.

On the left is the heat exchanger historical data, presented as the previous values for effectiveness as a function of total operation time. The current value for 2010-08-17 is presented with a distinct marker. The linear fit of the ε decrease is superimposed to the daily values. The Type A limits (power and cost-balance ε) are traced on the same graph. In terms of the heat exchanger state, no critical limit is reached. The operation could continue for thousands of hours before reaching the limit effectiveness values requiring heat-exchanger cleaning.

From the process point of view, considering current operation conditions, the RR value is near the limit of the reference state, but not in transgression; no warning would be displayed.
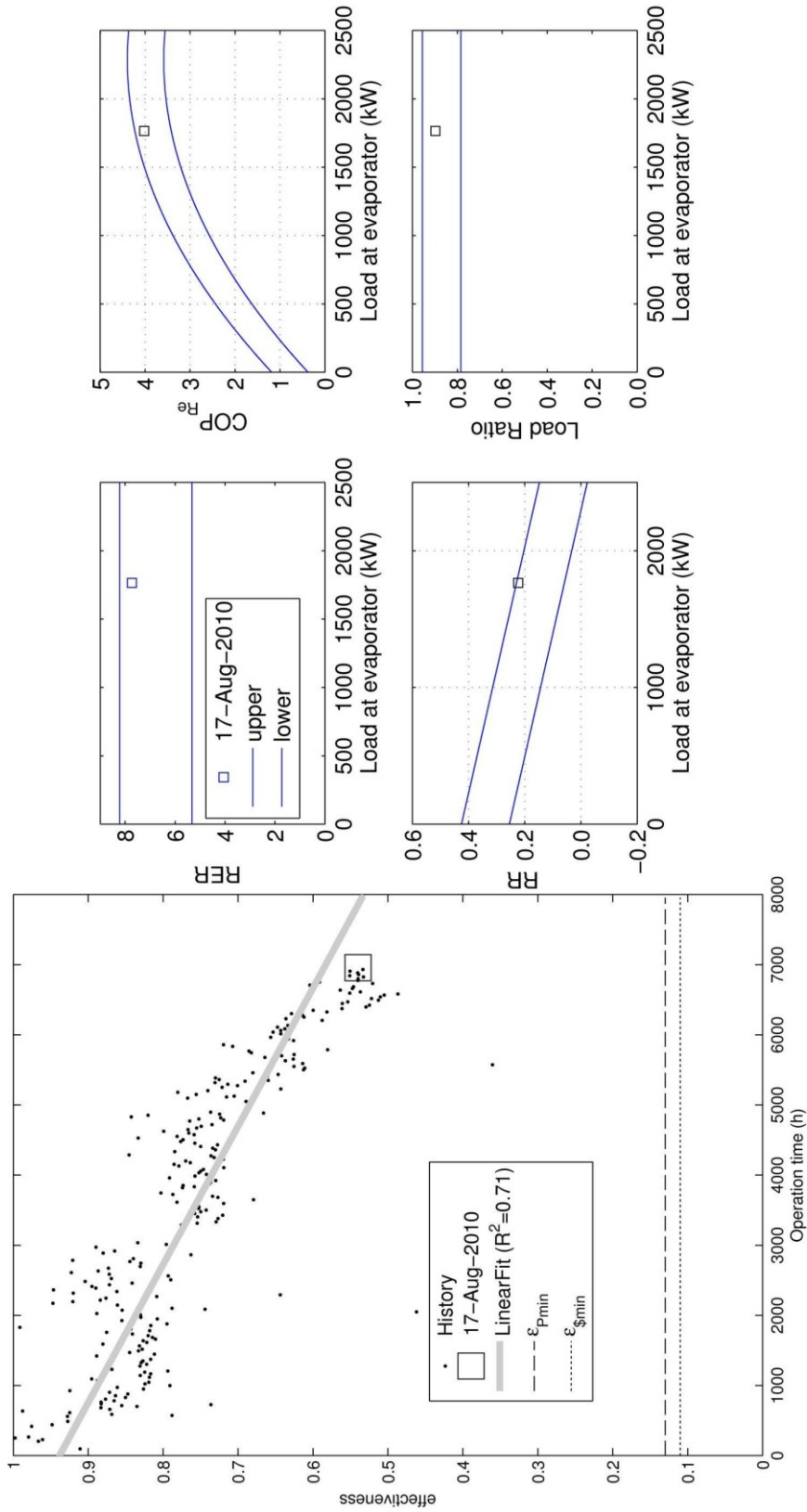
Figure 6-8 Proposed ongoing commissioning interface

7. Conclusions and future work

This is likely the first proposed ongoing commissioning methodology for a liquid-to-liquid HVAC heat-recovery process. The approach is based on comparing incoming operation data against two types of benchmarks. Type A benchmarking applies to the main equipment, here a plate heat-exchanger. Due to the nature of the equipment, the benchmarks are fixed performance limits expressed here in terms of the effectiveness ε. The limits were defined according to power and financial criteria. The Type B benchmarking applies to the heat recovery process and interactions with other systems. The benchmarks are a collection of performance indices, some of which undergoing variation according to the conditions of operation. These PIs were cast into simple inverse parametric benchmark models. Type B benchmarks allow for self-referencing of incoming data against expected behavior. The PIs and limits calculation require knowledge on the as-operated system and a training dataset. The methodology requires data assumed to be exempt of faults.

The ongoing commissioning could take the form of a functional block embedded in the building automation system. The suggested testing frequency here is daily, based on the steady-state requirements for heat exchanger analysis.

The case study used to demonstrate the methodology is based on operation data collected in a heating and chilled water plant located in Montreal. Passive liquid-to-liquid heat recovery from condenser water was performed any time the plant chillers were active between April and October. Three years of operation were selected and analyzed. The

process was continuous in the peak season, discontinuous in the shoulder season and inactive between November and March.

At the time-step available, the high dispersion affecting the data associated with process start-up made it unusable for dynamic modeling. Quasi steady-state hypothesis appeared valid for the remaining data.

Heat-exchanger fouling was targeted as the main fault likely to affect the heat-recovery. The variations in operation conditions caused by seasonal and occupancy patterns affected ε sufficiently to mask the generic effect of fouling during the first season. In terms of training set, this confirms the validity of the entire 2008 season as reference. Fouling was however confirmed and the regime assessed from the 2008-2010 data. It was dependent upon the cumulative hours of operation of the exchanger rather than calendar date, and obeyed a quadratic pattern. One main issue here was the large amount of data required in order to detect a potential fault. Having access to manufacturer data and models for the heat-exchanger would have allowed the compensation of the seasonal and daily variations in operation conditions (temperature), leading to a quicker confirmation of fouling growth.

Following the suggested methodology, the calculation of ε limits and process PI was performed from various sets from the reference season; the benchmarks based on June 2008 performed well in training and testing sets.

Some of the heat-exchanger performance limits (Type A) however proved incompatible with the case-study. They were based on the hypothesis that fouling would gradually impair heat recovery, leading to increasing needs in complementary heating. Despite the

fouling growth, the heat recovery rate did not decrease over the studied period. On the contrary, as the re-heat loads increased annually, the system could recover more heat from the condenser loop. This was made possible by a downward drift of the mean temperature in the heating water loop, however above the set-point triggering additional heat input. The lower temperature on the cold side of the exchanger increased the temperature difference and thus opposed the lower heat transfer capacity. At system scale, the only impact of fouling was higher flow requirement in the building heating water loop.

The comparison between all proposed benchmarks for the case study outlines one major thing: the degradation in the heat exchanger heat transfer capacity, monitored by Type A did not translate into significantly lower performance at process scale according to Type B benchmarks. In other words, the targeted fault, even confirmed, did not have the expected consequence. In that sense, the combination of the two benchmark types proved relevant: focusing on main equipment would not have been sufficient. Error messages based on fouling level might prove irrelevant at process scale.

7.1. Future work

Here are a few suggestions for the continuation of work on this topic:

- Future projects should include other case studies of passive heat-recovery, with different operation schedule, load patterns and possibly other fouling regimes.
- Data displaying faulty behavior should be included in order to evaluate the sensitivity of the tool, and thus its actual fault detection capability.

- Cases where complementary heat is required are likely to exist and should be investigated. This would allow the calculation of the two performance limits rejected here; optimization-based and standard-based effectiveness.

- The optimization based on increases in auxiliary power (for instance pumps) could be investigated.

- Various data formulation such as non-dimensional models or normalized versions of the performance indices (ex: the COP) might provide additional understanding.

- Finally, the methodology could eventually be applied to other liquid-to-liquid heat recovery systems with little adaptation. For instance, in an active process involving a heat-pump, the Type A benchmark could be based on COP rather than ε, and the power usage of the heat-recovery process would include the heat-pump power.

8. References

1. Office of Energy Efficiency (2006), *The State of Energy Efficiency in Canada*, Natural Resources Canada.

2. Katipamula, S., Brambley, M. R., Bauman, N., & Pratt, R. G. (2003). *Enhancing building operations through automated diagnostics: Field test results*. Proceedings of the ICEBO conference, Berkeley,USA.

3. ASHRAE (Ed.) (2005). *The commissioning process, ASHRAE guideline 0-2005*. Atlanta, GA, Unites-States of America: American Society for Heating, Refrigeration and Air-Conditioning Engineers.

4. LEED Canada (2004), *Rating System & Addendum for new construction & Major Renovations, LEED Canada-NC Version 1.0*, Canadian Green Building Council,. Available online from http://www.cagbc.org/Content/NavigationMenu/Programs/LEED/default.htm access date: January 7th, 2013.

5. Haasl, T., & Sharp, T. (1999). *A practical guide for commissioning existing buildings*.US Department of Energy, State and community programs.

6. Turner, W. D., Claridge, D. E., & Liu, M. S. (2003). In Wells J. (Ed.), *Continuous commissioning(SM) guidebook for federal energy managers*.

7. Canmet Energy (March 2008), *Recommissioning Guide for Building Owners and Managers*, Natural Resources Canada. Available online (http://canmetenergy.nrcan.gc.ca/buildings-communities/publications/3054) access date January 7th, 2013.

8. ARTI [currently AHRI] (2003). *Methods for automated and continuous commissioning of building systems*. (No. ARTI-21CR/610-30040-01). Technical Results, System Integration Project Reports. Retrieved from http://www.osti.gov/bridge/purl.cover.jsp?purl=/810800-vomrED/native/;http://www.ahrinet.org ;

9. Choinière, D., editor. *Cost Effective Commissioning of Existing and Low Energy Buildings*, Annex 47 of the ECBCS of the IEA (2010), available online from http://www.ecbcs.org/annexes/annex47.htm

10. LEED Canada, *LEED® Canada for Existing Buildings: Operations and Maintenance 2009, RATING SYSTEM*. Canadian Green Building Council, Available online from http://www.cagbc.org/Content/NavigationMenu/Programs/LEED/default.htm access date : January 7th, 2013.

11. BOMA Canada (2012), *Questionnaire BOMA BESt, Immeuble de bureaux de plus de 100000 pi²,* Building Owners and Managers Association of Canada.

12. Energy Star, http://www.energystar.gov/   Access date 30/11/2012.

13. Hun, B.D., Haberl, J.S., Davies, H, Owens,B. (2012). Measuring Commercial Building Performance, *ASHRAE Journal* Vol 54 (7), p. 50-59.

14. Djuric, N., & Novakovic, V. (2009). Review of possibilities and necessities for building lifetime commissioning. *Renewable & Sustainable Energy Reviews, 13*(2), p. 486-492.

15. IPMVP (Ed.). (2010). *International performance measurement and verification protocol, concepts and options for determining energy and water savings*. Washington D.C., USA: Efficiency Valuation Organization.

16. IEA (1996). *Real Time HVAC Simulation; Building Optimization and Fault Diagnosis Source Book*, Annex 25 of the ECBCS, Finland. Available online from http://www.ecbcs.org/annexes/annex25.htm

17. Jagpal R., editor (2004). *Computer Aided Evaluation of HVAC System Performance, Technical Synthesis Report*, Annex 34 of the ECBCS of the IEA. Available online from http://www.ecbcs.org/annexes/annex38.htm

18. Cui, J. T., & Wang, S. W. (2005). A model-based online fault detection and diagnosis strategy for centrifugal chiller systems. *International Journal of Thermal Sciences, 44*(10), p. 986-999.

19. Reddy, T.A. (2007) Development and Evaluation of a Simple Model-Based Automated Fault Detection and Diagnosis (FDD) Method Suitable for Process Faults of Large Chillers, *ASHRAE Transactions*, Vol. 13 part 2, p. 27-39.

20. ASHRAE (Ed.), (2009). *Fundamentals*. ASHRAE, Atlanta, USA.

21. Baumann, O. (2004). *Operation diagnostics-use of operation patterns to verify and optimize building and system operation*. Proceedings of the ICEBO conference, Paris, France.

22. Yang, J., Rivard, H., & Zmeureanu, R. (2005). On-line building energy prediction using adaptive artificial neural networks. *Energy and Buildings, 37*(12), p. 1250-1259.

23. Reddy, T. A. (2011). *Applied data analysis and modeling for energy engineers and scientists*, first edition, Springer, New-York, USA.

24. Monfet, D. (2011). *New ongoing commissioning approach of central plants: Methodology and case study.* (PHD Thesis, Concordia University, Montréal, Canada).

25. Deng, S., Turner, W. D., Claridge, D. E., Liu, M., Bruner Jr., H. L., & Wei, G. (2002). Retrocommissioning of central chilled/hot water systems. *ASHRAE Transactions 2002, June 22, 2002 - June 26, 108 PART 2* 75-81.

26. ASHRAE (Ed.), *(*2012) *ASHRAE Handbook--HVAC Systems and Equipment*, ASHRAE, Atlanta, USA.

27. Müller-Steinhagen, H., editor. (2000), *Heat Exchanger Fouling, Mitigation and cleaning technologies*, Publico Technologies, Essen, Germany, p. 319-332.

28. Zhou, Q., Wang, S., & Ma, Z. (2009). A model-based fault detection and diagnosis strategy for HVAC systems. *International Journal of Energy Research, 33*(10), p. 903-18.

29. Tatara, R. A., & Lupia, G. M. (2011). Assessing heat exchanger performance data using temperature measurement uncertainty. *International Journal of Engineering, Science and Technology* (Multicraft Publishers), Vol. 3(No. 8), p. 1-12

30. Mohanty, D. K., & Singru, P. M. (2011). Use of C-factor for monitoring of fouling in a shell and tube heat exchanger. *Energy, 36*(5), p. 2899-2904.

31. Pogiatzis, T. A., Ishiyama, E. M., Paterson, W. R., Vassiliadis, V. S., & Wilson, D. I. (2012). Identifying optimal cleaning cycles for heat exchangers subject to fouling and ageing. *Applied Energy, 89*(1)

32. Markowski, M., Trafczynski, M., & Urbaniec, K. (2013). Identification of the influence of fouling on the heat recovery in a network of shell and tube heat exchangers. *Applied Energy*, 102, p. 755-764.

33. Genić, S. B., Jaćimović, B. M., Mandić, D., & Petrović, D. (2012). Experimental determination of fouling factor on plate heat exchangers in district heating system. *Energy and Buildings, 50*(0), p. 204-211.

34. Weyer, E., Szederkenyi, G., & Hangos, K. (2000). Grey box fault detection of heat exchangers. *Control Engineering Practice, 8*(2), p. 121-131.

35. Hu, Q. H., So, A. T. P., Tse, W. L., & Ren, Q. C. (2005). *Development of ANN-based models to predict the static response and dynamic response of a heat exchanger in a real MVAC system.* Proceedings of the International Conference on Control and Synchronization of Dynamical Systems (Csds-2005)*, 23*, p. 110-121.

36. Astorga-Zaragoza, C., Alvarado-Martinez, V., Zavala-Rio, A., Mendez-Ocana, R., & Guerrero-Ramirez, G. (2008). Observer-based monitoring of heat exchangers RID B-6286-2009. *ISA Transactions, 47*(1), p. 15-24.

37. Siemens (2011), *Products and functions for efficient maintenance in the process automation, Brochure October 2011*, Siemens Automation and Maintenance division, Nürnberg, Germany.

38. Siemens (2010), *Applications for Process Automation, Applications & Tools, Monitoring of Heat Exchangers using the HeatXchMon Function Block*, Version V1.0

39. Hortelan, H. (2009). *Rapport d'internat,* Concordia University.

40. Durkin, T. H., & Rishel, J. B. (2003). Dedicated heat recovery. *ASHRAE Journal, 45*(10), p. 18-24.

41. Kaushik, S. C., Panwar, N. L., & Siva R. V. (2011). Thermodynamic evaluation of heat recovery through a canopus heat exchanger for vapor compression refrigeration (VCR) system. *Journal of Thermal Analysis and Calorimetry*, p. 1-7.

42. Gong, G., Chen, F., Su, H., & Zhou, J. (2012). Thermodynamic simulation of condensation heat recovery characteristics of a single stage centrifugal chiller in a hotel. *Applied Energy, 91*(1), p. 326-333.

43. ASHRAE (Ed.). (2010) *Energy Standard for Buildings Except Low-Rise Residential Buildings, ANSI/ASHRAE/IESNA 90.1-2010.* Atlanta, GA, USA.

44. Monfet, D., Zmeureanu, R., Charneux, R., & Lemire, N. (2009). Calibration of a building energy model using measured data. *ASHRAE Transactions* 2009, Vol 115, Pt 1, 115, p. 348-359.

45. Monfet, D., & Zmeureanu, R. (2010). Ongoing commissioning approach for a central cooling and heating and plant. *ASHRAE Transactions* 2010, p. 117.

46. Monfet, D., & Zmeureanu, R. (2012). Ongoing commissioning of water-cooled electric chillers using benchmarking models. *Applied Energy, 92*, p. 99-108.

47. Monfet, D. (2009). *Évaluation des performances énergétiques d'une centrale thermique d'un campus universitaire*. Proceedings of the IXième Colloque interuniversitaire Franco-Québécois sur la thermique des systèmes, Lille, France.

48. McQuinston, F. C., Parker, J. D., & Spitler, J. D. (Eds.). (2005). *Heating, ventilating, and air conditioning, analysis and design, Sixth edition,* Wiley, NewYork, USA.

49. Consortium PMA - Pellemon. (2003). *Université Concordia, complexe des sciences – campus Loyola, manuel de description et d'opération du bâtiment, 2072-00-W1*. Montréal, Canada.

50. Kakaç, S. and Liu, H., (1998). *Heat exchangers selection, rating and thermal design*, CRC press, USA.

51. Incropera, F., & DeWitt, D. *Fundamentals of heat and mass transfer* (3rd ed.). John Wiley and sons, Inc. New York USA.

52. Hydro-Québec, *Comprendre Votre Consommation*, online ressource, http://www.hydroquebec.com/affaires/moyen/tarif-affaires.html access date 18-01-2013. access date 2013-01-18.

53. Ministère des ressources naturelles du Québec, *Gros plan sur l'Énergie, prix du gaz naturel*, website http://www.mrn.gouv.qc.ca/energie/statistiques/statistiques-energie-prix-gaz.jsp access date 2013-01-18.

54. Somerscales E.F and Knudsen, J. (editors), (1981). *Fouling of heat transfer equipment*, Hemisphere publishing corp. USA.

55. ASHRAE (Ed.). (2002). *ASHRAE guideline 14-2001, Measurement of Energy and Demand Savings*. ASHRAE, Atlanta, USA.

56. ASHRAE (Ed.). (2005). *ASHRAE guideline 2-2005, Engineering Analysis of Experimental Data*. ASHRAE, Atlanta, USA.

57. Coleman, H.W. Steele, W.G., (1989). *Experimentation and uncertainty analysis for engineers,* Wiley & Sons. New York USA.

58. Wheeler, A. J., & Ganji, A. R. (2004). Introduction to engineering experimentation (2nd ed.). Prentice Hall, Upper Saddle River, USA.

59. Karassik, I. J. (2001). *Pump handbook* (3rd ed.). McGraw-Hill, New York, USA.

Appendices

Appendix A **Design values for the plant equipment**

Most of the following is quoted from Monfet [24]. The remaining is gathered in specification sheets and design data [49].

Table A-1 Design values for major plant elements

Item	Design Information		Pumps & fans	Design information	
CH1 & CH2 (each)	Power (kW) / RLA (A)	549 / 587	P1& P2 (Chilled water, each)	Flow (L/s) / Power (kW)	72.6 / 75
	Evaporator T_{in} /T_{out} (°C) / Evaporator Flow (L/s)	13.3 / 5.6 / 97	P3 & P4 (Condenser water, each)	Flow (L/s) / Power (kW)	131.5 / 56
	Condenser T_{in} /T_{out} (°C) / Condenser Flow (L/s) / COP	29.4/35.0 / 162 / 5.76	P5 & P6 (HX3, each)	Flow (L/s) / Power (kW)	107.3 / 30
CT1 & CT2 (each)	Flow (L/s) / T_{in}/T_{out} (°C) / T_{WB} (°C)	131.5 / 25.3/29.4 / 24.3	CT fan	Max P (kW)	30
BR1	Max Power (kW)	1020	P04CBT (to electrical boiler)	Power (kW) / Flow (L/s)	1.2 / 11
Heat Exchangers					
Item	Cold side		Warm side		
HX3	T_{in} /T_{out} (°C) / Flow (L/s)	29.4 / 35.0 / 107.3	T_{in} /T_{out} (°C) / Flow (L/s)		37.8 / 32.2 / 107.3
HX2	T_{in} /T_{out} (°C) / Flow (L/s)	35.2 / 51.7 / 107.3	Steam (kg/h) / Pressure (kPa)		12 701 / 414
HX1	T_{in} /T_{out} (°C) / Flow (L/s)	29.4 / 51.7 / 107.3	T_{in} /T_{out} (°C) / Flow (L/s)		57.1 / 32.2 / 38.5
SOFAME	T_{in} /T_{out} (°C) / Flow (L/s)	32.2/57.1 / 38.5	Max Fan power (kW) / Max Fan capacity (m³/s) / Flue Gas Spec /Max temperature (°C)		11.2 / 7.1 / 238/343
	Pump Power (kW)	37.3	Auxiliary burners (each of 2) (kW)		3.22

The as-operated values are different, as mentioned in sections 3.2 and 5.1.

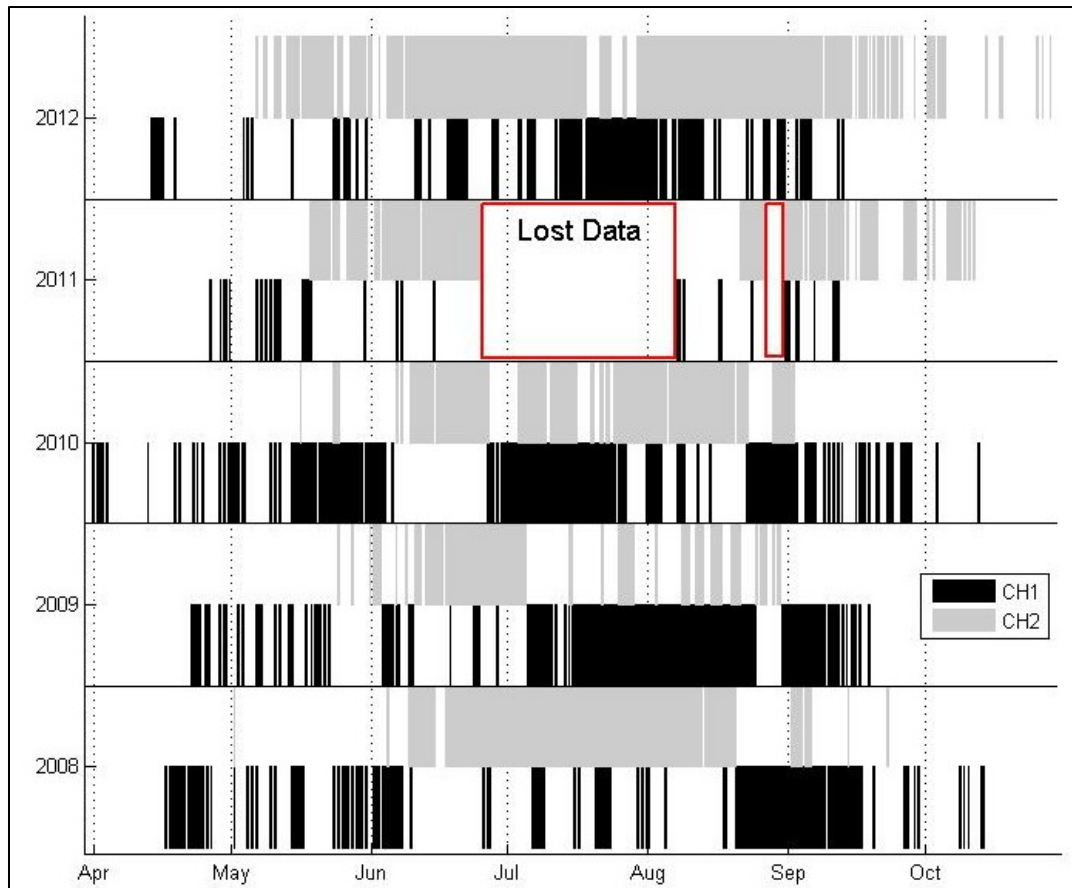# Appendix B **Chiller operation for all years, graphical summary**

Figure B-1 Cooling groups operation

Appendix C **Plant performance in 2011-2012**

The seasons of 2011 and 2012 were not included in the main text of this thesis. The current section describes briefly the characteristics of these seasons and discusses their compatibility with the proposed ongoing commissioning tool.

2011 and 2012 are characterized by modifications to loads and equipment following the addition of a new building to the plant loops: the Genomic research center. New equipment, an electric boiler, was also installed. It is located downstream (Figure C-2) HX2 and fed by a constant speed pump for which the flow measured in 2012 is 12.1 ±0.5 L/s.
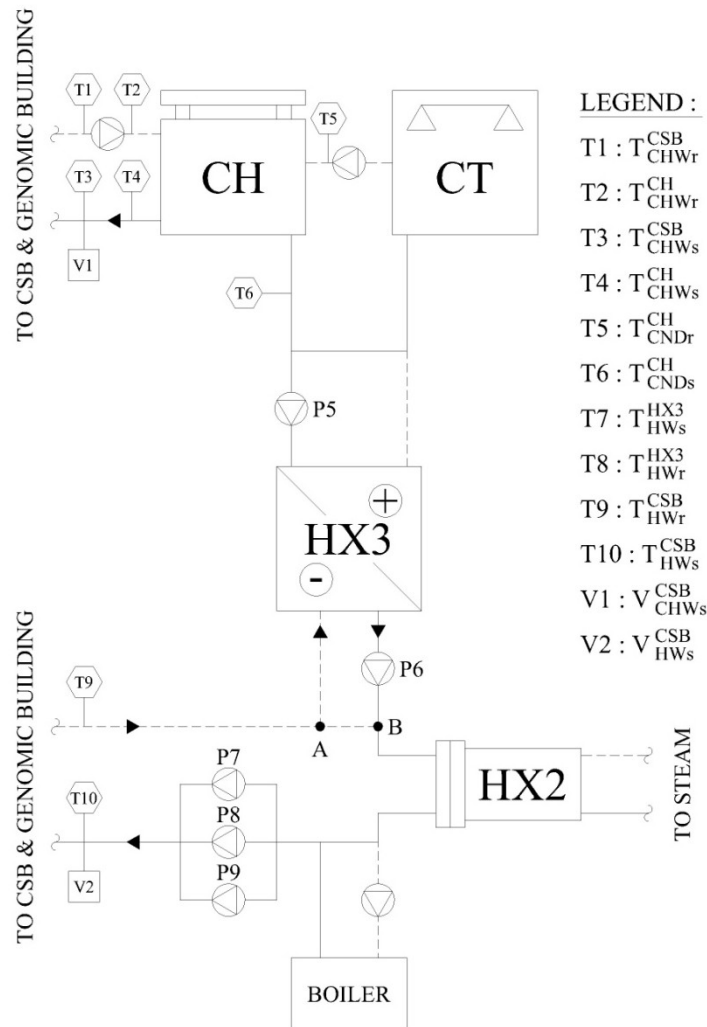

Figure C-2 Plant schematic in cooling mode

Acquisition issues lead to the loss of several weeks of data in 2011 (see Appendix B). The whole month of July and a week of August are missing, which is the peak season.

Table C-2 Mean measured values during chilled water production and heat recovery

	unit	2010		2011 (partial)		2012	
		Mean	S	Mean	S	Mean	S
Toa	°C	23.2	4.8	21.6	4.8	23	5.1
RH	%	42	23	41	23	35	19
V_{CHW}^{CSB}	L/s	100	26	93	17	108	30
T_{CHWs}^{CSB}	°C	7.07	0.41	7.17	0.30	7.14	0.39
T_{CHWr}^{CSB}	°C	11.4	1.5	11.2	1.4	11.4	1.7
V_{HW}^{CSB}	L/s	52	8	66	12	61	11.14
T_{HWs}^{CSB}	°C	30.7	1.4	30.3	1.6	33.4	2.1
T_{HWr}^{CSB}	°C	28.2	1.1	28.2	1.4	31.3	1.9
T_{CNDs}^{CH1}	°C	32.3	1.5	32.0	1.3	32.5	1.4
T_{CNDr}^{CH1}	°C	28.36	0.44	28.4	0.68	28.43	0.35
T_{EVs}^{CH1}	°C	6.8	0.5	6.82	0.72	6.8	0.48
T_{EVr}^{CH1}	°C	11.1	1.5	11.1	1.3	11.3	1.5
P_{CH1}	kW	288	80	283	67	308	80
$VFDT_{CT1}$	%	47	17	51	14	59	18
T_{CNDs}^{CH2}	°C	32.4	1.3	32.2	1.4	32.2	1.4
T_{CNDr}^{CH2}	°C	28.50	0.35	28.46	0.45	28.49	0.42
T_{EVs}^{CH2}	°C	6.74	0.42	6.74	0.43	6.73	0.35
T_{EVr}^{CH2}	°C	11.3	1.4	10.9	1.5	11.0	1.6
P_{CH2}	kW	297	77	284	85	290	89
$VFDT_{CT2}$	%	55	20	43	13	52	16
T_{HWin}^{HX3}	°C	29.5	1.3	28.9	1.5	31.6	1.8
T_{HWout}^{HX3}	°C	30.4	1.4	29.8	1.4	31.9	1.7

The mean chilled and heating water flows were higher than in the previous seasons, which is likely due to the newly added building. The HW pumping power calculated from drive data increased consequently, with 42±1.2kW in 2011 and 32±1.1kW in 2012 (see Table 5-13 for comparison).

The main stream temperatures are presented in Table C-3. The decreasing tendency for the HW stream continued from 2008 to 2011. The 2012 season however involved a temperature rise which explains the pumping power reduction from 2011 to 2012, as mentioned above. This is coherent with the temperature-flow dependency for the building (chapter 5, Figure 5-13).

Table C-3 Seasonal mean stream temperature T_{avg}

Season	Seasonal mean temperature of the water streams (°C)						
	CH1e	CH2e	CSB CHW	CH1c	CH2c	CSB HW	HX3 HW
2008	8.58	8.79	9.03	30.39	30.92	30.92	31.57
2009	8.98	8.87	9.31	30.74	30.82	30.47	31.04
2010	8.92	9.00	9.25	30.33	30.44	29.46	29.97
2011	8.96	8.81	9.21	30.19	30.31	29.26	29.37
2012	9.04	8.88	9.28	30.47	30.33	32.37	31.74

The heat transfer and loads are presented in Table C-4. The missing peak-season data for 2011 affects the seasonal mean. Considering this, an increasing tendency in cooling and heating loads for the CSB over the five years is present.

Table C-4 Mean heat transfer rates during chilled water production by the plant

item	Seasonal mean heat flow rate ± uncertainty (kW)														
	2008			2009			2010			2011(partial)			2012		
Q_{ev}^{CH1}	1200	±	160	1527	±	170	1456	±	160	1397	±	160	1546	±	170
Q_{ev}^{CH2}	1400	±	160	1470	±	170	1537	±	170	1512	±	180	1564	±	180
Q_{CHW}^{CSB}	1500	±	180	1716	±	190	1891	±	210	1613	±	190	2011	±	220
Q_{c}^{CH1}	1870	±	310	2215	±	290	1797	±	290	1660	±	290	1865	±	290
Q_{c}^{CH2}	2200	±	310	2109	±	290	1780	±	290	1695	±	290	1691	±	290
Q_{HW}^{CSB}	440	±	110	485	±	120	504	±	140	521	±	170	531	±	170
Q_{HW}^{HX3}	390	±	290	414	±	290	419	±	280	414	±	280	129	±	290

The ongoing commissioning tool presented in section 6.3 used June 2008 as reference. According to the Type B benchmarks based on this training set, new conditions such as the lower heat recovery rates (Table C-4) of 2012 appear as anomalies. This illustrates the capability of the proposed tool to detect unusual operation. As a matter of fact, upon the re-commissioning following significant changes in a system, the benchmarks need a revision; future studies of the data will require new benchmarks and performance limits.

The robustness of Type A benchmarking is challenged in the presence of very narrow temperature differentials at the heat-exchanger. These were more frequent in 2011-2012 than before. The use of the measured T_{CNDs} leads to non-physical calculated ε. Although a correction for the heat input of pump 5 (Figure C-2) can be calculated, the best solution would be to consider the installation of temperature sensors on the condenser-side of HX3.

Appendix D Sub-daily effectiveness calculations

Two kinds of impossible (non-physical) values for ε occur in 2008 and 2009. First, there are 28% cases where ε is calculated as greater than 1. The delay in the propagation of a temperature variation from the CND side to the HW side was mentioned in section 5.2.4. The denominator will momentarily be lower for one to two time-steps if T_{CNDs} decreases, and higher in the opposite case. This is illustrated in Figure D-3. The ratio ε thus oscillates about its "normal" value. The upper part of the oscillation cycle raises questions because it violates energy conservation laws when exceeding 1.
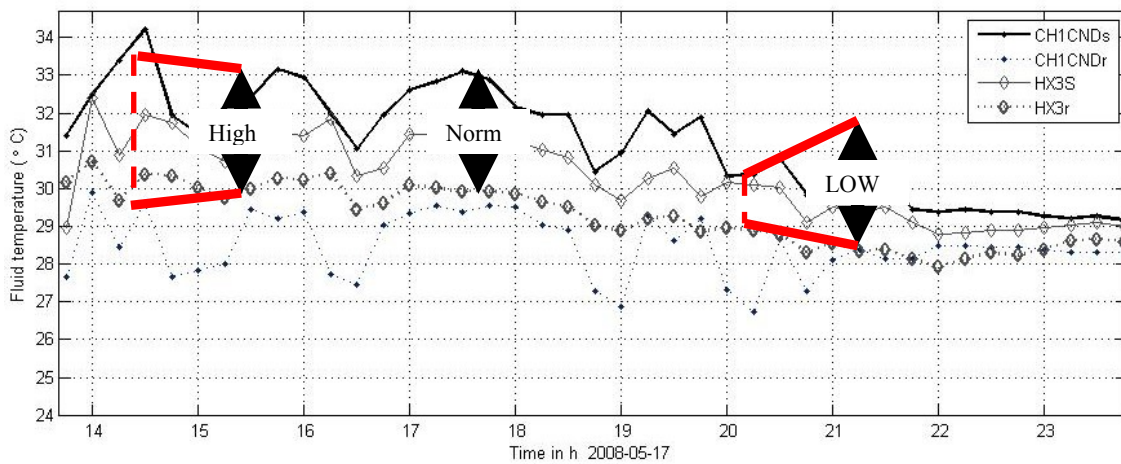

Figure D-3 Time dependence of temperatures with $T_{diff\ HX3\ Max}$ variation illustrated

Values of ε below zero occur too (1.7%) because the denominator of Equation 4-2 is negative. This is an extreme case of the phenomenon presented above. If the cooling load (and thus the T_{CNDs}) decreases very abruptly, for instance at the transition from one to two chillers-mode (Figure 5-11), T_{HWin} at the exchanger can be warmer than the T_{CNDs} for one or two time-steps. These observations explain why ε assumes values out of the natural range for the criterion.

From a physical point of view, a value of ε under 0 has no meaning. In most cases, it occurs because of the delay in temperature change on the condenser-side.
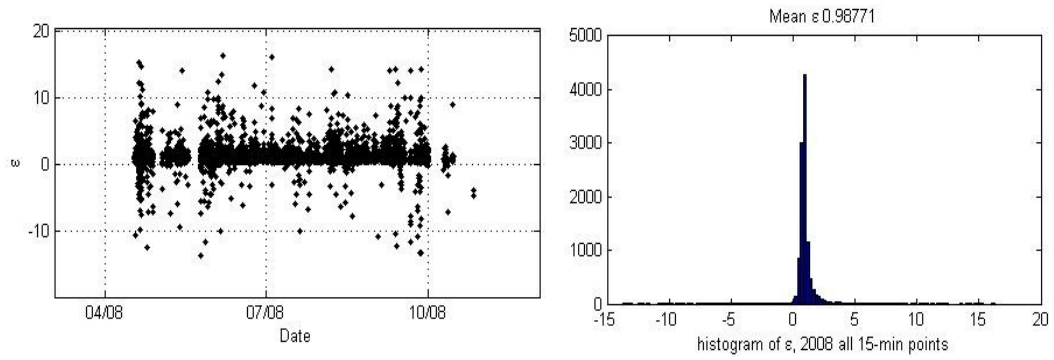
Figure D-4 Effectiveness, raw data 2008

After filtering for quasi steady-state and averaging on a day-night pattern, the distribution becomes more coherent with the expected behaviour. The distribution also appears to be less skewed.
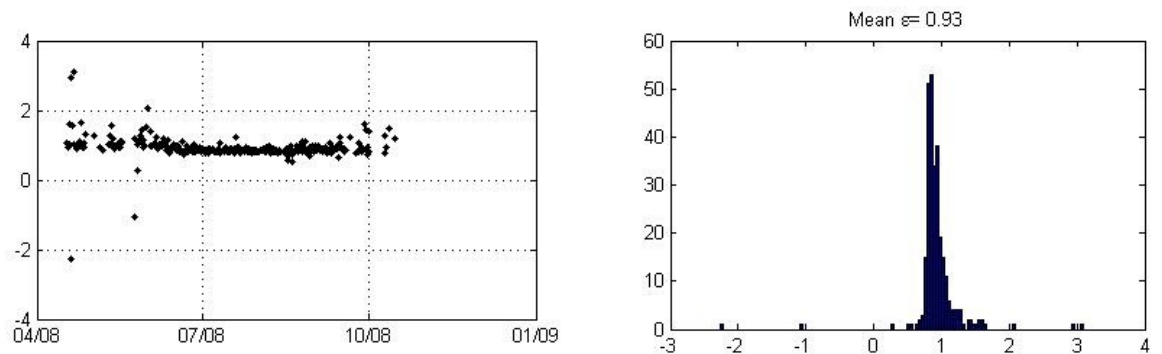

Figure D-5 Day-night quasi steady state values for effectiveness, 2008

111

Appendix E **Mean value of effectiveness in 2008**

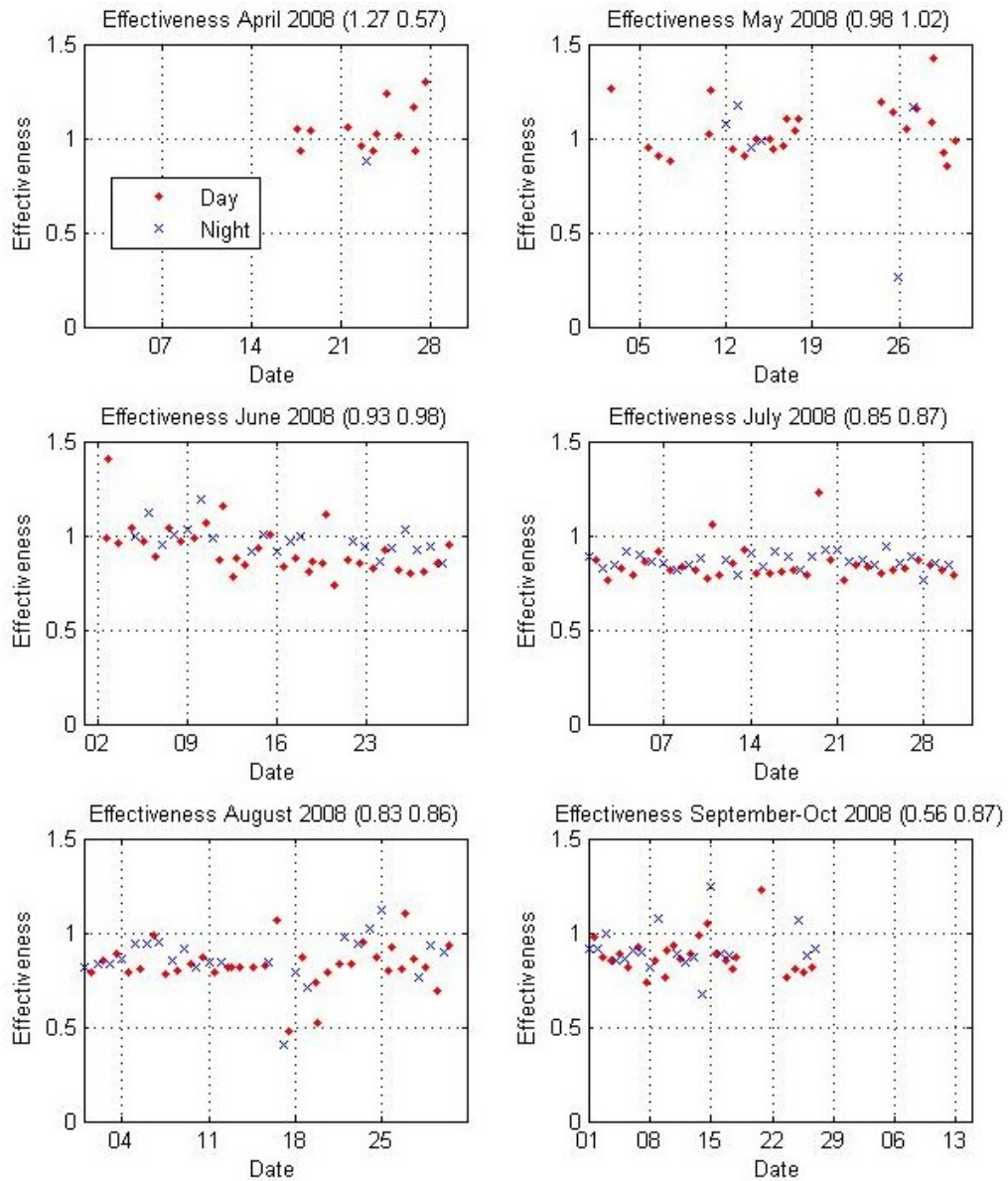The mean night-time ε is typically higher than the day (in parenthesis in subplot titles)

Figure E-6 Daily variation of ε 2008

The reheat and cooling load patterns for day versus night seem to have an impact. If two mean values per day instead of one are calculated, one for the day/occupied and one for the night/unoccupied periods, the mean ε is higher for the latter.